DEVELOPMENT OF METALLODITHIOLATES AS A NEW CLASS OF VERSATILE LIGANDS TO TRANSITION METALS

A Dissertation

by

TIFFANY ANNE PINDER

Submitted to the Office of Graduate and Professional Studies of
Texas A&M University
in partial fulfillment of the requirements for the degree of

DOCTOR OF PHILOSOPHY

Chair of Committee,	Marcetta Y. Darensbourg
Committee Members,	Sumana Datta
	Francois P. Gabbai
	Timothy R. Hughbanks
Head of Department,	David H. Russell

August 2013

Major Subject: Chemistry

ABSTRACT

Metallodithiolate ligands play an important role in providing the appropriate electronic environment for the catalytic function of various metalloenzymes; acetyl coA synthase serves as paradigm. Using tetradentate N_2S_2 ligands to bind transition metals, a library of well-characterized synthetic analogues has been established. These metal-bound cis-dithiolates, display a wide range of reactivity, including S-based metallation, oxygenation, and alkylation.

Sulfur's affinity for gold(I) is well known and typically follows Pearson's HSAB theory. With this in mind, the NiN_2S_2 moieties were used to synthesize propeller-type nickel-gold complexes within a group of $[Ni(N_2S_2)_xAu_y]$ (x = 1 or 2; y = 1, 2, or 4) complexes. The solid-state molecular structures of these square planar cis-dithiolate nickel complexes to which gold(I) is bound contain within them classical aurophilic interactions. Electrochemical studies reveal a positive shift in the $Ni^{II/I}$ couple for the $[Ni(N_2S_2)_xAu_y]$ complexes as compared to the NiN_2S_2 precursors.

The incorporation of the paramagnetic vanadyl ion, $[V{\equiv}O]^{2+}$, in N_2S_2 motifs has been studied in our laboratory. Previous studies of $M(N_2S_2)$ complexes where M is Ni^{2+}, $ZnCl^{+}$, and Fe(NO) with the $W(CO)_x$ reporter unit have been explored to determine the donor ability of these metallodithiolate ligands.

According to their response or binding to a tungsten carbonyl unit, we have found that the sulfurs of the dianionic $[(V{\equiv}O)(ema)]^{2-}$ are activated as nuclephilies. To

further investigate the donor ability of the neutral vanadyl-bound thiolate sulfurs, the oxidized $\{Fe(NO)_2\}^9$ unit was used.

Cleavage of the $(\mu\text{-}I)_2[Fe(NO)_2]_2$ dimer (in the $\{Fe(NO)_2\}^9$ form) was achieved with two metalloligands, Ni(bme-daco) and (V≡O)bme-daco, and also N-heterocyclic carbene, IMes. Using infrared spectroscopy, the ν(NO) stretching frequencies of the $LFe(NO)_2I$ (L = Ni(bme-daco), (V≡O)bme-daco, and IMes) complexes were used to report the donor ability of the ligands. Cyclic voltammetry for the $LFe(NO)_2I$ complexes show a more accessible $\{Fe(NO)_2\}^{9/10}$ couple for stronger donors. Electron paramagnetic resonance (EPR) measurements of the $LFe(NO)_2I$ complexes demonstrate super-hyperfine coupling of the ^{127}I to the unpaired electron on iron, and complex equilibria that indicates dissociation of the metallodithiolate ligand from the dinitrosyl iron unit.

DEDICATION

This dissertation and all work herein, is dedicated to my loving and supportive parents.

ACKNOWLEDGEMENTS

It's unbelievable how time flies!! My time here at A&M has definitely been rewarding, and has significantly contributed to my personal and professional development. I am indebted to many!

First, I would like to express my deepest gratitude to my research advisor and mentor Marcetta Y. Darensbourg, whose dedication for science has inspired me. I cannot thank her enough for all the support, encouragement and guidance from day one. Marcetta's constant pursuit of perfection has motivated me to be a better scientist. Over these five years, my mentor has believed in me, shared her expectations for me in the sciences, and I intend to meet and possibly exceed those expectations, by embracing a thirst for knowledge, discipline, and a strong work ethic. I will always remember and appreciate my mentor Marcetta Y. Darensbourg. I acknowledge with thanks my committee members, Prof. Sumana Datta, Prof. Francois Gabbai, and Prof. Timothy Hughbanks. They have been supportive and very encouraging with this project.

Special thanks to Prof. Francois P. Gabbai and Prof. Timothy R. Hughbanks for being great professors for my first year courses. I learned so much and gained a greater understanding of group theory and main group chemistry principles. I thank Dr. Joseph H. Reibenspies and Dr. Nattamai Bhuvanesh, for their help in the X-ray Diffraction Laboratory, and acknowledge with thanks Dr. Joseph H. Reibenspies for his work, in solving two of my structures presented in this work. I would like to thank Prof. Donald

J. Darensbourg for his assistance with the interpretation of some IR spectra and for choosing me to be the teaching assistant for the Green Chemistry course.

I appreciate all the help I received from the chemistry graduate office, especially Sandy Manning and Dr. Joanna Pellois. Prof. James Batteas, has encouraged and helped me in so many ways. He facilitated the establishment of the NOBCChE chapter at TAMU and I am fortunate to be affiliated with NOBCChE.

I express my gratitude to Nancy Magnussen, Bonnie Schiller, and all the women of WISE, who have provided an outlet for women to share their experiences through graduate school. My involvement with the outreach programs, and networking at the WISE conferences have been extremely beneficial.

Three past MYD group members, Dr. Roxanne Jenkins, Dr. Michael Singleton, and Dr. Chung-Hung Hsieh have assisted me with lab techniques and understanding chemistry principles. I am so grateful for their friendship. When they left, the lab definitely wasn't the same. Thanks to the current MYD and DJD group members, especially Randara Pulukkody, Steven Montalvo, Allen Lunsford, and Samuel Kyran. Steven and Allen's hard work contributed to the completion of these projects and I enjoyed their company over the years. Randara and Sam, have been so supportive, and I cherish our friendship. Ethel, our administrative assistant, thank you for all your help.

Casie, Morgan, and Johannes, started the program with me and we have shared so much. In fact, I'm certain that the many positive experiences would not have been the same without them.

Jayde, words can never express how much you mean to me! You have always encouraged and supported me through everything. Our bond can never be broken and I love you so much.

To my family and friends back home in the Bahamas, thanks for encouraging me to fulfill my dreams. My sister Tai, thank you for your encouragement and support.

My parents have always encouraged me to realize my potential, and I owe them so much. They have financially supported me over the years, but most importantly, by their lifestyle, they have taught the values and principles that I have embraced, to ensure a fulfilling and productive life. Thank you so much mummy and daddy and know that you are indeed the wind beneath my wings. I love you more than words can say. Most importantly, I thank God for allowing me to accomplish all of this.

TABLE OF CONTENTS

Page

LIST OF FIGURES

Page

LIST OF TABLES

Page

CHAPTER I

INTRODUCTION

Largely because of its alleged therapeutic properties for type II diabetic patients, the coordination chemistry of vanadium has become a major area of research in the last two to three decades.[1] In addition, its paramagnetic properties has given it a prominent position as a spin probe for the characterization of metal binding sites of proteins.[2,3] Two forms of vanadium, vanadate, $V^{V}O_4^{3-}$, and the vanadyl ion, $[V^{IV}{\equiv}O]^{2+}$, are prevalent under most ambient (oxygen) conditions.[4] Vanadium administered in both forms demonstrates an insulin-enhancing property, which results from the inhibition of the phosphotyrosine phosphatase 1B enzyme.[1] Professor Christopher Orvig, along with other researchers have synthesized several square pyramidal vanadyl complexes that exhibit this insulin-enhancing property.[5,6]

Although the mechanism is not fully understood, it is expected that once the metal complex is orally administered, the vanadyl ion is absorbed and distributed through the body by proteins such as serum albumin and transferrin.[7,8]

As derived by Ballhausen and Gray, the molecular orbital description of the vanadyl ion, $[V{\equiv}O]^{2+}$, should represent the $[V{\equiv}O]^{2+}$ as a triple bond, Figure I-1.[9] With its d^1 electronic configuration, EPR spectroscopy becomes a valuable tool for characterizing ligand environments about vanadium(IV).[10,11] Several studies have proven the spin-probing capacity of the vanadyl ion by replacing spectroscopically "silent" metal ions in metallo proteins such as Zn^{2+} or Mg^{2+} to gain information of the

coordination environments of such sites, for example carbonic anhydrase (CA), Figure I-2.[12]

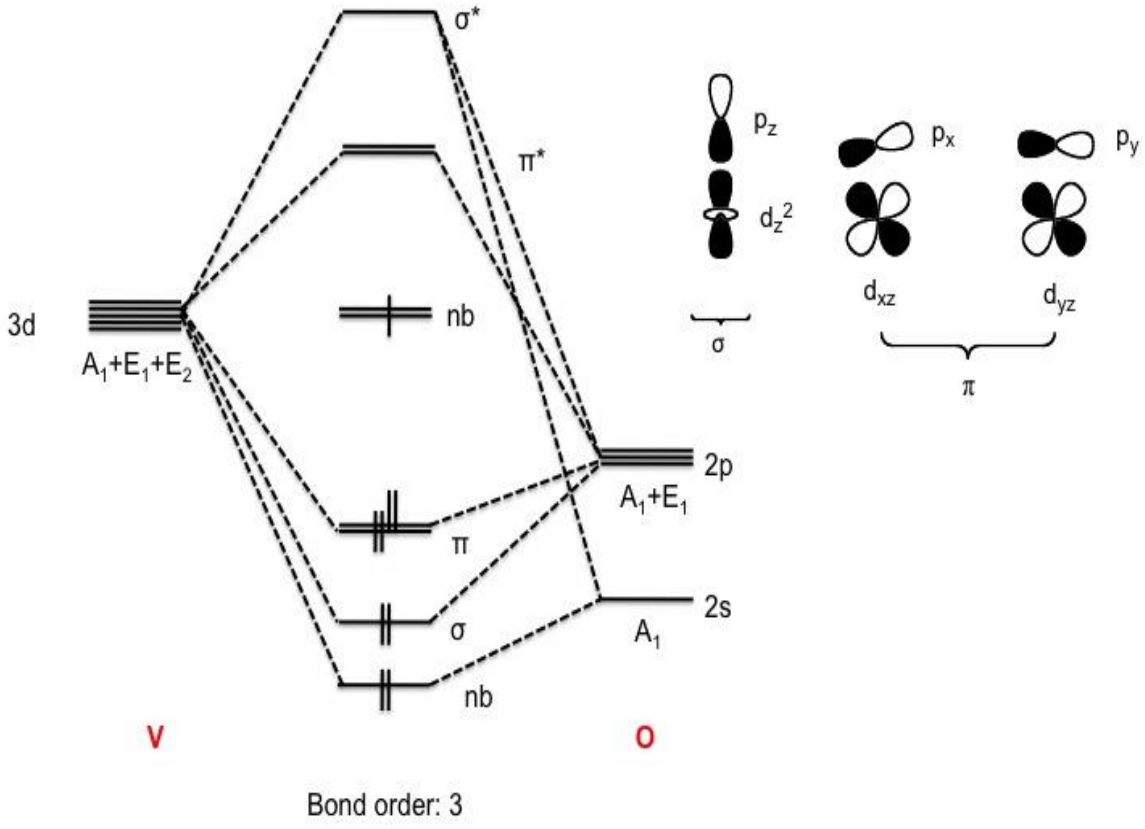

Figure I-1. Molecular orbital diagram of the vanadyl ion, $[V{\equiv}O]^{2+}$.[9]

In order to probe the structural and spectral properties of a series of $[(V{\equiv}O)N_2S_2]^{0,2-}$ complexes, our laboratory has incorporated the vanadyl ion into dianionic and tetraanionic N_2S_2 binding sites, Figure I-3.[13] The N_2S_2 ligands used in this

study were *N,N'*-bis(2-mercaptoethyl)-1,5-diazacyclooctane, (H_2-bmedaco),[14] *N,N'*-bis(2-mercaptoethyl)-1,5-diazacycloheptane, (H_2-bmedach), *N,N'*-ethylenebis(2-mercaptoacetamide), (H_4-ema),[15] and the cysteine-glycine-cysteine (CGC) tripeptide.[16] The CGC tripeptide ligand is analogous to the ema ligand because both are tetraanionic ligands with two carboxamido nitrogen atoms and two thiolate sulfur donor atoms. Three of the four complexes, (V≡O)bme-daco, (V≡O)bme-dach, and $[(V{\equiv}O)(ema)]^{2-}$ were structurally characterized by X-ray diffraction analysis showing square pyramidal geometry about the vanadium center.[13] The IR spectra of the $[(V{\equiv}O)N_2S_2]^{0,2-}$ complexes displayed a ν(V≡O) band in the range of 940 – 990 cm^{-1}, where the lower energy vibrations were observed for the dianionic complexes. Although the molecular structure of the $[(V{\equiv}O)(CGC)]^{2-}$ complex was not obtained, a strong ν(V≡O) stretch in the IR at 945 cm^{-1} (consistent with the ν(V≡O) stretch of $[(V{\equiv}O)(ema)]^{2-}$ at 941 cm^{-1}) confirmed formation of this $[(V{\equiv}O)N_2S_2]^{2-}$ complex.[13]

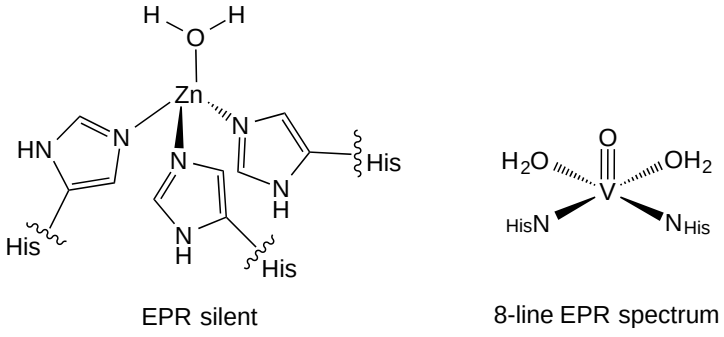

Figure I-2. Active site of carbonic anhydrase and the $[V{\equiv}O]^{2+}$ form of carbonic anhydrase.[12]

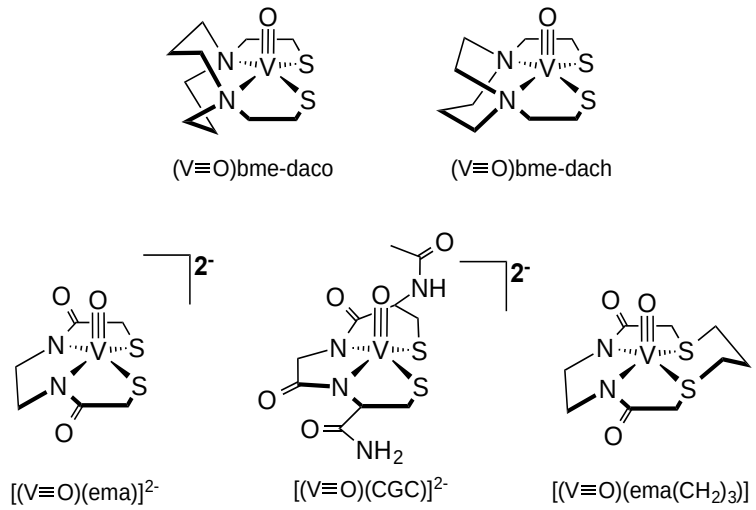

Figure I-3. $[(V{\equiv}O)N_2S_2]^{0,2-}$ complexes synthesized in the MYD laboratory.[13]

The EPR spectra of the paramagnetic $[(V{\equiv}O)N_2S_2]^{0,2-}$ complexes of Figure I-3 showed the distinctive eight-line pattern, indicative of the unpaired electron coupled to the ^{51}V center with a nuclear spin of 7/2.[13] These $[(V{\equiv}O)N_2S_2]^{0,2-}$ complexes (Figure I-3) are among five of the square pyramidal vanadyl ($V^{IV}{\equiv}O$) examples with contiguous N_2S_2 ligands in the literature and add to a collection of mononuclear MN_2S_2 complexes.[17,18,19,20]

Figure I-4 consists of several examples of mononuclear MN_2S_2 complexes prepared in our laboratory. The metal center of Ni(bme-daco),[21] Ni(bme-dach)[22] and Pd(bme-daco)[23] is in a regular square plane with cis-dithiolates and tertiary nitrogens within a 8- or 7- membered diazacycle. The Ni(bme-daco) served as the paradigm for this class of complexes, readily formed by reacting the protonated N_2S_2 ligand (H_2-bme-daco) with $Ni(acac)_2$ in toluene.[21] Minor differences in structure but important differences in solubility exist between the bme-daco and bme-dach analogues.[21,22] Both

NiN_2S_2 complexes exhibit similar Ni – N and Ni – S bond distances in the range of 1.940 – 1.979 Å and 2.159 – 2.164 Å, respectively; however, the ∠N – Ni – N is smaller in the dach derivative, at 83° as compared to 89° in the daco complex. This is compensated by a larger ∠S – Ni – S angle at 95° for Ni(bme-dach) that is ca. 6° smaller in Ni(bme-daco).[21,22] As with the nickel complexes, the Pd(N_2S_2) is a regular square plane with deviations from the plane of no more than 0.039 Å for all five atoms.[23] A distinguishing feature of penta-coordinate complexes such as $[(V{\equiv}O)N_2S_2]^{0,2-}$ described above (Figure I-3) and the Fe(NO) and Co(NO) complexes shown in Figure I-4 is the displacement of the metal out of the best N_2S_2 plane at 0.353 Å for $Co(NO)N_2S_2$ and 0.483 Å for $Fe(NO)N_2S_2$.[24] Presented below are similar data for the three $[V{\equiv}O]^{2+}$ complexes which show a vanadium displacement from the N_2S_2 plane of 0.672 Å on average. The N_2S_2 plane is again regular and the S – M – S angles for both the Fe(NO) and Co(NO) complexes are 95°, whereas for the $[(V{\equiv}O)N_2S_2]^{0,2-}$ the angles range from 89 – 98°.[13,24] In summary, this N_2S_2 motif shows great versatility by incorporating transition metal ions with different sizes and charge.

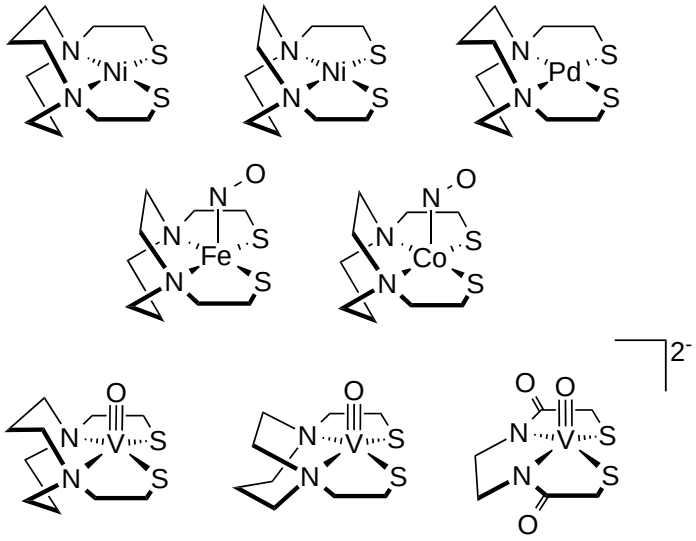

Figure I-4. Tetra- and penta-coordinate MN_2S_2 complexes in the MYD laboratory.[13,21-24]

Nucleophilicity of the Cis-Dithiolates

The reactivity of the nickel-bound cis-dithiolates has been well established for templating macrocycle formation.[25] Figure I-5 demonstrates macrocyclization with the Ni(bme-daco) complex along with several other examples of electrophilic – nucleophilic adduct formation. Alkylation with alkyl halides and cysteine modification agents such as iodoacetamide, oxygenation with hydrogen peroxide and other oxygen sources, and sulfur dioxide adduct formation are some of the reactions studied with Ni(bme-daco), Figure I-5.[21,26-28] Lastly in this reaction wheel of Ni(bme-daco), Figure I-4, metallation of the cis-dithiolates has been thoroughly investigated by exploring the structural and electronic properties of the metallodithiolates with a number of transition metals.[29-31]

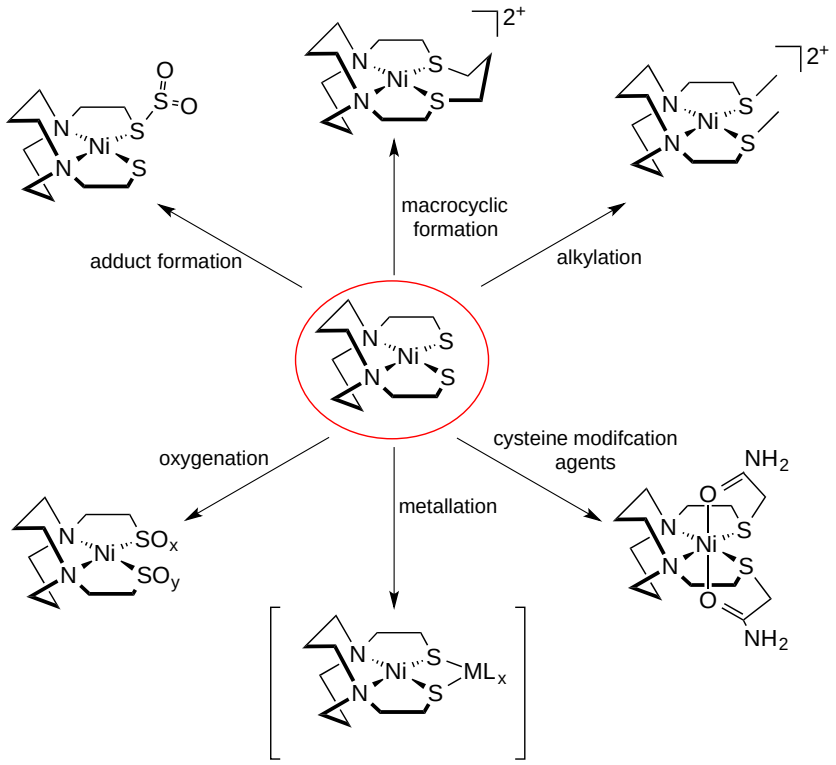

Figure I-5. S-based reactivity of Ni(bme-daco).[21,26-28,30-32]

Metallation as Reporter of MN_2S_2 Donor Abilities

Metallodithiolate ligands, MN_2S_2, have been used to synthesize a library of polymetallic complexes. Nature utilizes this MN_2S_2 framework as a structural motif in the metalloenzyme acetyl coA synthase, ACS, shown in Figure I-6.[33] The distal nickel, Ni_d, within the A-Cluster of ACS, contains a tripeptide motif (cysteine-glycine-cysteine), locking the distal nickel center, Ni_d, in a square planar geometry, providing the necessary electronic features to facilitate C-C and C-S coupling reactions performed by the proximal nickel, Ni_p, for the formation of acetyl coA.

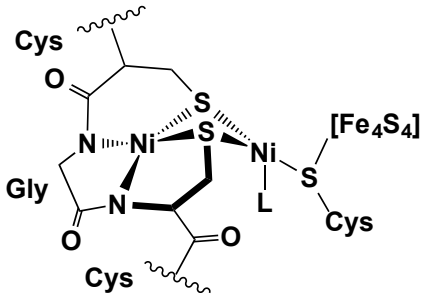

Figure I-6. The A-cluster of ACS.[33]

Tolman has developed a broadly accepted scale to describe the electronic and steric properties of phosphine ligands in organometallic complexes.[34] The electronic parameter, ν, based on the A_1 carbonyl vibrational mode of $Ni(CO)_3L$ complexes where L = PR_3, indicates lower ν(CO) stretching frequencies for stronger donor ligands as compared to weaker donors. The steric parameter, θ, Tolman's ligand cone angle, shows the difference in size of the substituents on the phosphine ligands; bulky substituents constitute large cone angles whereas smaller substituents diminish the cone angle.[34] Tunsgten (0) carbonyls also serve as reliable reporter units through ν(CO) IR values when bound to various ligands, including metallodithiolates.

Mimicking Tolman's approach, our laboratory has prepared a series of $(MN_2S_2)W(CO)_4$ complexes by reaction of MN_2S_2 with cis-$W(CO)_4(pip)_2$.[29,35] From this process, stable complexes are prepared. The ν(CO) stretching frequencies and calculated force constants of these metallodithiolate ligands have been compared to simple ligands prominent in coordination and organometallic chemistry.[29] From this study, the neutral NiN_2S_2 complexes show little differences in donor abilities; however, as a class they are better donors as compared to phosphine and nitrogen donor ligands, Figure I-7.[29] The

penta-coordinate complexes [Co(NO)bme-dach] and [Fe(NO)bme-dach] display similar donating properties as the neutral NiN_2S_2 complexes.[35] As will be shown in Chapter IV, the analogous $[(V{\equiv}O)N_2S_2]^{2-}$ complex is a slightly better donor than the analogous M(NO) complexes. The dianionic $[Ni(ema)]^{2-}$ complex is the strongest donor from this series, increasing the electron density on the $W(CO)_4$ moiety, thereby giving the lowest ν(CO) stretching frequencies and force constants.[29] Further discussion on the donating ability of the $[(V{\equiv}O)N_2S_2]^{0,2-}$ complexes will be addressed in Chapter IV.

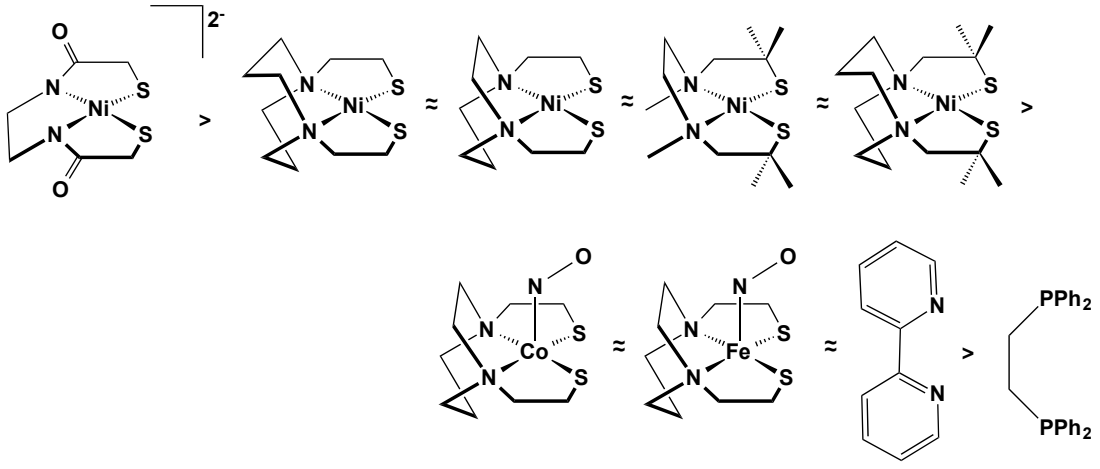

Figure I-7. Ranking of donor abilities of MN_2S_2 complexes determined from $(MN_2S_2)W(CO)_4$ complexes.[29,35]

A by-product of the donor ability study was the discovery that the cis-dithiolates of the MN_2S_2 complexes were shown to be hemi-labile ligands. Rauchfuss and coworkers first coined this term on observation of displacement of a donor atom from a chelating ligand to a metal complex upon addition of a π-accepting ligand.[36] In these

cases the conversion of the bidentate to a mono-dentate ligand results in a stronger bond of the latter. This process is important in catalysis, in that partial dissociation of a chelating ligand opens up a binding site to which a substrate can bind. The ring-opening process of the $(NiN_2S_2)W(CO)_4$ shown in Figure I-8 was observed in the presence of CO. A kinetic study established, in collaboration with the Donald Darensbourg laboratory, that the ring-opening process (Figure I-8) is first-order with respect to the tetracarbonyl species, $(NiN_2S_2)W(CO)_4$.[37] This dissociative mechanism leads to a short-lived penta-coordinate intermediate with an open site on W, leading to the formation of the penta-carbonyl species, $(NiN_2S_2)W(CO)_5$ (Figure I-8) upon CO capture.

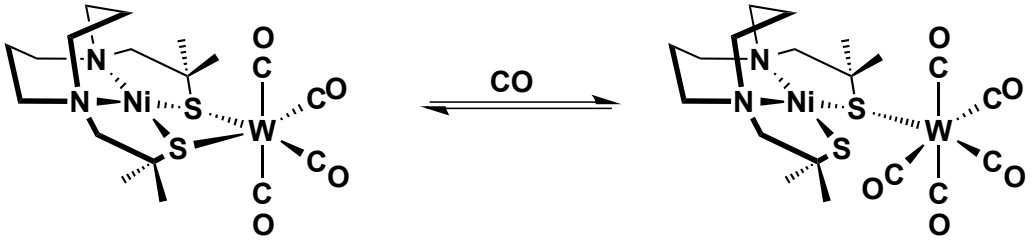

Figure I-8. Ring-opening process of $NiN_2S_2{\cdot}W(CO)_4$.[37]

Metallation in Assembly of Unique Polymetallic Structures

As mentioned earlier, the nucleophilic thiolates are susceptible to a variety of electrophiles such as alkyl halides, coordinatively unsaturated tungsten carbonyls, and oxygen sources, Figure I-5.[21,26,29,32] The reactivity of *cis*-dithiolates in MN_2S_2 complexes has demonstrated the ability of this motif for construction of polymetallic

complexes in the form of C_3 and C_4 paddlewheels, shown in Figures I-9 and I-10.[38-42] Paddlewheel complexes are distinct structures where two metals, whether bonded or not, become the axle and the bridging bidentate ligands (either three or four) are the paddles of the paddlewheel. They are prominent with metals prone to M-M bonds but can also be found with metals with no possibility for M-M bonds such as Zn^{2+}. The key feature is the bite angle of the bidentate ligands. Classic studies of the F. A. Cotton lab established the benefits of carboxylates, and amidates as bridging bidentate ligands.[43] The donor sites from the paddles are typically flat ligands with steric bulk on the periphery of the donor sites. The Cotton-type ligand paddles usually possess a negative charge. Whereas in most standard paddlewheels the lone pairs of the donor atoms of the paddles are pointed in a parallel arrangement, the soft sulfur atoms in cis-dithiolates are not confined to a set orientation.

The metallodithiolate ligand for six of the seven C_4 paddlewheel complexes of Figure I-9 contain $[NiN_2S_2]^{0/2-}$ paddles and a seventh is derived from a PdN_2S_2 complex paddle. Five of the cationic paddlewheel complexes originate from diazacycles in the form of 6-, 7-, and 8- membered rings as scaffolds that are outfitted with ethylene thiolate arms. The open chain MN_2S_2 ligand (M = Pd) where the tertiary amines have methyl substituents and ethylene thiolate linkers is roughly in the 3 o' clock position of Figure I-9.[40] The anionic species at the 5 o' clock position in Figure I-8 is derived from the $[Ni(ema)]^{2-}$ ligand.[42] Tables I-1 and I-2 contain the salient metric parameters of the C_3 and C_4-paddlewheel complexes. The Ni(II) or Pd(II) metallodithiolate ligands maintain a square planar coordination geometry in all C_4-paddlewheels.

Our laboratory has reported four of the seven known C_4-paddlewheel complexes containing a NiN_2S_2 motif from thiolate-modified diazacycles: $[Mo_2(Ni(bme\text{-}daco))_4]^{4+}$,[38] $[Mo_2(Ni(bme\text{-}dach))_4]^{4+}$,[38] $[Rh_2(Ni(bme\text{-}dach))_4]$,[39] and $[Pd_2(Ni(bme\text{-}dach))_4]^{4+}$,[40] found in Figure I-9 at 8, 10, 12, and 1 o' clock positions. Upon addition of Mo_2^{4+} (as the $[Mo_2(MeCN)_{10}][BF_4]_4$ precursor) to Ni(bme-daco) and Ni(bme-dach) in MeCN, the positions 8 and 10 o' clock, $[Mo_2(Ni(bme\text{-}daco))_4]^{4+}$ and $[Mo_2(Ni(bme\text{-}dach))_4]^{4+}$ complexes were isolated, respectively.[38] Formation of the $[Rh_2(Ni(bme\text{-}dach))_4]$ complex at 12 o' clock was obtained from displacement of the triflate ion from $Rh_2(O_2CCF_3)_4$ on addition to the Ni(bme-dach) metallodithiolate ligand in a MeCN solution.[39] The $[Pd_2(Ni(bme\text{-}dach))_4]^{4+}$ complex was synthesized by reacting Ni(bme-dach) and $Pd(NO_3)_2$ in a 2:1 ratio in MeCN.[40] Schroder and co-workers prepared two C_4-paddlewheel complexes, $[Pd_2(Pd(N_2S_2))_4]^{4+}$, from the reaction of L^2H_2 (L^2H_2 = N,N'-dimethyl-N,N'-bis(2-mercaptoethyl)propandiamine) with $[Pd(MeCN)_4](BF_4)_4$ in MeCN and $[Ni_2(Ni(N_2S_2))_4]^{4+}$ from a stoichiometric ratio of $[Ni(H_2O)_6](BF_4)_2$ and L^1H_2 (L^1H_2 = *N,N'*-bis(2-mercaptoethyl)-1,5-diazacyclohexane).[41] These are the structures in Figure I-9 at positions 3 and 7 o' clock, respectively. Lastly, an anionic C_4-paddlewheel complex, $[Ni_2(Ni(ema))_4]^{4-}$ was prepared on addition of $Ni(OAc)_2{\cdot}4H_2O$ to $[Et_4N^+]_2[Ni(ema)]^{2-}$ by the Hegg research group.[41]

In both $[Mo_2(Ni(bme\text{-}daco))_4]^{4+}$ and $[Mo_2(Ni(bme\text{-}dach))_4]^{4+}$ complexes, a Mo-Mo axle and eight sulfur atoms from the NiN_2S_2 metallodithiolate bidentate bridging paddles form the paddlewheel. A quadruple bond exists between the Mo atoms with a bond distance of 2.14 Å for $[Mo_2(Ni(bme\text{-}daco))_4]^{4+}$ and 2.16 Å for $[Mo_2(Ni(bme\text{-}$

dach))$_4$]$^{4+}$.[38] These values are similar to the quadruply-bonded Mo_2^{4+} unit in $Mo_2(S_2CR)_4$, reported by the late Professor F. A. Cotton.

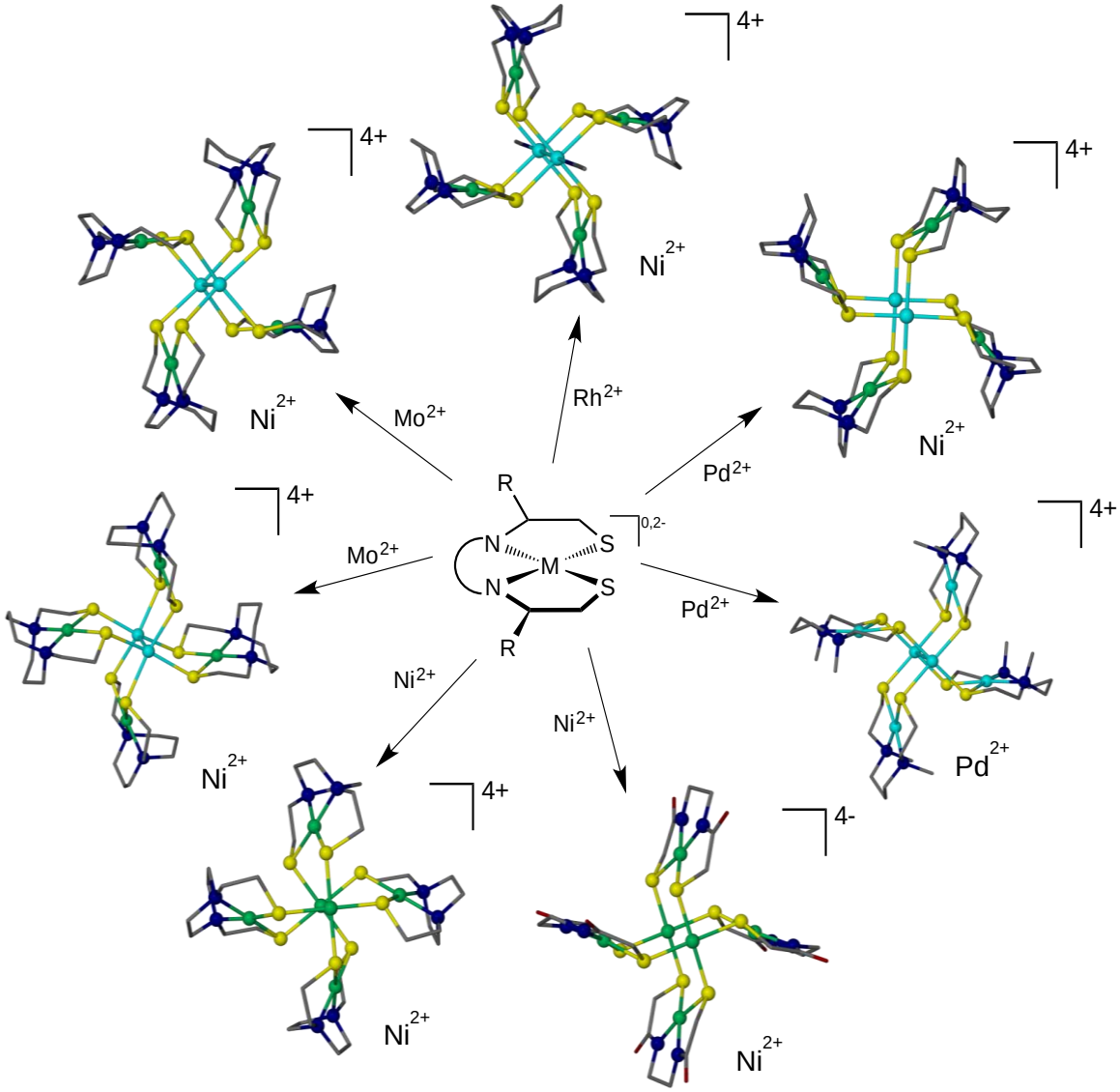

Figure I-9. C_4 paddlewheel complexes with NiN_2S_2 paddles except in 3 o'clock position where M = Pd^{2+}. Metals on arrows become axles.

Table I-1. Selected bond distances for the MN_2S_2 C_4-paddlewheel complexes.

C_4 paddlewheel	M-M (in axle) (Å)	S-S (Å)	Ni•••Ni (M'-M') (Å)	M_{disp} (axle) (Å)
$[Mo_2(Ni(bme\text{-}daco))_4]^{4+}$	2.142(1)	3.001(3)	5.334(2)	0.428
$[Mo_2(Ni(bme\text{-}dach))_4]^{4+}$	2.162(7)	3.097(1)	5.049(1)	0.467
$[Rh_2(Ni(bme\text{-}dach))_4]$	2.892(6)	3.044(1)	4.935(1)	0.076
$[Pd_2(Ni(bme\text{-}dach))_4]^{4+}$	3.132(8)	3.198(2)	4.859(1)	0.033
$[Pd_2(Pd(L^2H_2))_4]^{4+}$	3.095(2)	3.224(8)	4.997(3)	0.066
$[Ni_2(Ni(L^1H_2))_4]^{4+}$	3.024(5)	3.389(6)	4.658(9)	0.067
$[Ni_2(Ni(ema))_4]^{4-}$	3.209(5)	3.308(2)	4.726(7)	0.049

The cationic $[Rh_2(Ni(bme\text{-}dach))_4]$ complex, 12 o'clock position in Figure I-9, crystallizes with two MeCN molecules bound to the Rh_2^{4+} unit; the Rh-Rh single bond distance is 2.89 Å.[39] The other four C_4-paddlewheel complexes have M-M interactions ranging from 3.02 – 3.22 Å in which the longest interaction is seen in the anionic $[Ni_2(Ni(ema))_4]^{4-}$ complex.[40-42]

As seen in Table I-1, the S-S distance for the C_4 paddlewheels ranges from 3.00 – 3.39 Å, roughly following the trend for M-M distance/interaction in the C_4-paddlewheels in which the shorter M-M distances correlate with shorter S-S distances. Another important feature from this family is the M'•••M' distance between the metals in the

paddles. The largest separation is observed for the $[Mo_2(Ni(bme\text{-}daco))_4]^{4+}$ complex, due to the size of the Mo atom in the axle of the paddlewheel.[38]

In addition to the C_4-paddlewheels deposited in the Cambridge Crystallographic are ten C_3-paddlewheels (Figure I-10) with a N_2S_2 backbone analogous to the C_4-paddlewheel complexes described above. The C_3-paddlewheel complexes at the 1 o'clock position through the 7 o'clock position are derived from ethylene thiolate modified diazaccyles.[31,44-46] Five of the six complexes include a Ni^{II} center within this N_2S_2 motif as the paddles of the paddlewheel complexes; an exception at the 6 o'clock position is derived from a $Fe(NO)N_2S_2$ complex.[46] The NiN_2S_2 paddles at the 8 o'clock position are derived from tertiary amines with ethyl substituents and ethylene thiolates.[47] The C_3-paddlewheel complexes at the 10 and 11 o'clock positions of the wheel were derived from CuN_2S_2 with either carboxylate or cyclohexyl substituents on the tertiary amines.[48,49] Lastly, the NiN_2S_2 paddles in the 12 o'clock position contain a rigid backbone with cyclohexyl substituents on the amines and gem-dimethyl groups on the carbon alpha to the thiolate sulfurs.[50] All of these complexes have as axles metals such as Cu^{I}, Zn^{II}, or Ag^{I}, i.e., metals that prefer either trigonal planar (Ag^{I}) or tetrahedral geometries. The latter is found for Zn^{II} in which case the fourth ligand is chloride. The 7 o' clock position contains a Cu^{I} and a $Cu^{I}Br$ as components of the axle, the former existing in a trigonal plane and the latter in a $BrCu^{I}S_3$ tetrahedral environment.

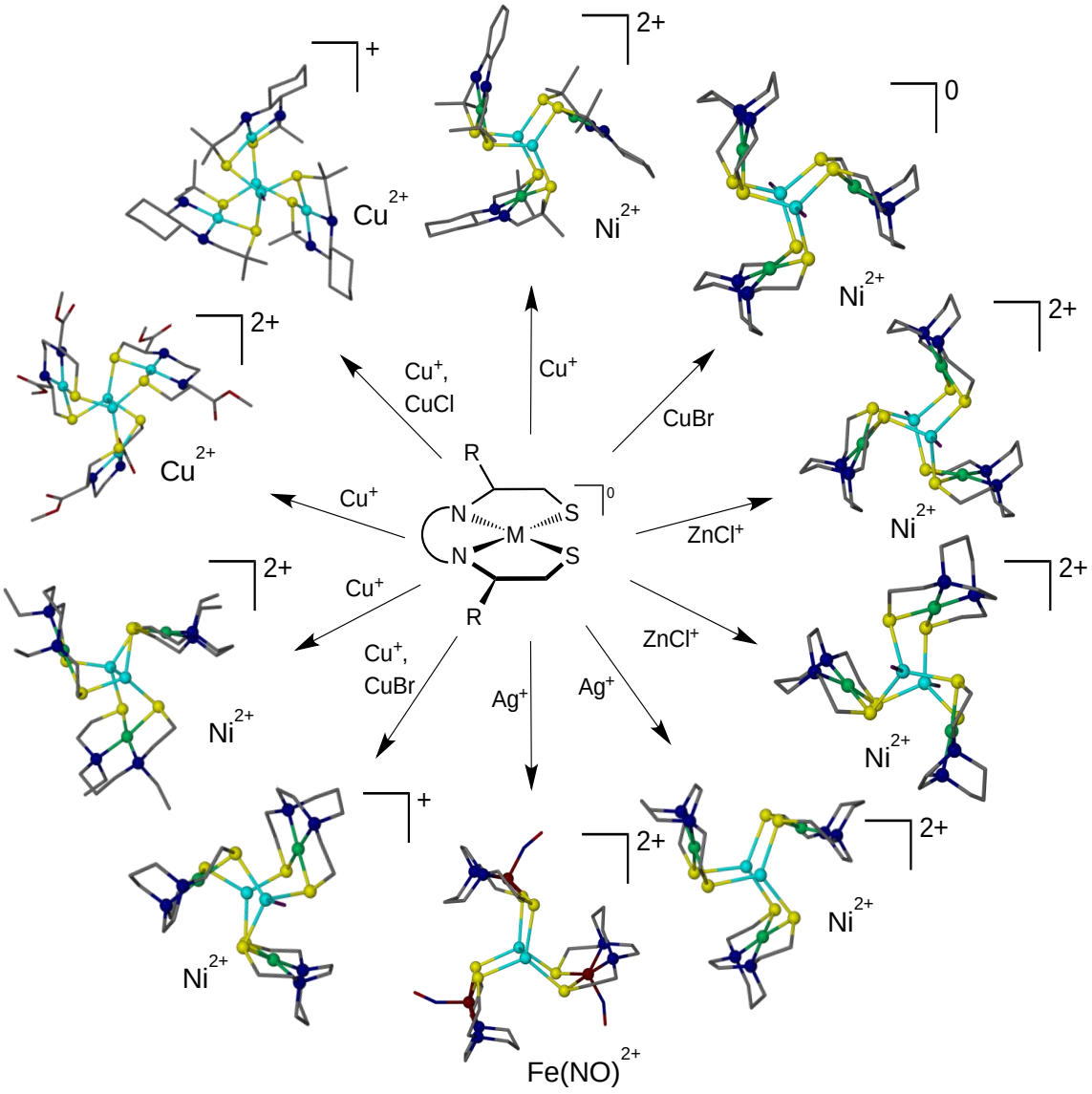

Figure I-10. C_3 paddlewheel complexes with MN_2S_2 paddles, (M = Ni^{2+}, $Fe(NO)^{2+}$, Cu^{2+}) as indicated in each position. Metals on arrows become axles.

Upon analysis of the metric parameters, the M-M distances range from 2.87 – 4.35 Å, with no complex displaying a M-M bond. As the number of the paddles decrease, as seen in the C_3-paddlewheels, the symmetry within these complexes decrease as well compared to the C_4-paddlewheels.

Table I-2. Selected bond distances for the MN_2S_2 C_3-paddlewheel complexes.

C_3 paddlewheel	M-M (in axle) (Å)	S-S (Å)	Ni•••Ni (M'-M') (Å)	M_{disp} (axle) (Å)
$[[ZnCl]_2(Ni(bme\text{-}daco))_3]^{2+}$	4.354(2)	3.040(3)	5.108(2)	0.658
$[[ZnCl]_2(Ni(bme\text{-}dach))_3]^{2+}$	4.277(1)	3.204(1)	5.086(1)	0.542 0.719
$[[CuBr]_2(Ni(bme\text{-}daco))_3]$	4.052(3)	3.031(8)	5.050(6)	0.510
$[Cu_2(Cu(bme\text{-}COOMe\text{-}Et))_3]^{2+}$	3.016(4)	3.468(6)	4.973(3)	0.125
$[Ag_2(Ni(bme\text{-}dach))_3]^{2+}$	2.998(1)	3.195(1)	5.218(1)	0.111
$[Cu_2Br(Ni(bme\text{-}dach))_3]^{+}$	3.373(1)	3.200(2)	4.987(1)	0.229 0.533
$[Cu_2(Ni(bme\text{-}DiEt\text{-}Pro))_3]^{2+}$	2.644(1)	2.993(2)	5.290(9)	0.175
$[Cu_2(Ni(bme^*\text{-}dahex))_3]^{2+}$	3.094(2)	3.228(4)	4.827(2)	0.075
$[Cu_2Cl(Cu(bme^*\text{-}dahex))_3]^{+}$	3.923(2)	3.597(3)	4.9035(4)	0.026 0.885
$[Ag_2(Fe(NO)(bme\text{-}dach))_3]^{2+}$	2.866(3)	3.314(3)	6.279(3)	0.423

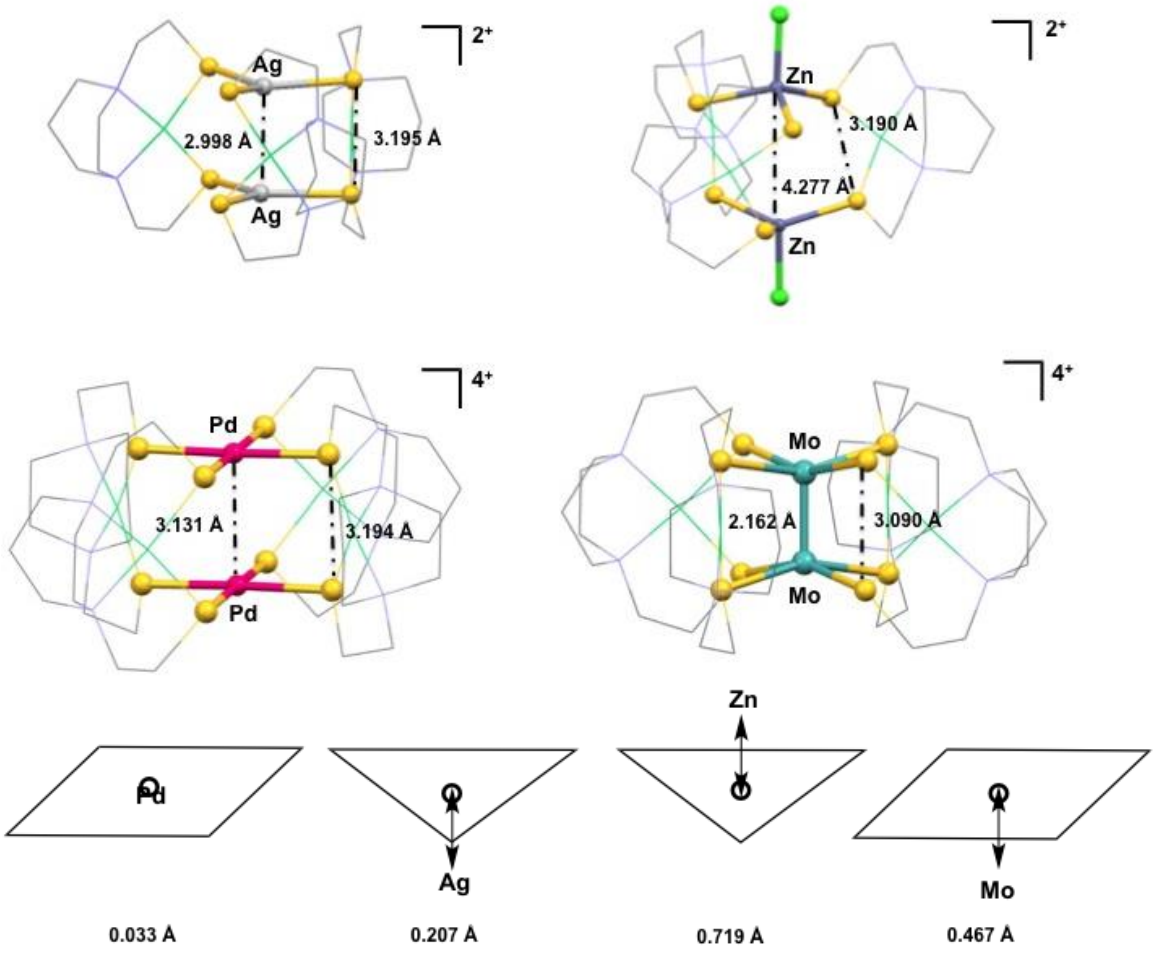

Figure I-11. (a) $[M_2(N_2S_2)_x]$ in different coordination environments around the axle of the paddlewheel and (b) metal displacement from S_3 or S_4 plane. O= centroid of N_2S_2 plane.

Figure I-11 displays graphics of two C_4 and two C_3 paddlewheel complexes, with all paddles consisting of the Ni(bme-dach) complex and the metal atoms of the axle in different coordination environments. It is a graphic intended to illustrate the sulfur coordination planes and positions of the two metals relative to those planes. The average distance between the best planes comprised of S_3 or S_4 within the complexes are comparable. A shorter distance of the S_4 planes is observed in the [Mo_2(Ni(bme-

dach))$_4$]$^{4+}$ complex which adjusts to accommodate binding to the quadruply bonded Mo_2^{4+} unit.[38] Additionally, the sulfur atoms are in a plane where the metal atom of the axle is displaced out of the S_3 or S_4 plane dependent on the presence or absence of a M-M interaction. The largest metal displacement is observed in [[ZnCl]$_2$(Ni(bme-dach))$_3$]$^{2+}$ at 0.719 Å with a pseudo-tetrahedral geometry around the Zn^{2+} center, leading to the largest M•••M distance.[45] The inverse of this "outside" displacement exists for the Mo_2^{4+} for which the [Mo-Mo]$^{4+}$ unit requires square pyramidal geometry about each Mo, and an inward displacement from the S_4 best plane of 0.476 Å. For [Pd$_2$(Ni(bme-dach))$_4$]$^{4+}$, the Pd^{II} center is nestled in an almost perfect S_4 square plane with slight displacement of 0.033 Å, whereas one Ag^I in [Ag$_2$(Ni(bme-dach))$_3$]$^{2+}$ is displaced out of the S_3 plane at 0.207 Å and the other is within the S_3 plane.[40,45]

Metallodithiolates as ligands can accommodate a variety of metals and give rise to unique polymetallic structures by utilizing the soft binding surface of the sulfur lone pairs. With this overview of the versatility of the MN_2S_2 motif, Chapter III of this dissertation details the chemistry of the NiN_2S_2 ligands to a Au^+ synthon according to the synthesis and characterization of unique heterobimetallic structures that demonstrate different types of aurophilic interactions.

To extend the study of MN_2S_2 complexes as metalloligands, the reactivity of the $[(V{\equiv}O)N_2S_2]^{0,2-}$ with dinitrosyl iron complexes (DNICs) have explored the redox properties and spectroscopic behavior of a heterobimetallic complex containing two EPR active metal centers. An important question addressed from this study is as follows: will the odd electrons on the dinitrosyl iron unit and on the $[V{\equiv}O]^{2+}$ be spin-paired or

localized? Comparison of the vanadyl-iron dinitrosyl complex with a diamagnetic NiN_2S_2 metallodithiolate and N-heterocyclic carbene will be discussed including full characterization of these complexes.

CHAPTER II

GENERAL EXPERIMENTAL DETAILS

General Procedures

All solvents used were purified and degassed via a Bruker solvent system. Anaerobic standard Schlenk-line techniques or an argon-filled glovebox were employed for air sensitive reagents and complexes. Reagents were purchased from commercial vendors and used as received unless noted.

General Physical Measurements

Electronic absorption spectra were recorded on a Hewlett-Packard 8453 diode-array spectrometer and a Cary 1E spectrophotometer using quartz cells (1.00 cm path length). Elemental analyses were performed by Atlantic Microlab, Inc., Norcross, GA. Infrared spectra were recorded on a Bruker Tensor 37 Fourier transform IR (FTIR) spectrometer. Solution IR spectra were obtained using a CaF_2 cell with a 0.1 mm path length; solid sample IR spectra were obtained using an attenuated total reflectance attachment equipped with a ZnSe crystal. Electrospray ionization mass spectrometry (ESI-MS) was performed in the Laboratory for Biological Mass Spectrometry at Texas A&M University. All NMR spectra were obtained on a Varian Mercury-300 MHz NMR spectrometer. ^{31}P NMR shifts are referenced to 100% H_3PO_4 (0 ppm).

Electron paramagnetic resonance, EPR spectra were collected on two different instruments, a Bruker (Billerica, MA) EMX Plus spectrometer equipped with a bimodal

resonator (Bruker model 4116DM); low-temperature measurements were made using an Oxford ESR900 cryostat and an Oxford ITC 503 temperature controller, and on a Bruker ESP 300 spectrometer. EPR spectra parameters were determined by simulations with SpinCount, developed by Professor Michael P. Hendrich of Carnegie Mellon University.

Electrochemistry

Cyclic voltammograms and differential pulse voltammograms were recorded on a BAS-100A electrochemical analyzer using a three-electrode cell: a glassy carbon disk (0.071 cm^2), the working electrode; reference electrode, a Vycor-tipped $Ag/AgNO_3$; and a straight platinum wire, the counter electrode. Solutions were deaerated by an Ar purge for 5-10 min and a blanket of Ar was maintained over the solution while performing the measurements. All experiments were performed at room temperature in CH_3CN or DCM solutions, 2.0 mM in analyte, and containing 0.1 M $(n\text{-}Bu)_4N^+PF_6^-$ as supporting electrolyte. Ferrocene, Fc, served as the internal reference and all potentials are reported relative to the Fc/Fc^+ couple as 0.00 V.

X-ray Diffraction and Analyses

Low-temperature (110 K) X-ray data were obtained on a single-crystal APEXii CCD diffractometer (Texas A&M University; molybdenum-sealed X-ray tube, $K\alpha$ = 0.71073 Å). Space groups were determined on the basis of systematic absences and intensity statistics. Structures were solved by direct methods and refined by full-matrix least squares on F^2. Hydrogen atoms were placed at idealized positions and refined with fixed isotropic displacement parameters, and anisotropic displacement parameters were

employed for all non-hydrogen atoms. The following programs were used: data collection, APEX2;[51] data reductions, *SAINTPLUS*, version 6.63;[52] absorption correction, *SADABS;*[53] structure solutions, *SHELXS-97* (Sheldrick);[54] and structure refinement, *SHELXL-97* (Sheldrick).[55] Structure plots were generated in Mercury, version 2.3. Experimental conditions and crystallographic data are listed in the Appendix.

CHAPTER III

ADVANCED VERSATILITY OF N_2S_2 NICKEL-DITHIOLATES IN COORDINATION CHEMISTRY: MONO- AND BIDENTATE, S-DONOR LIGANDS TO GOLD(I)[*]

Introduction

The controlled aggregation of bimetallics using nickel dithiolates to bind a second metal has proven effective for the design and synthesis of biomimetics for the acetyl CoA synthase (ACS) and nickel-iron hydrogenase enzyme active sites (Figure III-1).[33,56]

Further versatility of the contiguous N_2S_2 binding motif metallated by nickel has been demonstrated in structural studies of a large range of metals in bi-, tri-, and poly-metallic constructions, including those with M-M multiple bonds.[38,40,44] The cis-orientation of thiolate sulfurs in Ni(bme-daco), (N,N'-bis(2-mercaptoethyl)-1,5-diazacyclooctane),[21] Ni(bme-dach), (N,N'-bis(2-mercaptoethyl)-1,5-diazacycloheptane),[22] and $[Ni(ema)]^{2-}$, (*N,N'*-ethylenebis(2-mercaptoacetamide),[15] permit them to serve as S- donor bidentate ligands similar to chelating diphosphine ligands. By use of ν(CO) as a marker for electron density donated to the $W(CO)_4$ unit, studies for

---

[*] Pinder, T. A.; Montalvo, S. K.; Lunsford, A. M.; Hsieh, C.-H.; Reibenspies, J. H.; Darensbourg, M. Y. *Dalton Trans.* **2013**, *in press*. DOI: 10.1039/C3DT52295D. Figure III-1 on following page reproduced by permission of the Royal Society of Chemistry (RSC). http://pubs.rsc.org.lib-ezproxy.tamu.edu:2048/en/content/articlepdf/2013/dt/c3dt52295d?page=search

benchmarking the NiN_2S_2 complexes as ligands have established that such dithiolates are superior to phosphines and bipyridine.[29]

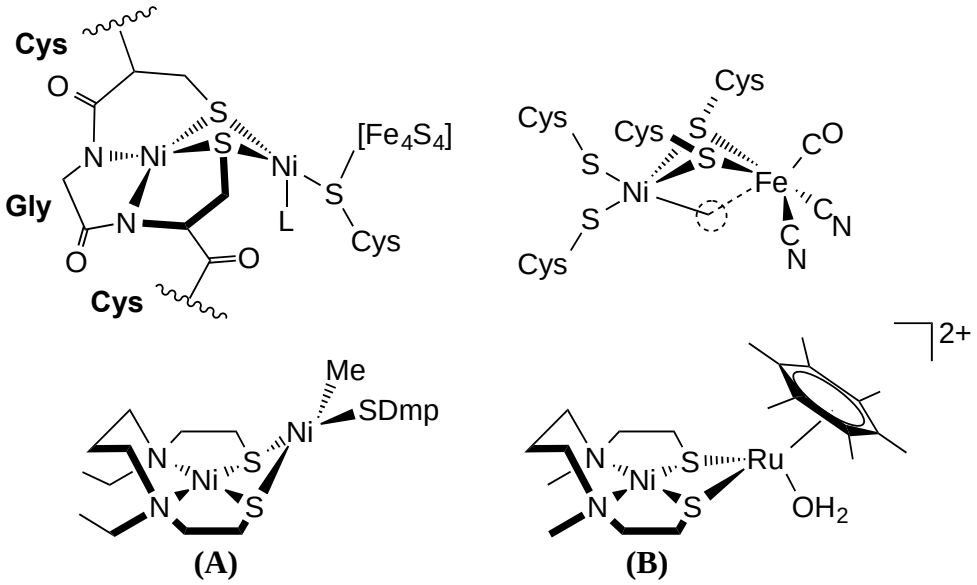

Figure III-1. Nickel Dithiolate metalloligands in Nature: active sites of acetyl CoA synthase (**A**)[33] and [NiFe]-hydrogenase (**B**),[56] with selected synthetic analogues below each.[57,58]

A selection of such complexes, based on the Ni(bme-daco) as ligand, is given in Figure III-2; the Ni(bme-dach) and $[Et_4N^+]_2[Ni(ema)]^{2-}$ have similar reactivity wheels, however a remarkably comprehensive series based on the 8-membered diazacycle has been more extensively explored. As bridging bidentate ligands to paddlewheel-type complexes, M—M distances may span from 2.14 Å (in $[(NiN_2S_2)_4Mo_2]^{4+}$ complexes where there is a formal Mo-Mo quadruple bond)[38] to over 4 Å in $[(NiN_2S_2)_3(CuBr)_2]$ where the copper(I) ions are exo to the S_3 planes and are not bonded.[44] As the S to S

distance in the $Ni(SR)_2$ metallodithiolate ligating units is relatively constant at 3.05 (± 0.05) Å, the ability of the ligand to adapt to the preferences of the metallo-axles of the paddlewheels is attributed to the non-directionality of the S-lone pairs, i.e., the cis dithiolate provides a soft donor bonding surface.[21,22,29,38,40,44] Classical bridging bidentate N-donor and P-donor ligands can be chosen to perform the same binding tasks as the metallated S-donors shown in Figure III-2, however to our knowledge *no one bidentate ligand has been demonstrated to cover such a range of binding capability as does the NiN_2S_2 metallo ligands*.

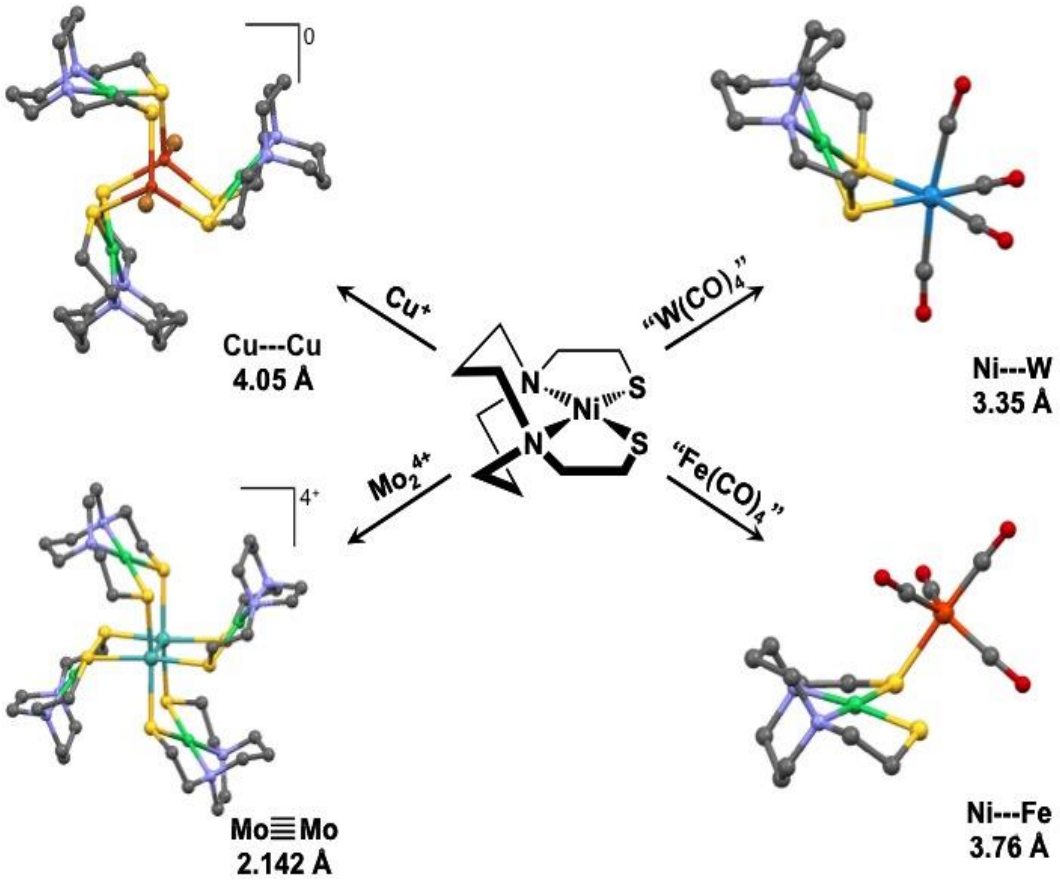

Figure III-2. Examples of Ni(bme-daco) as a mono- or bidentate metallodithiolate ligand.[29,38,44,59]

Phosphine and diphosphine ligands are known to bind gold(I) and facilitate aurophilic interactions described as fully or semi-supported (dependent on the chelating ligand bite angle), Figure III-3. Even in the absence of bridging bidentate ligands, linear R_3P-Au-X complexes may have (solid state) Au---Au distances in the range of 2.50 – 3.50 Å, taken as evidence for the existence of aurophilic interactions.[60-62] These are described as "unsupported" and are depicted in Figure III-3 as well. The [$(Ph_3P)_4Au_4$(μ-

$SCH_2Ph)_2$] complex reported by Fackler, *et al*., is an example of a mixture of semi-supported/unsupported interactions within a tetranuclear rhombic cluster.[63]

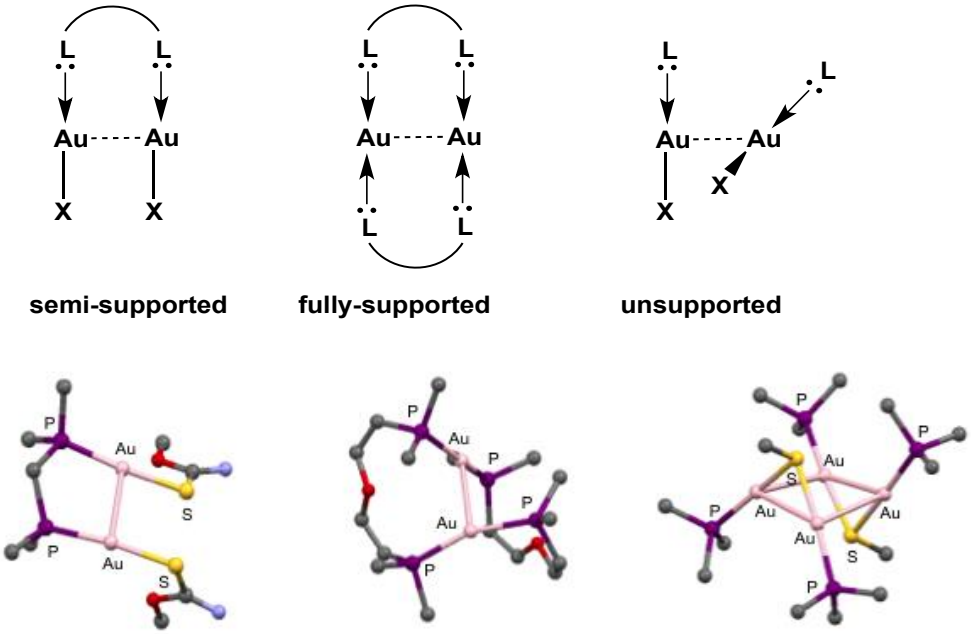

Figure III-3. Representations and examples of aurophilic interactions in the presence of bidentate bridging and mono-dentate ligands.[60-63]

Phosphine derivatives of Au(I) have received attention for treatment of rheumatoid arthritis in the form of auranofin, an FDA approved drug composed of linear two-coordinate gold(I) complexed with triethylphosphine and thiol-glucose ligands.[64] Advancements in antibody therapy have resulted in a shift away from gold-based therapies for arthritis,[65] however, auranofin and other gold(I) compounds have gained attention for their strong inhibition of tumor and cell growth.[66] Further, phosphine-gold(I) compounds are currently explored as both oxidation and C-C coupling catalyst

prospects.[67-69] Phosphine-gold(I) catalyzed cycloisomerization reactions of alkynes to cyclic products in excellent yields has been reported by Toste and coworkers.[67] Hence the study of fundamental structures and properties and the development of new ligands remains to be of consequence to gold(I) chemistry.

In view of the diversity of structural forms available to the NiN_2S_2 metallodithiolate ligand, the affinity of Au^+ for sulfur, and the structural influence of aurophilic interactions, we have explored products of Ph_3PAuCl as Au^+ synthon and the NiN_2S_2 complexes described above. Our results add to literature reports of cis-dithiolato nickel complexes as bidentate ligands to digold as has been found in a deprotonated, dianionic (NS) bidentate ligand, D-penicillaminate, in $[Ni^{II}(NS)_2]^{2-}$ and $[Ni^{II}(NS)_3]^{4-}$ complexes of gold(I). Linear S^---Au^+--S^- arrangements with fully-supported aurophilic interactions at 2.98 Å are found in the former, and 3.27 Å in the latter.[70] A simpler NS^- ligand, $^-SCH_2CH_2NH_2$, yields an analogous Ni_2Au_2 complex with linear S^---Au^+--S^- units and a Au---Au aurophilic distance of 3.00 Å.[71] More detailed comparisons will be given in the Results section below.

Experimental Details

General Procedures. The known complexes Ni(bme-daco), Ni(bme-dach), and $[Ni(ema)]^{2-}$ as its Et_4N^+ salt, were prepared according to published procedures.[15,21,22] Anhydrous CH_3CN and chlorotriphenylphosphine gold(I) were purchased from commercial vendors.

Synthesis of N,N'-bis(2-mercaptoethyl)-1,5-diazacyclooctane nickel(II)[{Ni(bme-daco)AuPPh$_3$}]$^+$(Cl$^-$). To a deep purple solution of Ni(bme-daco)

(0.059 g, 0.203 mmol) in MeCN (15 mL) was added dropwise a suspension of chlorotriphenylphosphine gold(I) (0.100 g, 0.202 mmol) in MeCN (20 mL) resulting in a light purple translucent solution upon stirring for 30 min. The solvent was removed in *vacuo* and the residue was washed with 30 mL of ether to remove impurities (0.062 g, 39% yield). X-ray quality purple crystals were obtained by layering a MeCN solution of the product with ether. Anal. Calc'd (found) $C_{28}H_{35}N_2AuClNiPS_2$ (MW = 786 g/mol): C, 42.80 (42.36); H, 4.49 (4.51); N, 3.56 (3.33). Absorption spectrum [MeCN; λ_{max}, nm (ε, M^{-1} cm^{-1})]: 506 (296), 409 (579), 246 (7476). $^{+}$ESI-MS (MeCN): *m/z* $[M\text{-}Cl^-]^+$ = 749 $[\{Ni(bme\text{-}daco)AuPPh_3\}]^+$ NMR data in CD_3OD $^{31}P\{^1H\}$ 40 (s) ppm.

$[Au_2\{Ni(bme\text{-}daco)\}_2]^{2+}(Cl^-)_2$, Complex 2. To a deep purple solution of Ni(bme-daco) (0.031 g, 0.11 mmol) in MeOH (15 mL) was added dropwise a suspension of Ph_3PAuCl (0.104 g, 0.210 mmol) in MeCN (20 mL) resulting in a magenta solution after 30 min. The solvent was removed *in vacuo* and washed with 30 mL of ether to remove impurities (0.049 g, 85% yield). X-ray quality purple crystals were obtained by layering a MeOH solution of the product with ether. Anal. Calc'd (found) $C_{20}H_{40}N_4Au_2Cl_2Ni_2S_4$ (MW = 1047 g/mol): C, 22.9 (22.6); H, 3.85 (3.79); N, 5.35 (5.09). Absorption spectrum [MeOH; λ_{max}, nm (ε, M^{-1} cm^{-1})]: 525 (172), 276 (14133), 267 (14090), 238 (38754). $^{+}$ESI-MS (MeOH): *m/z* $[M\text{-}2Cl^-]^{2+}$ = 488 $[Au_2\{Ni(bme\text{-}daco)\}_2]^{2+}$.

$[Au_2\{Ni(bme\text{-}dach)\}_2]^{2+}(Cl^-)_2$, Complex 3. In a manner similar to that described above, a suspension of Ph_3PAuCl (0.117 g, 0.237 mmol) in MeOH (20 mL) was added dropwise to a brown suspension of Ni(bme-dach) (0.033 g, 0.12 mmol) in

MeOH (20 mL) resulting in a transparent orange solution. After stirring for 30 min, solvent was reduced in vacuo to 10 mL and a light orange solid was obtained after addition of diethyl ether (0.055 g, 90% yield). X-ray quality crystals were obtained by layering a MeOH solution of the product with ether. Anal. Calc'd (found) $C_{18}H_{36}N_4Au_2Cl_2Ni_2S_4$ (MW = 1019 g/mol): C, 21.2 (21.7); H, 3.56 (3.88); N, 5.50 (4.89). UV-vis: [MeOH; λ_{max}, nm (ε, M^{-1} cm^{-1})]: 455 (335), 267 (11735), 238 (10476). $^{+}$ESI-MS (MeOH): *m/z* $[M\text{-}2Cl^-]^{2+}$ = 473 $[Au_2\{Ni(bme\text{-}dach)\}_2]^{2+}$.

$(NEt_4^+)_2[Au_2\{Ni(ema)\}_2]^{2-}$ and $[\{Ni(ema)\}_2Au_4(PPh_3)_4]$, Complexes 4 and 5. A suspension of Ph_3PAuCl (0.100 g, 0.202 mmol) in MeCN (20 mL) was added dropwise to a reddish-brown solution of $(NEt_4^+)_2[Ni(ema)]^{2-}$ (0.053 g, 0.10 mmol) in MeCN (20 mL) with immediate dissolution to a transparent bright orange-red solution. After stirring for 10 min, the solvent was reduced in vacuo to 10 mL and an orange solid was obtained upon addition of diethyl ether (0.041 g, 69% yield). X-ray quality crystals for complex **4** were obtained by layering a MeCN solution of the product with ether at -20 °C. Crystalline complex **5** was obtained from slow evaporation of a MeCN solution of the product at 22 °C. Anal. Calc'd (found) $C_{28}H_{56}N_6Au_2Ni_2O_4S_4$ (MW = 1180 g/mol): C, 28.5 (28.2); H, 4.78 (5.65); N, 7.12 (6.46). Absorption spectrum [CH_2Cl_2]; λ_{max}, nm (ε, M^{-1} cm^{-1})]: 528 (273), 428 (876), 246 (1638). $^{-}$ESI-MS (MeCN): *m/z* $[M+H]^-$ = 919 $[Au_2\{Ni(ema)\}_2]^{2-}$ For $C_{84}H_{76}N_4Au_4Ni_2P_4O_4S_4$, Anal. Calcd (found) (MW = 2363 g/mol): C, 42.70 (41.43); H, 3.24 (3.41), N, 2.37 (2.36). ESI-MS (CD_2Cl_2): *m/z* = 2363 $[\{Ni(ema)\}_2Au_4(PPh_3)_4]$ NMR data in CD_2Cl_2 $^{31}P\{^1H\}$ 36 (s) ppm.

Synthesis and Structural Characterization

Synthesis and isolation of complexes 1 – 5. Scheme III-1 shows the three NiN_2S_2 metallo ligands used in this study and summarizes the synthesis of the five new Ni-Au complexes. Two product compositions, dependent on solvent, resulted from mixing stoichiometric amounts of Ni(bme-daco) and Ph_3PAuCl. The simple1:1 $[NiN_2S_2\text{-}AuPPh_3]^+$ adduct, **1**, retaining the PPh_3 ligand on gold, was obtained from MeCN at 22 °C and isolated as its chloride salt; with MeOH as solvent, the two NiN_2S_2 metallo ligands assembled about a digold unit, producing light purple crystals of **2** on layering with Et_2O. A better yield of the latter was obtained on use of an excess of Ph_3PAuCl.

While both Ni(bme-dach) and Ph_3PAuCl are poorly soluble in MeOH, heterogeneous mixtures at 22 °C immediately resulted in dissolution and a transparent orange solution from which bright orange crystals of **3** were obtained. The Et_4N^+ salt of $Ni(ema)^{2-}$ was dissolved in CH_3CN prior to addition of Ph_3PAuCl, resulting in a color change from the deep maroon of the dianionic nickel complex to a fully transparent, red-orange solution of product **4**, isolated as its Et_4N^+ salt. Complex **5** was obtained from the same reaction mixture as complex **4**, but under different crystallization conditions: complex **4** was isolated from layering MeCN solution with ether at -20 °C, complex **5** resulted from slow (over days in open container) evaporation of MeCN solution at room temperature affording ruby red crystals. Elemental analysis and mass spectrometry of the isolated compounds indicated the absence of PPh_3 in complexes **2**, **3,** and **4**, however

complex **5** contained two $AuPPh_3$ per NiN_2S_2 unit, and hence will be described below as an analogue of complex **1**.

Scheme III-1. The NiN_2S_2 ligands of this study and their NiN_2S_2-Au complexes.

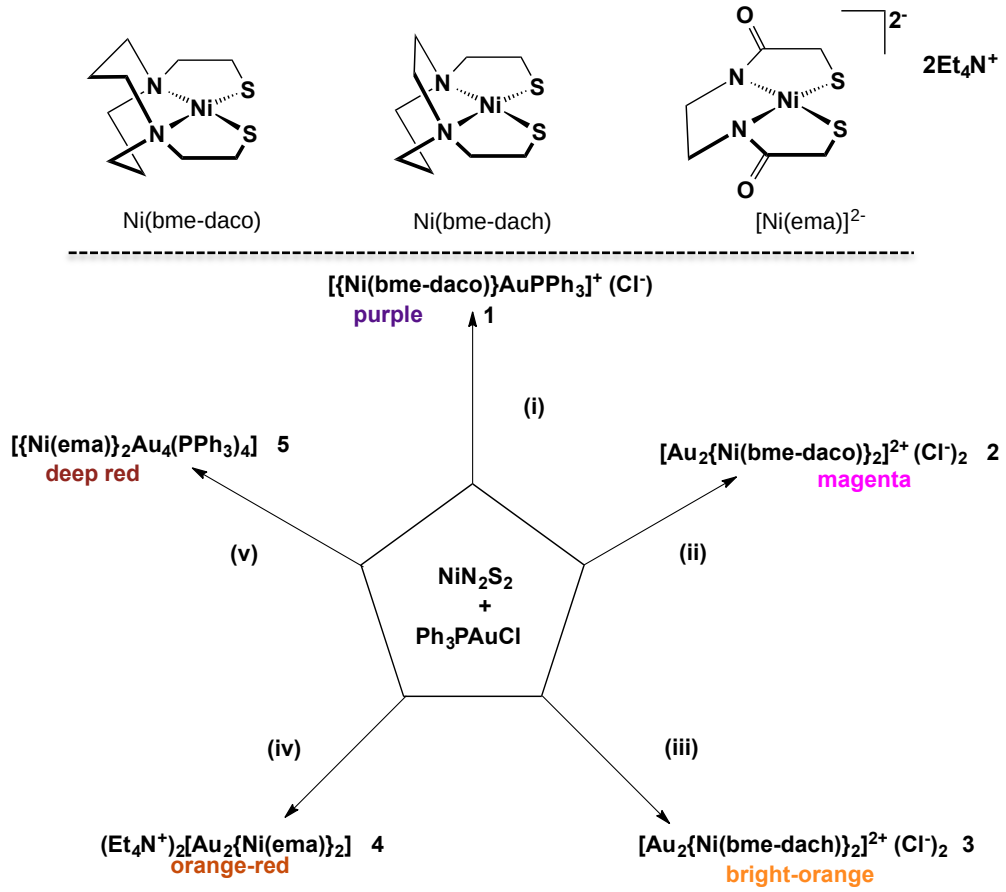

(i) MeCN, RT (NiN_2S_2:Ph_3PAuCl), 1:1
(ii) MeOH, RT (NiN_2S_2:Ph_3PAuCl), 1:2
(iii) MeOH, RT (NiN_2S_2:Ph_3PAuCl), 1:2
(iv) MeCN, RT (NiN_2S_2:Ph_3PAuCl), 1:2
(v) MeCN, RT (NiN_2S_2:Ph_3PAuCl), 1:2

All complexes of this study are stable in air, both in solid and solution states. Complexes **1** – **5** are water soluble, presumably because of exposed hydrophilic centers RS^- and Au^+, however they vary in their solubility properties in organic solvents.

Molecular structures. The molecular structures of complexes **1 – 5** were characterized by X-ray diffraction analysis and are displayed as thermal ellipsoid plots in Figures III 4 – 6. Salient metric parameters are listed in Table III-1, and full listings are in the Appendix. The nickel(II) ion within the N_2S_2 donor sites maintains rigorous square planar coordination geometry in all. Complex **1** represents the expected first step in formation of the larger clusters in that a single thiolate sulfur has been aurolated with a $AuPPh_3^+$ unit, giving rise to a ∠Ni-S-Au = 81.56°, and a largely linear geometry about the gold(I), ∠S-Au-P = 176.2°. Notably, the metric data that define the free Ni(bme-daco) ligand show no significant differences to that of complex **1** with the exception of a slight elongation of the Ni-S bond bearing the $AuPPh_3^+$ unit. An analogous structure involving an I_2 – thiolate sulfur adduct of Ni(bme-daco)*, (bme-daco* = N,N'-bis(2-mercapto-methyl-propane)-1,5-diazacyclooctane) is known where the Ni-S-I angle is 101.02°.[72]

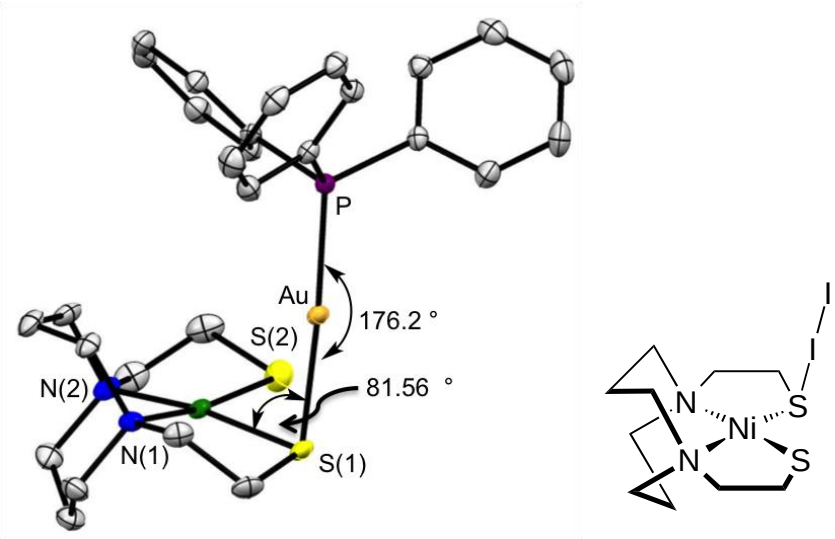

Figure III-4. Thermal ellipsoid plots drawn at 50% probability level of the complex **1** cation. Hydrogen atoms, the Cl^- counterion, and the H_2O of crystallization are not shown. Inset is the Ni(bme-daco)•I_2 analogue.[72]

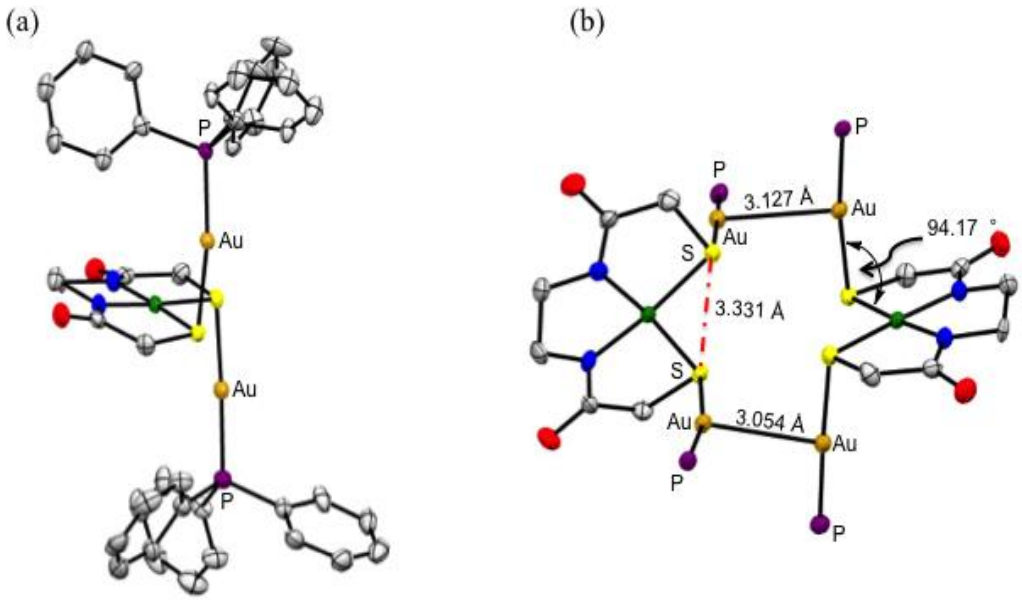

Figure III-5. Thermal ellipsoid plots drawn at 50% probability level of complex **5** with selected metric data. (a) One [Ni(ema)$Au_2(PPh_3)_2$] unit of complex **5**; (b) The dimeric assembly with Ph rings and hydrogens omitted, as are solvent molecules of crystallization.

Neutral complex **5**, originating from the dianionic $[Ni(ema)]^{2-}$ as metallodithiolate ligand, has both thiolate sulfurs engaged in binding to $AuPPh_3^+$ units, arranged in an anti-configuration with respect to the N_2S_2Ni plane (Figure III-5a). Whereas there are no intermolecular contacts between the cationic complex **1** units that would suggest unsupported gold-gold interactions, the neutral complex **5** crystallizes as a dimer in which one NiN_2S_2 plane is roughly oriented perpendicular to the other, (Figure III-5b); in fact the dihedral angle taken from the intersection of the lines normal to the best N_2S_2 planes is 76°. This arrangement, which minimizes steric repulsions from the large PPh_3 ligands also finds unsupported aurophilic interactions at 3.054 and 3.127 Å.

In complexes **2**, **3,** and **4** both the chloride and the PPh_3 ligands of the gold precursors have been displaced by thiolate sulfurs from the metallodithiolate ligand, leading to digold units attached to cis-dithiolate sulfurs and arranged in the stair-step type structure shown in Figure III-6. Despite the charge difference of the complexes derived from the neutral NiN_2S_2 ligands in **2** and **3** vs. the dianionic $[Et_4N^+]_2[Ni(ema)]^{2-}$ ligand of **4**, the Ni_2Au_2 structures are largely identical. The Au-Au distances are well within aurophilic interactions at 3.13 Å for **2**, 3.11 Å for **3,** and 3.12 Å for **4**, and the S to S distances are 3.05 Å for **2,** 3.22 Å for **3,** and 3.30 Å for **4**. The dihedral angles between the NiN_2S_2 planes (the tread of the step) and the $S_2Au_2S_2$ plane (the riser) vary by only 5° (from 94 to 99°); Figure III-7 illustrates this. The height of the riser in the three complexes averages to 4.6 Å, and the depth of the tread is 2.9 Å. Konno et al., report a similar stair-step complex composed of a non-contiguous N_2S_2 complex of

nickel $\{[Ni(NS)_2]_2(Au^+)_2\}^{2+}$, NS = $^-SCH_2CH_2NH_2$.[71] The metric parameters are remarkably similar to complexes **2 – 4**, including a $Au^+ \bullet\bullet\bullet Au^+$ separation of 3.00 Å and S to S distances averaging to 3.13 Å. The stair-step is slanted (plane-rise-plane angle ~ 107°) somewhat similar to the Figure III-7 structures. For comparison, the analogous stair-step structures of the nickel trimetallics, $[(NiN_2S_2)_2Ni]^{2+}$ and $[(NiN_2S_2)_2Ni]^{2-}$ find the S_2NiS_2 plane that makes up the "riser" to have a S to S span distance of 3.3 Å, and the step angles are larger, in the range of 107 to 122°, prompting a more appropriate description of "slant chair" rather than "stair-step".[26,40,73]

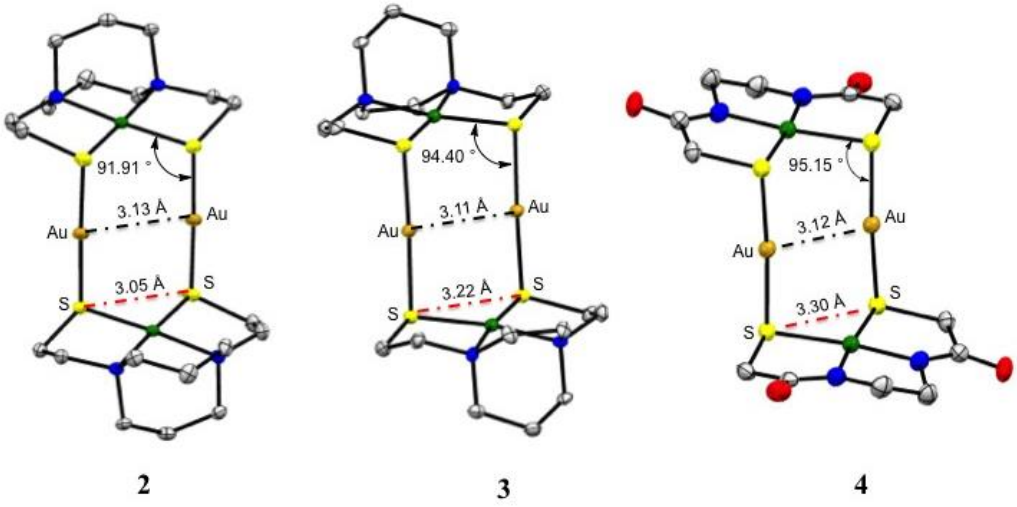

Figure III-6. Thermal ellipsoid plots drawn at 50% probability level of complexes **2, 3** and **4** with selected metric data. Hydrogen atoms have been removed for clarity. The Cl^- counterion for **2** and **3** and Et_4N^+ counterion for **4** are not shown.

This stair-step structure of the digold derivatives is related to the di-metal paddlewheel complexes such as $[(NiN_2S_2)_4Pd_2]^{4+}$ and the $[(NiN_2S_2)_4Mo_2]^{4+}$ shown in

Figure III-2 by the removal of two paddles. The Pd—Pd distance is 3.13Å, and the dihedral planes made by the NiN_2S_2 paddles and the $S_2Pd_2S_2$ planes is 132°, notably larger than the digold structures and rationalized by the added steric hindrance from four paddles.[38,40] The bite angle, ∠S-Ni-S and the S to S distances, for complexes **1 – 5**, show no major differences compared to that of the NiN_2S_2 ligand precursors, demonstrating optimal binding to the Au^+ center(s).

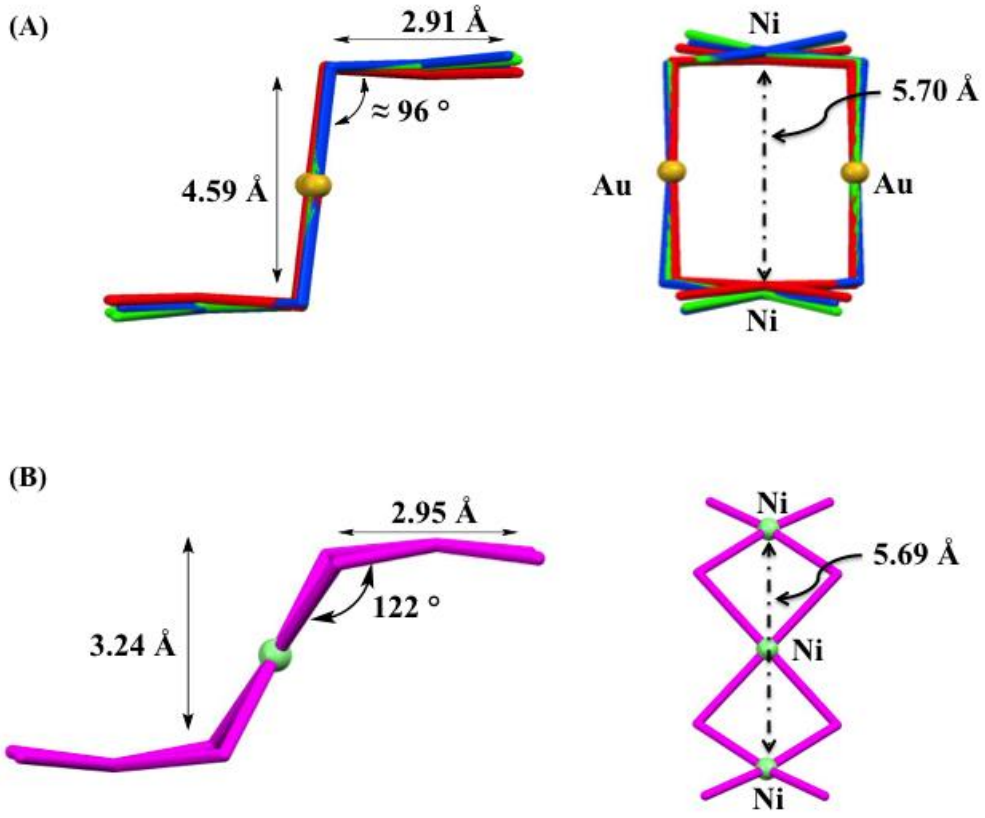

Figure III-7. (A) Overlay of complexes **2 – 4** in "stair-step" configurations (red – **2**, green – **3**, blue – **4**). (B) "Slant chair" configuration of $[(Ni(bme\text{-}dach)_2Ni]^{2+}$.[40]

Table III-1. Metric Data for Complexes **1** – **5** (Distance, Å; Angle, deg).

	1	**2**	**3**	**4**	**5**
Ni – S	2.171(8)	2.180(9)	2.180(1)	2.185(1)	2.189(2)
	2.185(7)[a]	2.192(9)	2.185(2)	2.199(1)	2.203(2)
Au – S	2.333(7)	2.300(9)	2.300(1)	2.293(1)	2.339(2)
S – S	3.055(7)	3.050(9)	3.215(2)	3.302(1)	$3.336(2)_{avg}$
Au – Au	-	3.13(5)	3.11(4)	3.12(6)	3.09(6)
∠Au-S-Ni	81.56(2)	91.93(3)	93.12(5)	95.13(4)	79.41(6)
					94.19(7)
∠S-Ni-S	89.05(3)	88.47(3)	94.90(5)	97.70(4)	98.67(7)

a) Ni – S distance corresponding to the sulfur which is also bonded to the gold

Electronic Absorption Spectra

The UV-Vis absorption spectra for complexes **1 – 4** exhibit d-d transitions in the range of 400 – 600 nm, typical of square planar nickel(II) complexes. LMCT transitions for nickel complexes with RS^- ligands show an intense absorbance in the region of 250 – 350 nm assigned to $RS^- \rightarrow Ni^{II}$ charge transfer transitions.[74] Analysis of the electronic absorption spectra for complexes **1 – 4** showed no significant differences from the NiN_2S_2 precursors.[15,21,22]

Electrochemistry

The solution electrochemistry of the aurolated NiN_2S_2 complexes readily fits into the results from analogous studies of S-metallated and S-alkylated NiN_2S_2.[26,75] Reduction events assignable to the $Ni^{II/I}$ couple of the NiN_2S_2 unit within the

polymetallics become more accessible relative to the free or unbound NiN_2S_2 as electron density from thiolate S is engaged by the interacting electrophile. Multiple events correspond to the number of NiN_2S_2 units in the S-metallated $[NiN_2S_2]_xM_y$ clusters, and the separation between those events arguably reflects the degree of coupling mediated by the connecting metals. Table III-2 lists electrochemical parameters of complexes **1 – 3** of this study, along with those of a selection of alkylated NiN_2S_2 complexes for comparison.

The reversible cathodic event, assigned to $Ni^{II/I}$ reduction, at $E_{1/2}$ = -2.34 V for both Ni(bme-dach) and Ni(bme-daco) in acetonitrile solution, is moved beyond the solvent window for the dianionic $Ni(ema)^{2-}$. The reduction potential of Ni(bme-daco) is shifted positively by ca. 700 mV for successive S-methylations and the buildup of positive charge on the resulting thioether complexes. Metallation by Ni^{II}, generating the $[NiN_2S_2]_2Ni^{2+}$ trimetallic, also finds the first $Ni^{II/I}$ reduction wave for the trimetallic at a quite positive value of -1.11 V (ref to Fc/Fc^+).

Complex **1** shows complexities in its cyclic voltammogram relating to the presence of further aggregates, however the most prominent event in freshly prepared solutions was a quasi-reversible wave centered at -1.10 V. This value is consistent with the $Ni^{II/I}$ reduction of the di-methylated, di-cationic, $Ni(bme\text{-}daco)Me_2^{2+}$ species which is seen at -1.11 V.[26] That the complexities are related to the larger aggregates is confirmed by monitoring the degradation of solutions and by studies of complexes **2** and **3**.

Figure III-8 displays the cyclic voltammogram (CV) cathodic region results for complex **3**, showing two $Ni^{II/I}$ events as expected. Scan reversal at various potentials verified the reversibility of the more positive event, while the more negative is quasi-reversible. That there are only two reductions, separated by ca. 200 – 210 mV, is confirmed by the square wave voltammogram results, also shown in Figure III-8 for complex **3**. The cyclic voltammograms of complexes **2** and **3** are very similar; electrochemical parameters are compared with appropriate analogues in Table III-2. The more positive $Ni^{II/I}$ event is shifted over 700 mV from the respective parent Ni(bme-daco) or Ni(bme-dach) complexes.[26]

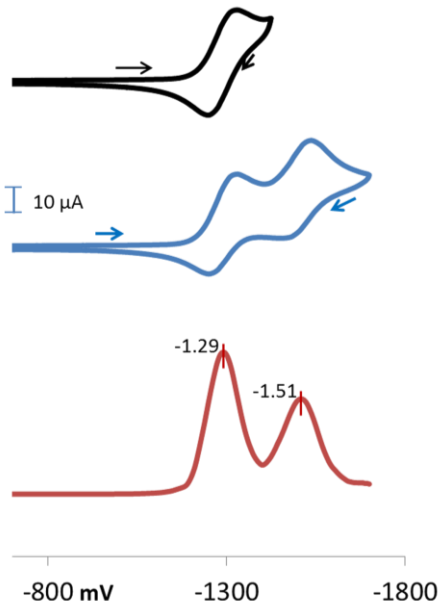

Figure III-8. Cyclic voltammograms (with scan reversals to isolate successive waves) of 2 mM solutions of complex **3** in 0.1 mM $(n\text{-}Bu)_4N^+PF_6^-/CH_3CN$ with a glassy carbon working electrode at 150 mV/s scan rate. Scans of the squarewave voltammograms are initiated in the negative direction; square-wave voltammogram amplitude = 25 mV; frequency = 15 Hz; *E*step = 4 mV.

The dianionic complex **4** shows no cathodic event within the solvent window. A largely irreversible anodic wave of E_a(max) = ca. +0.7 V could be sulfur or gold(I) based, according to literature reports.[76]

The difference between the most accessible NiN_2S_2 reduction and each subsequent NiN_2S_2 reduction redox event in these cluster complexes is directly related to electronic coupling between the metallic units: a large separation in the case of strongly coupled and electronically delocalized species and small in the case of weakly coupled and localized species. Factors influencing such coupling include distance between the redox centers, geometric optimization of the overlapping molecular orbitals, and the nature of connecting units. In the case of complex **3**, the difference of 210 mV between the first and second events is small in comparison to that of 900 mV seen in the more strongly coupled $[NiN_2S_2]_2Ni^{2+}$ complex in Table III-2. The distances involved range from 5.6 to 5.8 Å between the nickel centers in the cationic Ni_2Au_2 complexes as compared to the analogous $\underline{Ni}N_2S_2$ to $\underline{Ni}N_2S_2$ distance of 5.370 Å in the case of the $[Ni(bme\text{-}daco)]_2Ni^{2+}$ complex. As the difference is not great, perhaps the explanation for the smaller coupling in **2** and **3** is the poor overlap between the 5d orbitals of the gold with the 3p orbitals of the sulfur.

Table III-2. Listing of cyclic voltammetry parameters.[a]

Compound	$E_{1/2}$ $Ni^{II/I}$ [V]	E_{pc1} [V]	E_{pc2} [V]	$\Delta E_{cat(max)}$[b] [V]
Ni(bme-daco)	-2.34[31]			
Ni(bme-dach)	-2.34[9]			
Ni(bme-daco)Me^+	-1.60[31]			
Ni(bme-daco)Me_2^{2+}	-1.08[31]			
[Ni(bme-daco)]$_2Ni^{2+}$	-1.11[34]	-1.14	-2.04	0.91
[Ni(bme-daco)]$_2Au_2^{2+}$, **2**	-1.36	-1.41	-1.61	0.20
[Ni(bme-dach)]$_2Au_2^{2+}$, **3**	-1.38	-1.42	-1.63	0.21

[a]All measurements were done in MeCN solution, 0.1 M $(n\text{-}Bu)_4N^+PF_6^-$ electrolyte, measured vs $Ag/AgNO_3$ reference electrode, with a concentration from 1.0-2.5 mM in analyte. All potentials are referenced to Cp_2Fe/Cp_2Fe^+ = 0 mV as internal standard. [b]Separation of cathodic peaks taken as difference between the maxima of the cathodic waves.

Summary and Conclusions

The S- - -S distances in the cis-dithiolates of both anionic $NiN_2S_2^{2-}$ and neutral NiN_2S_2 complexes (3.28Å for $Ni(ema)^{2-}$; 3.04Å for Ni(bme-daco); and 3.20 for Ni(bme-dach)) make them ideal candidates for bridging bidentate ligands to Au^I- -Au^I units, at 3.11 -3.12 Å, i.e., with aurophilic interactions, shown in the unsupported complex **5** to be 3.09 Å. Hence the self-assembly of stair-step structures occurs for both forms of nickel dithiolate metallo ligands, using the planar NiN_2S_2 configurations as treads with connections through the digold unit through bridging thiolate sulfurs at interplane angles of ca. 90°. Demonstrating the similarity between phosphine P-donor ligands and the S-donors from nickel ditholates, the self-assembly process can be controlled by reaction conditions, resulting in complexes **1** and **5** that retain PPh_3 attached to gold.

The digold stair-step complexes are robust, water soluble, and oxygen insensitive. Electrochemical measurements find less communication between nickels in the N_2S_2 planes connected by $[Au_2]^{2+}$ units than in related complexes that have a Ni^{2+} ion in a bridging position, i.e., $[NiN_2S_2]_2Ni^{2+}$. Whether these attractive complexes have potential as gold catalysts, or as metallo pharmaceuticals, remains to be explored.

CHAPTER IV

METALLODITHIOLATES AS LIGANDS TO DINITROSYL IRON COMPLEXES: TOWARDS THE UNDERSTANDING OF STRUCTURES, EQUILBRIA, AND SPIN COUPLING

Introduction

An extensive class of homo- and heterobimetallic complexes has been developed through a bridging thiolate approach, M-(μ-SR)-M'.[77-79] The active sites of naturally occuring metalloenzymes such as the dinuclear [NiFe]- and [FeFe]- H_2ase also display metal thiolate bridges.[56,80] More appropriate to our study, is the Ni(Cys-Gly-Cys) motif which serves as a metallodithiolate ligand to the catalytically active nickel in the acetyl CoA synthase (ACS) active site, structure A, Figure IV-1.[33]

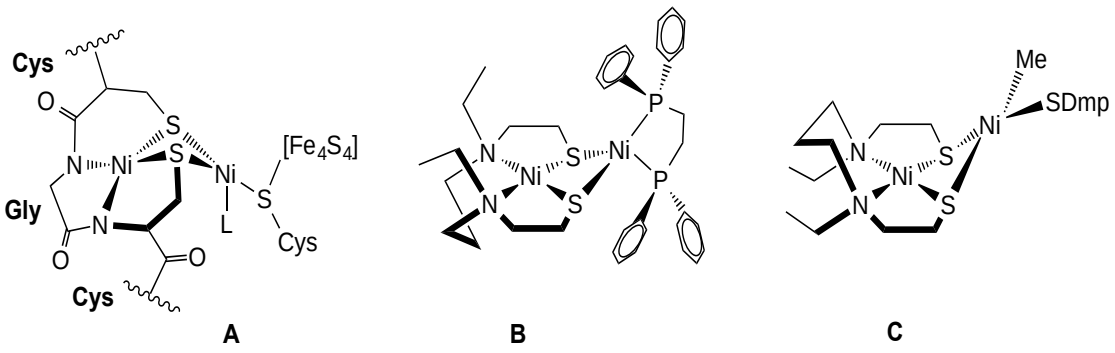

Figure IV-1. Representation of the A-Cluster in acetyl CoA synthase ($Ni_{d,p}$ = distal and proximal to 4Fe4S cluster),[33] and synthetic models, B[81] and C.[57]

The distal nickel, Ni_d, within the A-Cluster of acetyl CoA synthase, is in a square planar geometry, that serves as a suitable ligand required of the proximal nickel, Ni_p, for facilitation of the C-C and C-S coupling processes in the formation of acetyl CoA.[82,83] It is expected that such contiguous N_2S_2 binding sites are widespread in bioinorganic chemistry and as such has inspired extensive studies that have characterized other aspects of S-based chemistry including oxygenation, and alkylation.[26,84] In the past twenty years, *cis*-dithiolatonickel compounds as metalloligands have been used to mimic the structural and redox properties of acetyl CoA synthase, Figure IV-1, B and C.[35,85,86] Such metallodithiolates as ligands have been used to design other biomimetics including [NiFe]-H_2ase active site synthetic analogues.[58]

Attempts have been made to codify the electron donation properties of NiN_2S_2 as metallodithiolate ligands according to ν(CO) stretching frequencies in $W(CO)_{4,5}$ adducts, Figure IV-2, A.[29] While stable complexes are formed, as stability is a requirement of any analytical standard, the $W(CO)_4$ platform is attractive. However there is little discrimination between the various neutral NiN_2S_2 complexes, and another reference moiety was sought. For this and other reasons, vide infra, the $Fe(NO)_2$ unit has been explored. The dinitrosyliron unit, $Fe(NO)_2$, another transition metal acceptor fragment, has also been shown to bind to dithiolato-metalloligands; examples are given in Figure IV-2, C and D.[85,87] Complex C was prepared by Pohl *et al.*, as a structural analogue to the [NiFe]-H_2ase active site by replacing the $Fe(CO)(CN)_2$ unit with $Fe(NO)_2$.[85]

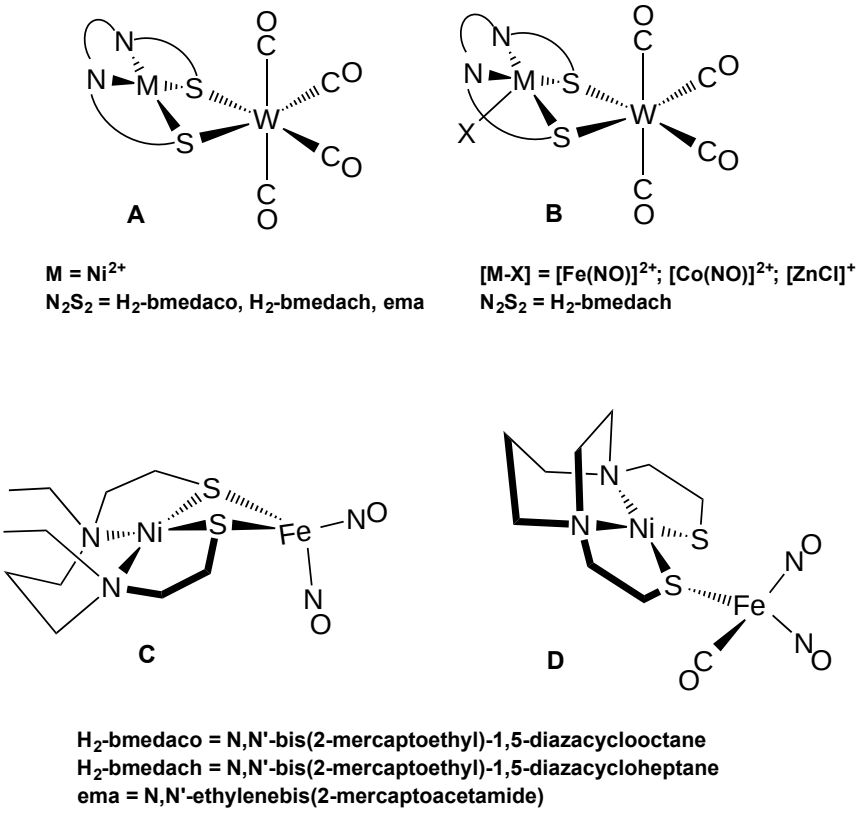

Figure IV-2. Structures of $MN_2S_2W(CO)_4$, $NiN_2S_2Fe(NO)_2$, and synthetic models of acetyl CoA synthase and [NiFe]-hydrogenase.[29,35,85-87]

The bimetallic molecules represented by Figure IV-2 B, include penta-coordinate metallodithiolate ligands in which the fifth donor site of the MN_2S_2 is NO or X^-. In this regard, the $[Fe(NO)(N_2S_2)]$, $[Co(NO)(N_2S_2)]$, and $[ZnCl(N_2S_2)]^+$ act as bidentate ligands to the tungsten carbonyl synthon.[35,86] Other penta-coordinate N_2S_2 complexes include metal oxo centers such as $[V{\equiv}O]^{2+}$,[13] $[Re{=}O]^{3+}$,[88] and $[Tc{=}O]^{3+}$.[89]

Dinitrosyliron complexes (DNICs) are found in biology and are presumed to play a major role in the storage and transport of NO in cells.[90,91] DNICs exist in two redox levels, which can be represented via the Enemark-Feltham notation.[92] The oxidized

form, $\{Fe(NO)_2\}^9$ with a distinctive EPR signal at g = 2.03, and the EPR silent, reduced form, $\{Fe(NO)_2\}^{10}$.[93,94] Synthetic models of the physiological DNIC complexes have engaged thiols and imidazoles as mimics of the biologically relevant cysteine and histidine amino acids, respectively.[95,96] We suggest that the $Fe(NO)_2$ unit serves as an additional tool for reporting donor properties of metallodithiolates. Not only are the two redox levels stabilized by different ancillary ligands in $L_2Fe(NO)_2$, $[X_2Fe(NO)_2]^-$, and $(L)(X)Fe(NO)_2$ complexes, but within each redox level, the ν(NO) values respond to supporting ligands.[97-99] While most $\{Fe(NO)_2\}^9$ derivatives are in anionic complexes, $[X_2Fe(NO)_2]^-$, the N-heterocyclic carbene ligand stabilizes a rare example of a neutral species, $(IMes)(SPh)Fe(NO)_2$.[100] The rareness of such species is due to the tendency of the $XFe(NO)_2$ moiety to dimerize into very stable $[(\mu\text{-}X)Fe(NO)_2]_2$, known in the case of $X = SR^-$, as Roussin's red "esters".

Both NiN_2S_2 and $Fe(NO)N_2S_2$ form S-bridged iron dinitrosyl complexes, for example, [Ni(bme-dach)•$Fe(NO)_2$CO],[87] and [Fe(NO)bme-dach•$Fe(NO)_2$]$^+$.[100] These metallodithiolates bind to the $Fe(NO)_2$ unit in a monodentate or bidentate manner. Substitution of a spectroscopically silent metal ion by the paramagnetic, EPR active $[V{\equiv}O]^{2+}$ ion may be used for characterization of reaction intermediates and verification of biological metal binding sites. Square pyramidal $(V{\equiv}O)N_2S_2$ complexes have been prepared with dianionic and tetraanionic ligands and show characteristic electron paramagnetic resonance signals indicative of the unpaired electron coupling to the ^{51}V metal center of nuclear spin 7/2.[13] Sulfur-based reactivity of the $(V{\equiv}O)N_2S_2$ thiolates with electrophiles such as 1,3-dibromopropane and methyl iodide occurs only when the

overall complex is dianionic $[(V{\equiv}O)N_2S_2]^{2-}$ i.e., N_2S_2 is the tetraanionic ema ligand, ema = N,N'-ethylenebis(2-mercaptoacetamide).

Herein, we report the reactions of a dianionic $[(V{\equiv}O)N_2S_2]^{2-}$ complex with the metallo acceptor $W(CO)_4$ and heterometallic cleavage products of $(\mu\text{-}I)_2[Fe(NO)_2]_2$ by an N-heterocyclic carbene, NiN_2S_2, and $(V{\equiv}O)N_2S_2$ metalloligands. The $Fe(NO)_2^+$ synthon, $(\mu\text{-}I)_2[Fe(NO)_2]_2$, is prepared by oxidation of $Fe(CO)_2(NO)_2$ with elemental iodine.[101]

Experimental Details

General Procedures. The known complexes $Fe(CO)_2(NO)_2$, V≡O(bme-daco), Ni(bme-daco), $[V{\equiv}O(ema)]^{2-}$, N,N'-ethylenebis(2-mercaptoacetamide) ligand, ema, and *cis*-$W(CO)_4(pip)_2$ (pip = piperidine) were prepared according to published procedures.[102] The IMes-NHC ligand (1,3-bis(2,4,6-trimethylphenyl)imidazol-2-ylidene) was prepared *in situ* by reaction of 1,3-Bis(2,4,6-trimethylphenyl)imidazolidinium chloride with NaOtBu in equivalent stoichiometric amounts. Throughout this chapter, the IMes-NHC ligand will be represented as IMes. The $\{Fe(NO)_2\}^9$ source for complexes **2**, **3**, and **4** was obtained by iodine oxidation of $Fe(CO)_2(NO)_2$, yielding $(\mu\text{-}I)_2[Fe(NO)_2]_2$, isolated as a black, air-sensitive solid, and identified by ν(NO) IR stretching frequencies. The following materials were reagent-grade and used as purchased from Sigma-Aldrich: sodium *tert*-butoxide, 1,3-Bis(2,4,6-trimethylphenyl)imidazolidinium chloride, nitrosyl tetrafluoroborate, and anhydrous dimethyl formamide.

Preparation of Compounds. **$[Et_4N]_2[V{\equiv}O(ema)W(CO)_4]$, Complex 1;** ema = N,N'-ethylenebis(2-mercaptoacetamide). A 0.026 g (0.056 mmol) sample of $(pip)_2W(CO)_4$

was dissolved in 15 mL of DMF and heated at 40 °C for 20 min. The $[Et_4N^+]_2[V{\equiv}O(ema)]^{2-}$ (0.029 g, 0.055 mmol) complex, dissolved in DMF, was added dropwise to this solution and heating continued for an additional 30 min producing a deep amber color. A tan-brown solid was obtained after precipitation with diethyl ether. X-ray quality crystals were grown by diffusion of ether into a DMF solution of the product. Isolation of the crystals afforded 0.021 g (46%) of product. IR (DMF, cm^{-1}) *ν*(CO) 1996(w), 1919(w), 1872(s), 1848(m), 1802(m). Anal. Calcd (found) $C_{26}H_{48}N_4O_7S_2VW$: C, 37.73 (33.11); H, 5.85 (6.18); N, 6.77 (6.25).

(IMes)Fe(NO)$_2$I, Complex 2. A 0.150 g (0.4 mmol) sample of 1,3-Bis(2,4,6-trimethylphenyl)imidazolidinium chloride and 0.043 g (0.4 mmol) of NaOtBu were dissolved in 20 mL of THF and stirred for 30 min prior to transfer to a Schlenk flask containing 1.0 mmol of $(\mu\text{-}I)_2[Fe(NO)_2]_2$ dissolved in 10 mL THF. Stirring for 30 min resulted in a deep greenish-brown solution, which was filtered through Celite. Diethyl ether (10 mL) was added resulting in a dark brown precipitate; the supernatant was removed from the solid via a football cannula. The precipitate was dried in vacuo and redissolved in a minimal amount of THF, transferred to degassed test tubes, and layered with ether to produce X-ray quality crystals. Isolation of the crystals afforded 0.15 g (70%) of product. IR (THF, cm^{-1}) *ν*(NO) 1782(s), 1726 (vs). Anal. Calcd (found) $C_{21}H_{24}FeIN_4O_2$: C, 46.1 (45.9); H, 4.42 (4.48); N, 10.24 (10.00).

[Ni(bme-daco)•(Fe(NO)$_2$I)$_2$] and [V≡O(bme-daco)•Fe(NO)$_2$I], Complexes 3 and 4. Complexes **3** and **4** were prepared similarly to **2** by addition of *ca.* (0.3-0.4 mmol) of the metalloligand, Ni(bme-daco) or V≡O(bme-daco), dissolved in 20 mL of THF to a

Schlenk flask containing 1.0 mmol of the $(\mu\text{-I})_2[Fe(NO)_2]_2$ in 10 mL of THF. Stirring for 30 min resulted in a black (the Ni derivative) or deep green (the V≡O derivative) solution, which was then filtered through Celite. Diethyl ether (10 mL) was added resulting in black and deep green precipitates, respectively; the supernatant was removed from the solid via a football cannula. The precipitate was dried and redissolved in THF. The solutions were concentrated in vacuo, transferred to degassed test tubes, and layered with ether to produce X-ray quality crystals. Isolation of the crystals afforded from 0.075 to 0.17 g (45-50%) of product. The IR spectrum of [Ni(bme-daco)•$(Fe(NO)_2I)_2$], (THF, cm^{-1}) ν(NO) 1793(s), 1731 (vs). Anal. Calcd (found) $C_{10}H_{20}Fe_2I_2N_6NiO_4S_2$: C, 15.5 (15.4); H, 2.60 (2.45); N, 10.8 (10.5). For [V≡O(bme-daco)•$Fe(NO)_2I$], (THF, cm^{-1}) ν(NO) 1796(s), 1733 (vs). Anal. Calcd (found) $C_{10}H_{20}FeIN_4O_3S_2V$: C, 22.2 (22.0); H, 3.72 (3.60); N, 10.3 (10.2).

Synthesis, Isolation, and Physical Properties

The preparation of a series of MN_2S_2 derivatives of tungsten carbonyls has permitted conclusions regarding their electron donating ability based on ν(CO) frequencies as compared to classical phosphine and amine ligands.[29] Whereas the neutral $(V\equiv O)N_2S_2$ complexes displayed no reactivity to cis-$(pip)_2W(CO)_4$, the dianionic vanadyl-ema complex displaced the piperidine ligands, yielding complex **1**, eq 1. The yellow-brown crystalline product was isolated as its Et_4N^+ salt by layering an amber DMF solution with Et_2O. Both in solution and solid-state, complex **1** is very air-sensitive. The ν(CO) IR values are close matches of the Ni^{II}(bme-daco) complex (ν(CO) in DMF (cm^{-1}): 1995, 1871, 1853, 1819). We can assume that the dianionic character of

the $[Et_4N^+]_2[V{\equiv}O(ema)]^{2-}$ metalloligand compensates for the greater electrophilcity of the $[V{\equiv}O]^{2+}$ unit over the d^8 Ni^{II} center.

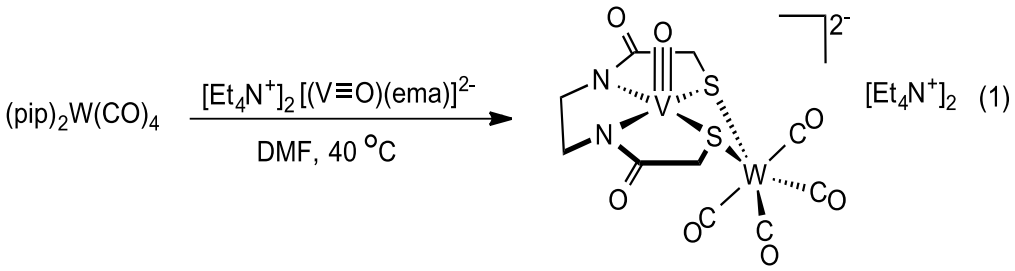

(1)

ν(CO) (DMF, cm^{-1}): 1996, 1872, 1848, 1802 (**1**)

The $[Fe(NO)_2]^+$ (i.e., the $\{Fe(NO)_2\}^9$ unit) synthon derives from dimeric $(\mu\text{-}I)_2[Fe(NO)_2]_2$, first reported by Hieber and Anderson in 1933.[101] Scheme IV-1 outlines its use in this study. Cleavage of $(\mu\text{-}I)_2[Fe(NO)_2]_2$ in THF readily occurred on addition of the N-heterocyclic carbene, (1,3-bis(2,4,6-trimethylphenyl)imidazol-2-ylidene), IMes, as well as the $Ni(N_2S_2)$ and $(V{\equiv}O)N_2S_2$ metalloligands where N_2S_2 = bis(2-mercaptoethyl)-1,5-diazacyclooctane. The $(IMes)Fe(NO)_2I$, **2**, [Ni(bme-daco)•$(Fe(NO)_2I)_2$], **3**, and [(V≡O)bme-daco•$Fe(NO)_2I$], **4**, complexes were isolated as deep brown, black, and dark green colored crystalline solids, respectively. The $\{Fe(NO)_2\}^9$ complexes are thermally stable in the solid state but should not be exposed to air. They decompose in solution, even under anaerobic conditions. Complexes **2** and **3** are highly soluble in THF and CH_2Cl_2, whereas **4** is only moderately soluble.

Scheme IV-1. Synthetic Route to L(I)Fe(NO)$_2$ complexes

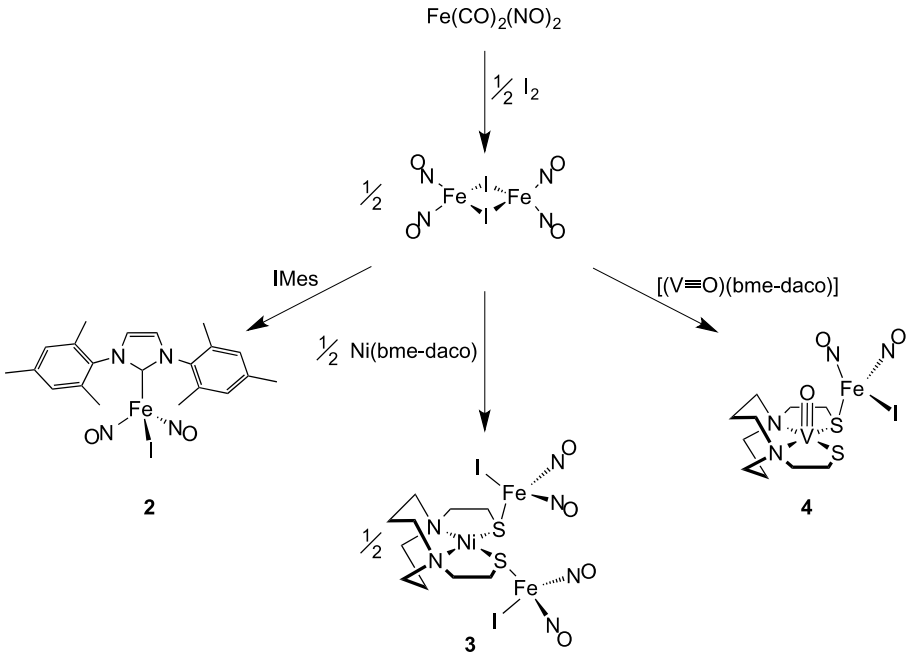

All three complexes (**2** – **4**) were insoluble in toluene, however toluene/THF mixtures in 3:1 ratio were used for EPR studies, vide infra, presumable in order to repress dissociation. The infrared spectra, Figure IV-3, for **2 – 4** in the diatomic ligand region show two *ν*(NO) bands of intensity pattern corresponding to the symmetric and asymmetric *ν*(NO) stretches in the Fe(NO)$_2$ groups. In comparison to the (μ-I)$_2$[Fe(NO)$_2$]$_2$ precursor, of *ν*(NO) = 1800 and 1736 cm^{-1}, complexes **2**, **3**, and **4** show shifts to lower *ν*(NO) stretching frequencies, Figure IV-3.

Complex	Sym (cm^{-1})	Asym (cm^{-1})
2	1782	1726
3	1793	1731
4	1796	1733

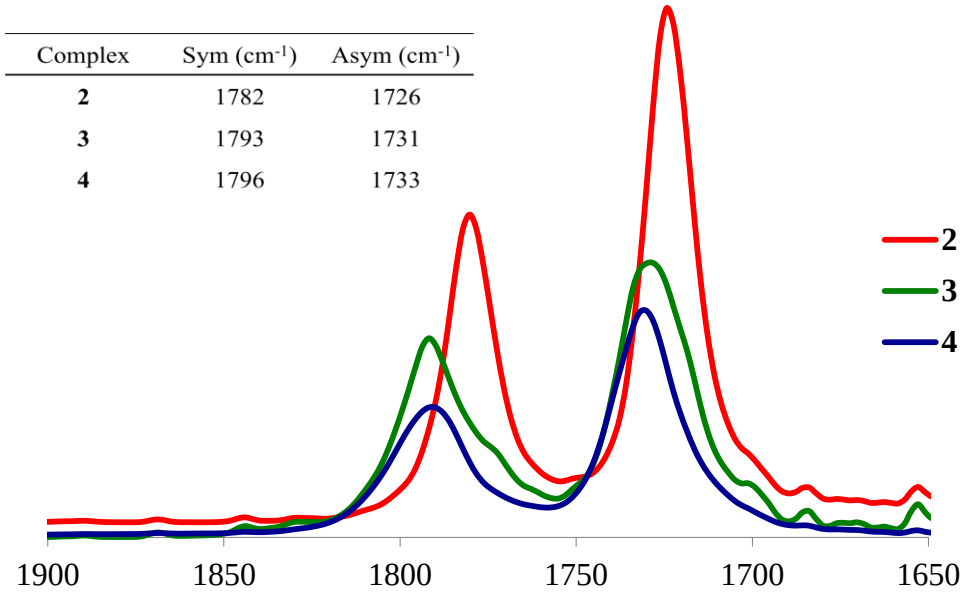

Figure IV-3. ν(NO) region IR spectra of L(I)Fe$(NO)_2$ complexes, THF solution.

Molecular Structures. The molecular structures of complexes **1 – 4,** characterized by X-ray diffraction analysis, are presented in Figures IV 4 – 7. Full structural reports are available in the Appendix. Selected bond distances and angles are listed in Table IV-1 for **2 – 4**.

Table IV-1. Selected bond distances (Å) and angles (deg) for complexes **2** – **4**.

	2	**3**	**4**
Fe-C_{NHC}	2.041(3)	—	—
Fe-S	—	2.330(13)	2.323(19)
Fe-I	2.573(8)	2.574(9)	2.599(16)
Fe-N_{av}	1.689(3)	1.730(3)	1.688(3)
N-Fe-N	111.9(1)	111.1(2)	117.1(2)
S-Fe-I	—	109.48(4)	107.01(6)
Fe-N-O	167.3(2) 162.3(3)	168.5(3) 161.6(4)	170.2(3) 166.2(3)

The tungsten carbonyl adduct of $[Et_4N^+]_2[(V{\equiv}O)(ema)]^{2-}$, **1**, adds to an analogous series of $(NiN_2S_2)W(CO)_4$ complexes.[29] Though the vanadyl center in $[Et_4N^+]_2[V{\equiv}O(ema)W(CO)_4]^{2-}$ still maintains the square pyramidal geometry of its precursor, $[Et_4N^+]_2[(V{\equiv}O)(ema)]^{2-}$, there are slight differences in the two complexes. The V-O bond distance of complex **1** is 1.612(5) Å, shown in Figure IV-4, whereas it is slightly elongated in the free metalloligand, $[Et_4N^+]_2[(V{\equiv}O)(ema)]^{2-}$, 1.623(19) Å. This value correlates within the IR data as the ν(VO) of **1** is about 12 cm^{-1} higher than that of $[Et_4N^+]_2[(V{\equiv}O)(ema)]^{2-}$. In both complexes, **1** and $[Et_4N^+]_2[(V{\equiv}O)(ema)]^{2-}$, the vanadium atom is displaced from the N_2S_2 plane by 0.729 Å and 0.713 Å, respectively.

The N-V-N angle in **1** and its precursor are largely identical, however, the S-V-S angle in **1** is ca. 4° (89.4°) smaller than $[Et_4N^+]_2[(V{\equiv}O)(ema)]^{2-}$ (93.9°).[13] This may be due to restriction by the $W(CO)_4$ unit in the bidentate binding mode.

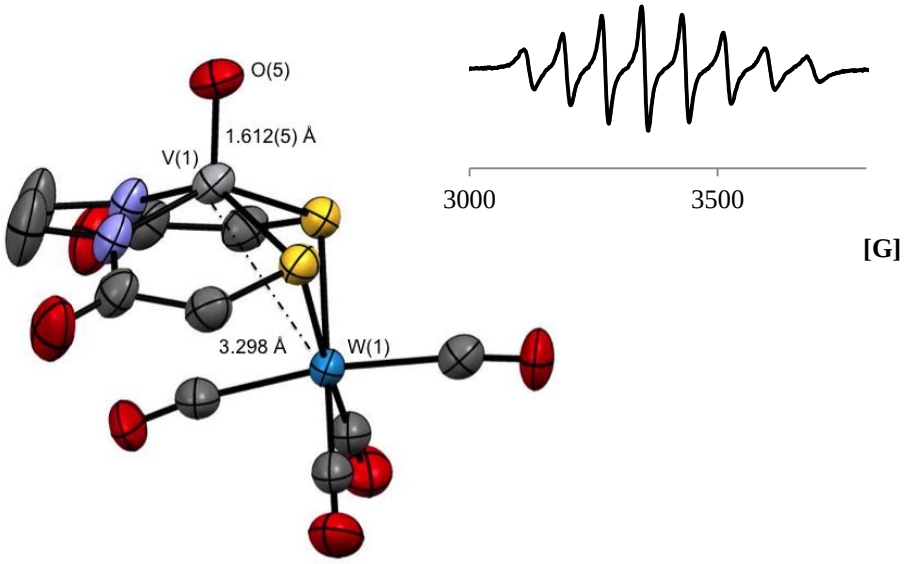

Figure IV-4. ORTEP drawing of complex **1**, $[Et_4N^+]_2[V{\equiv}O(ema)W(CO)_4]^{2-}$. Hydrogen atoms and the $[Et_4N^+]$ counterions have been removed for clarity. EPR spectrum of **1** at 298 K in CH_2Cl_2.

The iron is in pseudo-tetrahedral geometry in complexes **2 – 4**. The Fe-N-O angles display slightly greater linearity in **4,** with bond angles of 170.2° and 166.2° **(**avg. 168.2°) compared to **2,** bond angles of 167.3° and 162.3° (avg. 165.0°) and **3**, bond angles of 168.5° and 161.6° (avg 164.4°). Complex **2** adds to a growing list of DNICs based on and stabilized by N-heterocyclic carbene ligands, Figure IV-5. The $(IMes)Fe(NO)_2SPh$ is a precise analogue to **2**, and shows a similar Fe-C_{NHC} distance of 2.045(3) Å (2.041(3) Å for **2**).[100] Likewise, the average Fe-NO distances are 1.672(3) Å

in the thiolate as compared to 1.689(3) Å in complex **2**. Both are regular tetrahedra with slightly opened N-Fe-N angles.

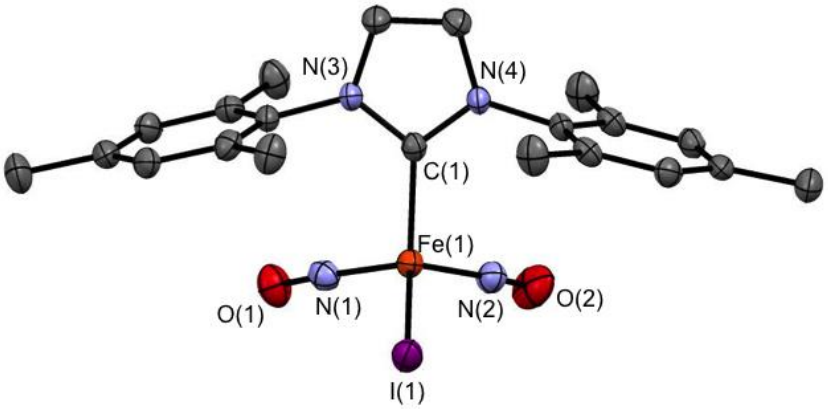

Figure IV-5. ORTEP drawing of complex **2** with thermal ellipsoids drawn at 50% probability level. Hydrogen atoms have been removed for clarity.

In complexes **3** and **4** the metallodithiolates are found as monodentate donor ligands to $Fe(NO)_2I$. Complex **3**, of formulation $NiN_2S_2[Fe(NO)_2I]_2$, displays a square planar NiN_2S_2 complex with pendant $Fe(NO)_2I$ units attached to each thiolato-sulfur in a transoid configuration, Figure IV-6. Metric data for the NiN_2S_2 free ligand is substantially the same as in complex **3** with the exception of a slightly elongated Ni-S distance for **3** vs. Ni(bme-daco).[21] Within the $Fe(NO)_2I$ unit, the N-Fe-N angle is the same as in complex **2**, and the Fe-I distances are identical. Hence from metric parameters the NiN_2S_2 metalloligand has a similar effect on the $Fe(NO)_2I$ metalloacceptor as does the IMes ligand.

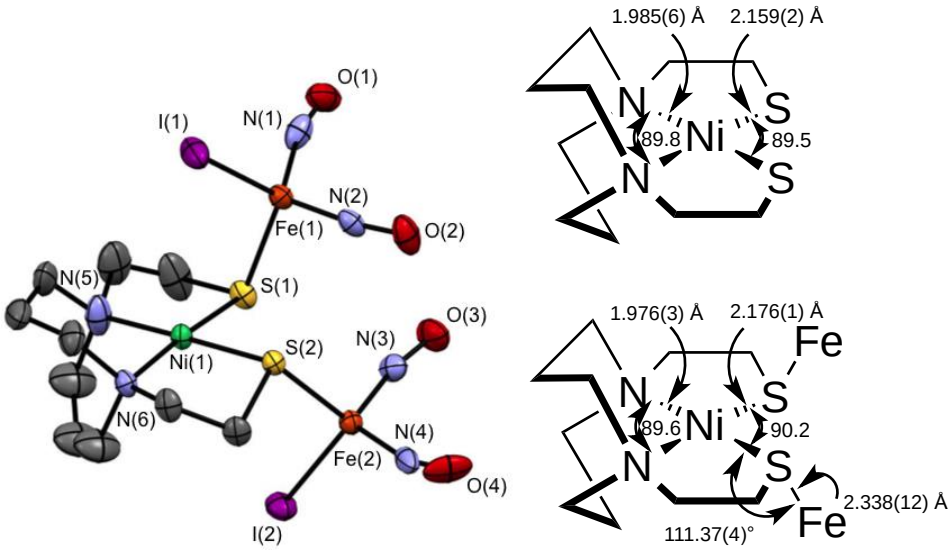

Figure IV-6. ORTEP drawing of complex **3** with thermal ellipsoids drawn at 50% probability level; The Ni(bme-daco) structure[21] and **3** are compared in Chemdraw line figures at right. Hydrogen atoms have been removed for clarity.

The $(V{\equiv}O)N_2S_2$ complex, (V≡O)(bme-daco), binds only one $Fe(NO)_2I$ unit through a bridging thiolate sulfur similarly to the [Ni(bme-dach)•$Fe(NO)_2(CO)$], a reduced $\{Fe(NO)_2\}^{10}$ DNIC. [87] As shown in Figure IV-7, the Fe-S distance of 2.343(2) Å in the Ni-Fe complex is substantially the same as in complex **4**. The displacement of V from the N_2S_2 plane is maintained the same as in the free $(V{\equiv}O)N_2S_2$ metalloligand with displacement of the $[V{\equiv}O]^{2+}$ unit from the N_2S_2 best plane equal to *ca*. 0.65 Å. This displacement is on the same side as the $Fe(NO)_2I$ to sulfur binding leading to a V---Fe distance of 3.731 Å, the vanadyl-oxygen to iron, (V)O---Fe, distance is 3.575 Å, and the closer $[V{\equiv}O]^{2+}$ to nitrogen, the (V)O---N distance, is 3.558 Å. The major difference in the two structures is the M-S-Fe angle, 103.7° in **4** and 91.3° in the [Ni(bme-dach)•$Fe(NO)_2(CO)$], Figure IV-7. Despite the difference in redox levels of **4** vs.

[Ni(bme-dach)•Fe(NO)$_2$(CO)], the N-Fe-N angle values are the same for both, 117°, and some 6° larger than those found in complexes **2** and **3**.

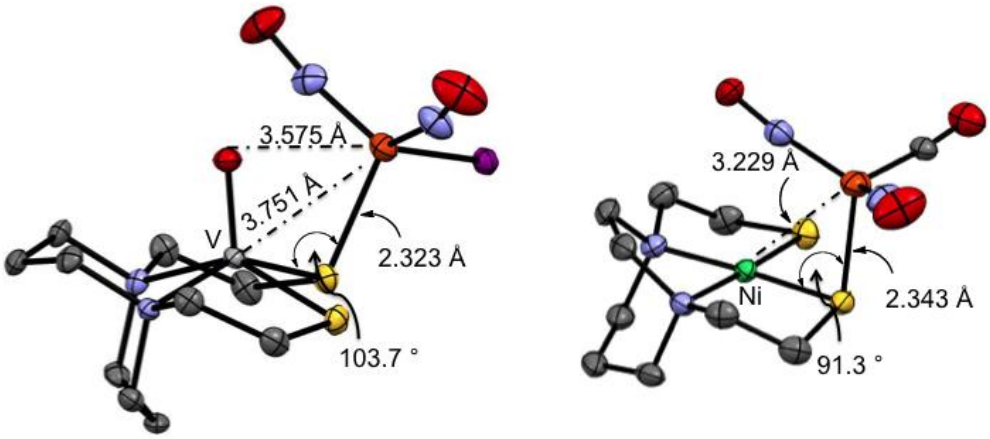

Figure IV-7. Ball and stick drawing of complex **4**, (a), and for comparison, the [Ni(bme-dach)•Fe(NO)$_2$(CO)], (b), structure.[87] Hydrogen atoms have been removed for clarity.

The fact that the Ni(bme-daco) binds two Fe(NO)$_2$I units would suggest superior electron-donating ability of the nickel versus the vanadyl complexes. In fact all three complexes of this study show ν(NO) spectra that are nearly identical in pattern and wavenumber position, consistent with the local C_{2v} symmetry of the Fe(NO)$_2$ unit. For comparison, the ν(NO) of the [Ni(bme-dach)•Fe(NO)$_2$(CO)], the reduced{Fe(NO)$_2$}^{10} redox level are at 1732 and 1689 cm^{-1}, lower than the {Fe(NO)$_2$}^{9} complexes.

Electron Paramagnetic Resonance Spectral Data

The paramagnetism due to the {Fe(NO)$_2$}^{9} unit that is latent within the spin coupled, diamagnetic (μ-I)$_2$[Fe(NO)$_2$]$_2$ may be revealed upon dimer cleavage by

exogenous ligands and coordinating solvents. For example, addition of tetraethylammonium iodide ($Et_4N^+I^-$) to $(\mu\text{-}I)_2[Fe(NO)_2]_2$, forms the monomeric and paramagnetic $[I_2Fe(NO)_2]^-$. Its room temperature EPR spectrum showed a characteristic isotropic signal centered at g = 2.077 with eleven lines from super hyperfine coupling to the two ^{127}I nuclei. These results are consistent with an earlier report of Bryar and Eaton.[103] Complex **2**, mono-iron dinitrosyl, $Fe(NO)_2\}^9$, complex is of S = ½ as determined by magnetic susceptibility, μ = 1.75 B.M. by both Evans' and Gouy balance measurements. Its EPR spectrum, Figure IV-8 a) displays a six line pattern resulting from super hyperfine coupling to the naturally occurring isotope of iodine ^{127}I with a g value of 2.070. The 298 K EPR spectrum of complex **3**, [Ni(bme-daco)•$(Fe(NO)_2I)_2$], shown in Figure IV-8 b), is highly similar to that of complex **2**. Solubility of complex **3** in toluene/THF mixture was decreased significantly as compared to a THF solution mixture of **3**.

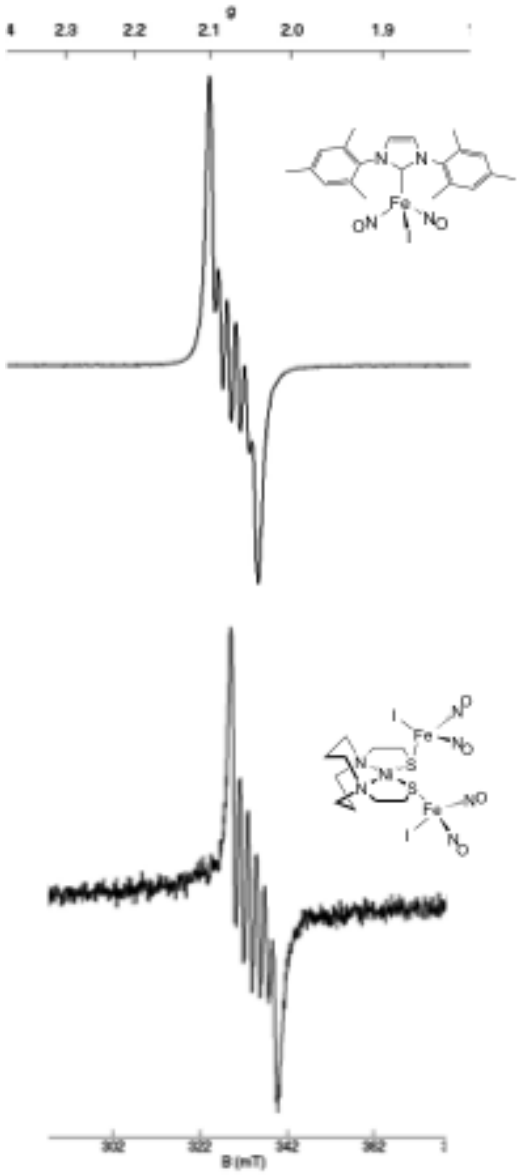

Figure IV-8. Displays the room temperature EPR spectrum of complex **2**, the mono-iron product of $(\mu\text{-}I)_2[Fe(NO)_2]_2$ cleavage by the IMes ligand in a toluene/THF mixture. b) The EPR spectrum of complex **3**, $[Ni(bme\text{-}daco)\bullet(Fe(NO)_2I)_2]$ at 298 K in a toluene/THF mixture.

EPR spectra of $[V{\equiv}O(bme\text{-}daco)\bullet Fe(NO)_2I]$, complex **4**, were obtained at 298 K and 10 K. The former is given in Figure IV-9 a) and shows the 6-line multiplet

superimposed on a identified 8-line pattern. The former arises from the unpaired electron on the $Fe(NO)_2I$, as seen in Figure IV-8 a) and b) while the latter is from the vanadyl moiety. Figure IV-9 b) is the low temperature spectrum recorded of **4** in the same 3:1 toluene/THF solution. Under these conditions, no evidence of the $Fe(NO)_2I$ moiety is observed; the spectrum is identical to that of the free (V≡O)(bme-daco) complex. From this we can only conclude that the equilibrium is shifted towards the products in equation 2, which the dimeric form of $(\mu\text{-}I)_2[Fe(NO)_2]_2$ is spin-paired. Nevertheless it must be noted that the 298 K spectrum of $(\mu\text{-}I)_2[Fe(NO)_2]_2$ in DCM and THF solvents displays a six-line pattern, indicating the ease of cleavage of the dimer to yield the solvated paramagnet, $(solv)Fe(NO)_2I$.

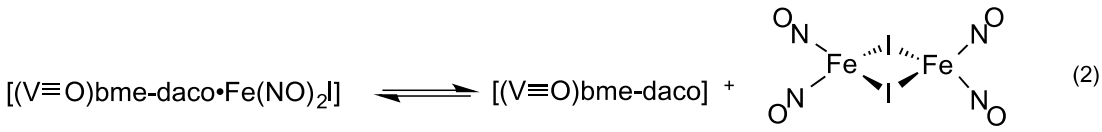

(2)

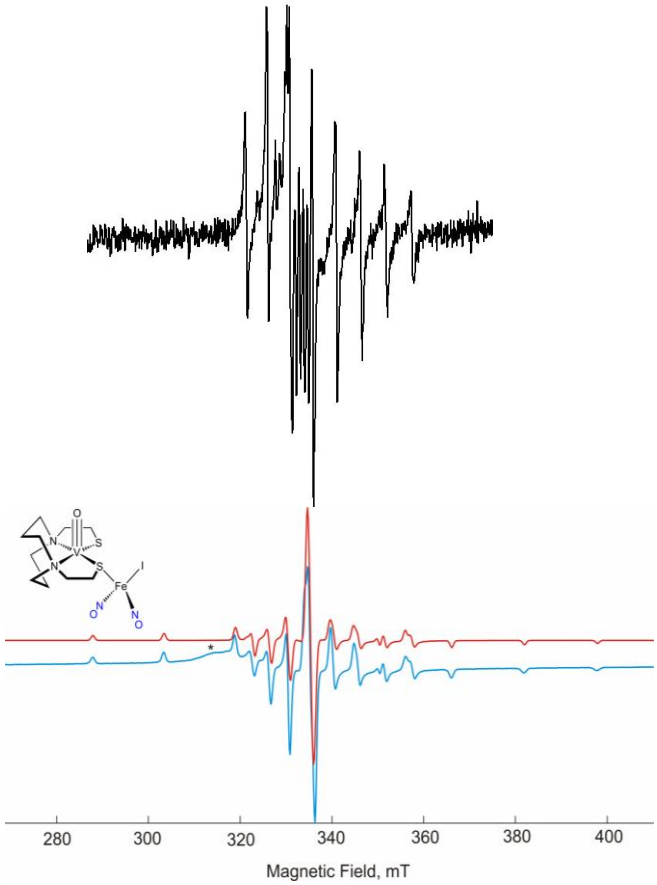

Figure IV-9. a) EPR spectrum of **4** in a 3:1 (toluene:THF) solution at 298 K, b) complex **4** in toluene/THF at 10 K.

Electrochemistry

The $\{Fe(NO)_2\}^9$ complexes of this study, **2 – 4,** exhibit irreversible oxidation events between 0.20 and 0.60 V. Complex **3,** [Ni(bme-daco)•$(Fe(NO)_2I)_2$], also shows a reversible anodic event centered at -0.17 V with an i_{pa}/i_{pc} of 0.89 that is currently unassigned. A possibility for this event maybe due to aggregate formation of the [Ni(bme-daco)•$(Fe(NO)_2I)_2$], resulting in metallation of multiple Ni centers in solution. The cathodic region of **2** shows one irreversible reduction event at -1.33 V assigned to

the $\{Fe(NO)_2\}^{9/10}$ couple, consistent with the $(NHC)Fe(NO)_2SPh$ complex.[100] Both complexes **3** and **4** show a similar couple at -1.37 and -1.47 V, respectively, that are also assigned to the $\{Fe(NO)_2\}^9/\{Fe(NO)_2\}^{10}$ couple, Figure IV-10**.** In complex **3**, a second quasi-reversible couple is centered at -0.70 V with an i_{pa}/i_{pc} of 0.79. This event is assigned to the Ni^{II}/Ni^{I} couple. It is positively shifted from the parent Ni(bme-daco) complex by 1.64 V. This shift to more positive potentials is consistent with previous studies where upon metallation or alkylation of the NiN_2S_2 unit results in more facile reduction of the Ni^{2+}. Examples of this trend can be seen in Table IV-2.

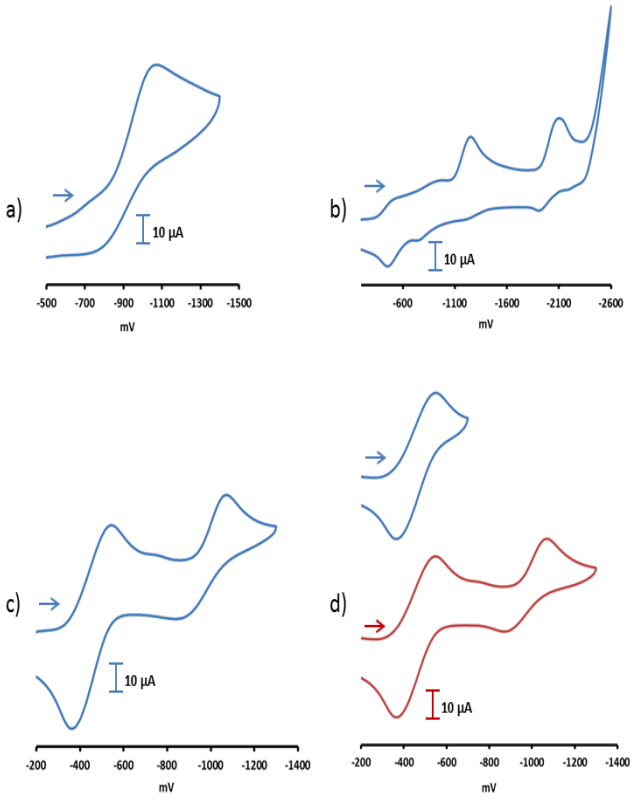

Figure IV-10. Cyclic voltammograms of 2 mM solutions of a) complex **2** b) complex **4** c) complex **3** and d) scan reversals of complex **3** in 0.1 mM $(n\text{-}Bu)_4N^+PF_6^-/CH_2Cl_2$ with a glassy carbon working electrode at 200 mV/s scan rate.

Table IV-2. Listing of cyclic voltammetry parameters.[a]

Compound	$E_{1/2}$ $Ni^{II/I}$ [V]	E_{pc2} [V]	E_{pc} $Fe(NO)_2^{9/10}$ [V]
Ni(bme-daco)	-2.34[2]		
Ni(bme-daco)Me^+	-1.60[2]		
Ni(bme-daco)Me_2^{2+}	-1.08[2]		
$[Ni(bme\text{-}daco)]_2Ni^{2+}$	-1.11[3]	-2.04	
2			-1.33
3	-0.70		-1.37
4			-1.47

[a]All measurements were done in CH_2Cl_2 solution, 0.1 M $(n\text{-}Bu)_4N^+PF_6^-$ electrolyte, measured vs $Ag/AgNO_3$ reference electrode, with a concentration from 1.0-2.5 mM in analyte. All potentials are referenced to Cp_2Fe/Cp_2Fe^+ = 0 mV as internal standard.

Summary and Conclusions

The synthesis and characterization of three heterobimetallic complexes and a N-heterocyclic carbene complex with $W(CO)_4$ and $Fe(NO)_2$ metallo-reporter units have been achieved. This study shows the superior sensitivity of the $Fe(NO)_2$ moiety within these complexes to its ligands according to analysis of the electronic environment using two techniques, cyclic voltammetry and infrared spectroscopy. The donor ability of the ligands within the three $\{Fe(NO)_2\}^9$ complexes can be ranked based on the *v*(NO) IR stretching frequencies in the order: (IMes) > Ni(bme-daco) > V≡O(bme-daco); however, the electrochemical data for the $\{Fe(NO)_2\}^9$ complexes contrasted to the *v*(NO) IR stretching frequencies. Previous studies indicated no reactivity of the *cis*-thiolates of neutral $(V{\equiv}O)N_2S_2$ complexes with alkylating agents as electrophiles. However, the V≡O(bme-daco) readily reacts with the $\{Fe(NO)_2\}^9$ unit but not with the $W(CO)_4$ precursor as does the dianionic metalloligand, $[(V{\equiv}O)(ema)]^{2-}$. Super hyperfine

coupling of ^{127}I with the unpaired electron on the iron center of the $\{Fe(NO)_2\}^9$ unit was observed for complexes **2** and **3** by EPR spectroscopy. Based on EPR analysis of complex **4**, [(V≡O)bme-daco•$Fe(NO)_2$I], the ^{51}V metal ion and ^{127}I contribute to two distinct super hyperfine patterns with no overlap. The long distance between the two paramagnetic metal centers, V---Fe, at 3.75 Å, indicates no interaction between the two S = ½ systems.

CHAPTER V

SUMMARY AND CONCLUSIONS

The coordination chemistry of metalloenzyme active sites consisting of a cysteine-X-cysteine (X = serine or glycine) tripeptide motif plays an important role in the fine-tuning of the reactivity and electronic structure of the distal nickel center of acetyl-coA synthase and the cobalt or iron centered nitrile hydratases.[33,104,105] As these N_2S_2 donor sites are not restricted solely to metalloenzymes, the ease of synthesis of their inorganic derivatives has resulted in a library of synthetic analogues that may be readily compared to their biological counterparts.

Metallodithiolates, a new class of ligands, can closely mimic the coordination environments of metalloenzymes described above. Compared to classical phosphines and amines, they give unique polymetallic structures because of the non-directionality of the lone pairs on the sulfurs. To further study N_2S_2 as a metal binding site in biomolecules, our laboratory has made use of such metallodithiolates specifically, the N_2S_2 tight binding site contains diazacycles bearing ethylene thiolate arms. As mentioned in Chapter I, metallodithiolate ligands are building blocks for C_4 and C_3 paddlewheel complexes. Propeller-shaped molecular structures with metallo S-donor ligands to Au(I) were described in Chapter III.

Gold thiolate clusters display-interesting geometries because of the versatility in thiolate bridges and aurophilic interactions.[62] Aurophilic interactions, ranging from 2.50 – 3.50 Å, commonly found in gold(I) compounds, can be used to describe some of the

unique properties of gold including photoluminescence. I have explored the coordination chemistry of nickel cis-dithiolates with gold (I), which led to the synthesis of complexes displaying several types of classical aurophilic interactions. Using Ph_3PAuCl as the Au^+ source and three NiN_2S_2 metallodithiolate ligands, Ni(bme-daco), Ni(bme-dach), and $[Ni(ema)]^{2-}$, five $[Ni(N_2S_2)_xAu_y]$ (where x = 1 or 2, y = 1, 2 or 4) compounds were synthesized. Two cationic complexes and one anionic complex $[\{Ni(bme\text{-}daco)\}_2Au_2]^{2+}(Cl^-)_2$, $[\{Ni(bme\text{-}dach)\}_2Au_2]^{2+}(Cl^-)_2$, and $(Et_4N^+)_2[\{Ni(ema)\}_2Au_2]^{2-}$, displayed fully-supported aurophilic interactions in the range of 3.11 to 3.13 Å, respectively. Based on the range of metal-metal distances of the NiN_2S_2 units, these gold complexes can be fitted in with a collection of other polymetallic complexes synthesized in our laboratory, Figure V-1.

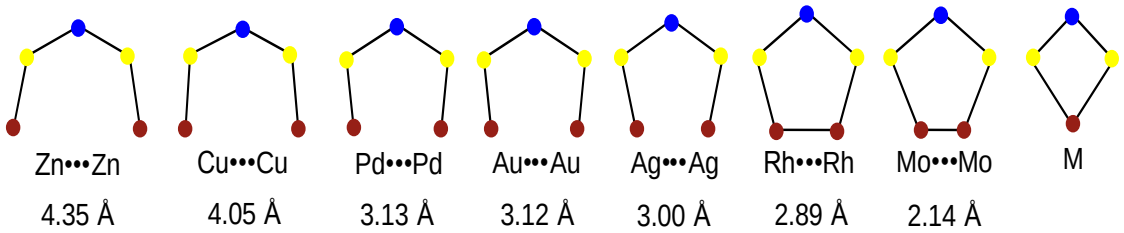

Figure V-1. Metal-Metal distances from a collection of polymetallic complexes containing the NiN_2S_2 unit.

X-ray diffraction analysis for these propeller-shaped complexes showed that the angle between the NiN_2S_2 plane and the $S_2Au_2S_2$ plane is at ca. 90° and the S---S distances in the cis-dithiolates show no major differences from the NiN_2S_2 metallodithiolate ligand precursors. The dianionic NiN_2S_2 metallodithiolate ligand,

$[Ni(ema)]^{2-}$ also produced a neutral complex, $[(Ni(ema))_2Au_4(PPh_3)_4]$ under different crystallization conditions. This complex retains the PPh_3 ligands on the Au(I) ion and contain unsupported aurophilic interactions in the range of 3.05 to 3.13 Å. The paradigm NiN_2S_2 ligand, Ni(bme-daco), also served as a mono-dentate ligand with Ph_3PAuCl to give $[Ni(bme\text{-}daco)\text{-}AuPPh_3]^+$.

Cyclic voltammetry measurements of the $[Ni(N_2S_2)_xAu_y]$ complexes, demonstrated positive shifts for the $Ni^{II/I}$ couple, as compared to the NiN_2S_2 precursors. The electrochemical results are consistent with the redox events seen for the mono-methylated and di-methylated cis-dithiolate NiN_2S_2 complexes; examples are shown in Figure V-2. The literature contains similar examples of the propeller-type $[Ni(N_2S_2)_xAu_y]$ complexes with bidentate cis-dithiolate nickel complexes from a chiral multidentate D-pencillaminate ligand.

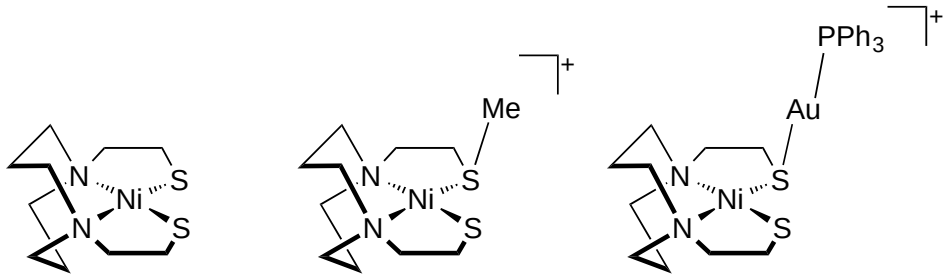

$E_{1/2}$ $Ni^{II/I}$: -2.34 V -1.60 V -1.10 V

Figure V-2. Comparison of $E_{1/2}$ $Ni^{II/I}$ redox couple for the Ni(bme-daco) and Ni(bme-daco) derivatives.

The chemistry of vanadium in biological systems has become a major area of research, aiding in the interpretation of the role of vanadium in biological or

physiological environments. Model square pyramidal compounds of $[V{\equiv}O]^{2+}$ have been synthesized with both soft (thiolates) and hard (amines, amides, alkoxides, hydroxides, etc.) donors.[1,106] With the assistance of a previous group member, Dr. Roxanne Jenkins, a series of $[(V{\equiv}O)N_2S_2]^{0,2-}$ complexes (where N_2S_2 = $(bme\text{-}daco)^{2-}$, $(bme\text{-}dach)^{2-}$, and $(ema)^{4-}$) was prepared and characterized. Prior to this work, there were only four other $[(V{\equiv}O)N_2S_2]$ complexes characterized by X-ray crystallography according to the Cambridge Crystallographic Data Centre, CCDC.

Another important finding from this study, was the neutral vanadyl complexes showed no reactivity with alkylating agents such as 1,3-dibromopropane or methyl iodide as compared to the dianionic vanadyl complexes.[13] This results from charge differences of the $[(V{\equiv}O)N_2S_2]$ vs $[(V{\equiv}O)N_2S_2]^{2-}$ complexes making the thiolates stronger nucleophiles in the dianionic complexes. The lack of reactivity of the neutral analogues of NiN_2S_2 complexes speaks to influence of the $Ni_{d(\pi)} - S_{p(\pi)}$ anti-bonding interaction on the nucleophilicity of the thiolato sulfurs.

Having established the structural and spectral properties of the $[(V{\equiv}O)N_2S_2]^{0,2-}$ complexes, reactivity of the $[(V{\equiv}O)N_2S_2]^{0,2-}$ complexes with reporter units such as tungsten carbonyls and dinitrosyl iron complexes was explored as described in Chapter IV.

Tunsgten (0) carbonyls serve as reliable reporter units when bound to various ligands, including metallodithiolates. Previous work in our laboratory compared the donating properties within a series of $(NiN_2S_2)W(CO)_4$ complexes with phosphines and amines.[29] Analogous studies with the $[(V{\equiv}O)N_2S_2]^{0,2-}$ derivatives were attempted however the

tungsten tetracarbonyl derivatives were only preparable with the dianionic $[(V{\equiv}O)N_2S_2]^{2-}$ complex, $[V{\equiv}O(ema)]^{2-}$. That is, the neutral vanadyl complexes were unreactive similarly to their behavior with carbon electrophiles. As shown in the introduction of this dissertation, Figure I-6 represents the ranking of the MN_2S_2 complexes determined from $(MN_2S_2)W(CO)_4$ complexes. This figure can now be adapted to include the $[V{\equiv}O(ema)]^{2-}$ complex, Figure V-3. With both $[Ni(ema)]^{2-}$ and $[V{\equiv}O(ema)]^{2-}$ containing the same ligand set, the dianionic nickel complex, $[Ni(ema)]^{2-}$, is a stronger donor as compared to the $[V{\equiv}O(ema)]^{2-}$ complex, based on ν(CO) IR stretching frequencies from the $W(CO)_4$ reporter unit. This is due to less electron density in the N_2S_2 motif of the $[V{\equiv}O(ema)]^{2-}$ complex because of the electrophilic oxygen atom on the vanadium and the low d-electron count.

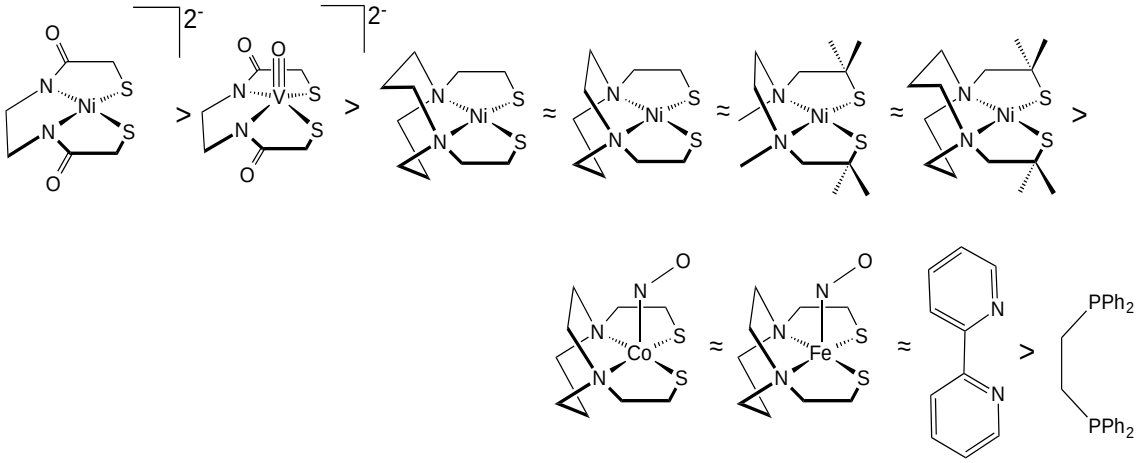

Figure V-3. Ranking of MN_2S_2 complexes from $(MN_2S_2)W(CO)_4$ complexes, adapted from Figure I-7.

Since the donating properties of the neutral vanadyl complexes could not be investigated using tungsten carbonyls, attempts were made to use the dinitrosyl iron reporter unit instead. The electronic environment of $Fe(NO)_2$ complexes can be studied by using ν(NO) IR stretching frequencies and the redox events of the $Fe(NO)_2$ unit from cyclic voltammetry. This is advantageous over the $W(CO)_{4,5}$ unit which only provides ν(CO) IR stretching frequencies, since the tungsten center is redox inactive. This approach can also provide information about the acceptor properties of the metal fragments.

Sulfur-based adduct formation of two N_2S_2 complexes and an N-heterocyclic carbene with the oxidized form of the $Fe(NO)_2I$ unit, derived from $(\mu\text{-}I)_2[Fe(NO)_2]_2$, have afforded (IMes)$Fe(NO)_2I$, [Ni(bme-daco)•$(Fe(NO)_2I)_2$], and [V≡O(bme-daco)•$Fe(NO)_2I$]. Infrared analysis of the ν(NO) values of these three complexes indicated that the N-heterocyclic carbene, IMes, is a stronger donor to the $Fe(NO)_2I$ unit, giving the lowest ν(NO) stretching frequencies. In support of this conclusion, addition of the IMes ligand to a solution of [Ni(bme-daco)•$(Fe(NO)_2I)_2$] yielded the (IMes)$Fe(NO)_2I$.

The electrochemistry data of the $Fe(NO)_2I$ complexes were obtained and the $E_{1/2}$ values contrasted to the ν(NO) IR stretching frequencies; stronger donor ligands allows a more negative $\{Fe(NO)_2\}^{9/10}$ couple. In the case of the (IMes)$Fe(NO)_2I$, the complex with the lowest ν(NO) stretching frequencies, the $Fe(NO)_2{}^{9/10}$ couple is at -1.33 V as compared to the metallodithiolate complexes, [Ni(bme-daco)•$(Fe(NO)_2I)_2$], and [V≡O(bme-daco)•$Fe(NO)_2I$] at -1.37 V and -1.47 V, respectively.

The solid state molecular structures of (IMes)Fe$(NO)_2$I, [Ni(bme-daco)•(Fe$(NO)_2$I$)_2$], and [V≡O(bme-daco)•Fe$(NO)_2$I] find for all a pseudo-tetrahedral geometry about the iron center. Both metallodithiolate ligands bind to the Fe$(NO)_2$I unit in a monodentate fashion; however, the Ni(bme-daco) ligand has two Fe$(NO)_2$I units, one on each thiolate sulfur, whereas the V≡O(bme-daco) only has one Fe$(NO)_2$I unit. The latter result is consistent with the greater nucleophilicity of the NiN_2S_2 complex.

The magnetic properties of (IMes)Fe$(NO)_2$I, [Ni(bme-daco)•(Fe$(NO)_2$I$)_2$], and [V≡O(bme-daco)•Fe$(NO)_2$I] were investigated by EPR spectroscopy. The EPR spectra of the Fe$(NO)_2$I complexes were found to be solvent dependent. Using THF as the solvent, the EPR spectrum of (IMes)Fe$(NO)_2$I, gave a distinctive six-line pattern from super hyperfine coupling of ^{127}I with a S = ½ system. Under identical conditions, the EPR signal for [Ni(bme-daco)•(Fe$(NO)_2$I$)_2$] was greatly attenuated. This can be attributed to the fact that in coordinating solvents, the [Ni(bme-daco)•(Fe$(NO)_2$I$)_2$] dissociates in solution, to give the diamagnetic Ni(bme-daco) ligand and the diamagnetic $(\mu\text{-I})_2[Fe(NO)_2]_2$ precursor. Similarly, the EPR signal for the [V≡O(bme-daco)•Fe$(NO)_2$I] complex has a lower intensity in THF solution. These experiments were designed to test the hypothesis that there might be no EPR signal for the [V≡O(bme-daco)•Fe$(NO)_2$I, because this complex contains two paramagnetic metal ions that may be spin-paired.

The EPR spectra indicated no spin-pairing of the two metal ions in the solution and gave individual super-hyperfine coupling for each moiety. With the 3:1 (toluene:THF) solution spectra of these complexes, the metallodithiolate complexes,

[Ni(bme-daco)•$(Fe(NO)_2I)_2$], and [V≡O(bme-daco)•$Fe(NO)_2I$] gave similar line patterns to those observed in a THF solution but with signals at normal intensities. The EPR spectrum of (IMes)$Fe(NO)_2I$ in a 3:1 (toluene:THF) solution gave an unresolved line pattern, with super hyperfine coupling to the naturally occurring isotopes of iodine and nitrogen, ^{127}I and ^{14}N.

Overall, the NiN_2S_2 complexes continue to produce unique polymetallic structures, and prove the versatility of cis-dithiolates as ligands. These NiN_2S_2 cis-dithiolate ligands are hemi-labile, capable of both monodentate and bidentate binding. With this property, and the use of gold(I) compounds as catalysts in oxidation processes, the $[Ni(N_2S_2)_xAu_y]$ complexes should be explored for catalysis of reactions such as hydrogenation, oxidation, and nucleophilic additions.

The N_2S_2 binding motif has been studied extensively over two decades, using different metals to investigate the electronic environment of such complexes. Further exploration of the N_2S_2 binding sites has been achieved with the vanadyl ion, $[V{\equiv}O]^{2+}$ in S-adduct formation with reporter units such as tungsten carbonyls and iron dinitrosyls to investigate the donor ability of $[(V{\equiv}O)N_2S_2]^{0,2-}$ complexes. The thiolate sulfurs of the neutral NiN_2S_2 complexes react with both reporter units, $W(CO)_{4,5}$ and $Fe(NO)_2$, whereas, the neutral $[(V{\equiv}O)N_2S_2]^0$ complexes only react with the $Fe(NO)_2$ unit. The less repulsion between the sulfur lone pairs and the V^{4+} ($[(V{\equiv}O)N_2S_2]^0$) metal center, makes the sulfurs less nucleophilic when compared to the electron rich Ni^{2+} (NiN_2S_2) complexes. In addition, paramagnetic studies of the bimetallic [V≡O(N_2S_2)]•$Fe(NO)_2I$

complex confirms no spin-coupling of the two paramagnetic metal centers. This work enhances the fundamental chemistry of metallodithiolates as ligands to other metals to further understand the electronic properties of such complexes.

REFERENCES

1. Crans, D. C.; Smee, J. J.; Gaidamauskas, E.; Yang, L. *Chem. Rev.* **2004**, *104*, 849-902.
2. Chasteen, N. D.; DeKoch, R. J.; Rogers, B. L.; Hanna, M. W. *J. Am. Chem. Soc.* **1973**, *95*, 1301-1309.
3. Petersen, J.; Hawkes, T. R.; Lowe, D. J. *J. Inorg. Biochem.* **2000**, *80*, 161-168.
4. Rehder, D. *Angewandte Chemie International Edition in English* **1991**, *30*, 148-167.
5. McNeill, J. H.; Yuen, V. G.; Hoveyda, H. R.; Orvig, C. *J. Med. Chem.* **1992**, *35*, 1489-1491.
6. Thompson, K. H.; Orvig, C. *Dalton Trans.* **2006**, *0*, 761-764.
7. Kiss, T.; Jakusch, T.; Hollender, D.; Dörnyei, Á.; Enyedy, É. A.; Pessoa, J. C.; Sakurai, H.; Sanz-Medel, A. *Coord. Chem. Rev.* **2008**, *252*, 1153-1162.
8. Sanna, D.; Ugone, V.; Micera, G.; Garribba, E. *Dalton Trans.* **2012**, *41*, 7304-7318.
9. Ballhausen, C. J.; Gray, H. B. *Inorg. Chem.* **1962**, *1*, 111-122.
10. Hwang, J. S.; Al-Turabi, M. O. H.; El-Sayed, L.; Al-Gwidi, H. A. M. *Energy & Fuels* **1999**, *14*, 179-183.
11. Kim, Y.-J.; Kim, Y.-I.; Choi, S.-N. *Polyhedron* **2000**, *19*, 2155-2161.
12. Fitzgerald, J. J.; Chasteen, N. D. *Biochemistry* **1974**, *13*, 4338-4347.

13. Jenkins, R. M.; Pinder, T. A.; Hatley, M. L.; Reibenspies, J. H.; Darensbourg, M. Y. *Inorg. Chem.* **2011**, *50*, 1849-1855.

14. Mills, D. K.; Font, I.; Farmer, P. J.; Hsiao, Y.-M.; Tuntulani, T.; Buonomo, R. M.; Goodman, D. C.; Musie, G.; Grapperhaus, C. A.; Maguire, M. J.; Lai, C.-H.; Hatley, M. L.; Smee, J. J.; Bellefeuille, J. A.; Darensbourg, M. Y.; Hancock, R. D.; Eng, S.; Martell, A. E. In *Inorg. Synth.*; John Wiley & Sons, Inc.: 2007, p 89-98.

15. Kruger, H. J.; Peng, G.; Holm, R. H. *Inorg. Chem.* **1991**, *30*, 734-742.

16. Krishnan, R.; Riordan, C. G. *J. Am. Chem. Soc.* **2004**, *126*, 4484-4485.

17. Sakurai, H.; Taira, Z.-e.; Sakai, N. *Inorg. Chim. Acta* **1988**, *151*, 85-86.

18. Dutton, J. C.; Fallon, G. D.; Murray, K. S. *Inorg. Chem.* **1988**, *27*, 34-38.

19. Hazari, S. K. S.; Kopf, J.; Palit, D.; Rakshit, S.; Rehder, D. *Inorg. Chim. Acta* **2009**, *362*, 1343-1347.

20. Farchione, D.; Wedd, A. G.; Tiekink, E. R. T. *Acta Crystallographica Section C* **1991**, *47*, 650-651.

21. Mills, D. K.; Reibenspies, J. H.; Darensbourg, M. Y. *Inorg. Chem.* **1990**, *29*, 4364-4366.

22. Smee, J. J.; Miller, M. L.; Grapperhaus, C. A.; Reibenspies, J. H.; Darensbourg, M. Y. *Inorg. Chem.* **2001**, *40*, 3601-3605.

23. Darensbourg, M. Y.; Tuntulani, T.; Reibenspies, J. H. *Inorg. Chem.* **1995**, *34*, 6287-6294.

24. Chiang, C.-Y.; Lee, J.; Dalrymple, C.; Sarahan, M. C.; Reibenspies, J. H.; Darensbourg, M. Y. *Inorg. Chem.* **2005**, *44*, 9007-9016.

25. Busch, D. H.; Jicha, D. C.; Thompson, M. C.; Wrathall, J. W.; Blinn, E. *J. Am. Chem. Soc.* **1964**, *86*, 3642-3650.

26. Farmer, P. J.; Solouki, T.; Mills, D. K.; Soma, T.; Russell, D. H.; Reibenspies, J. H.; Darensbourg, M. Y. *J. Am. Chem. Soc.* **1992**, *114*, 4601-4605.

27. Goodman, D. C.; Tuntulani, T.; Farmer, P. J.; Darensbourg, M. Y.; Reibenspies, J. H. *Angewandte Chemie International Edition in English* **1993**, *32*, 116-119.

28. Darensbourg, M. Y.; Tuntulani, T.; Reibenspies, J. H. *Inorg. Chem.* **1994**, *33*, 611-613.

29. Rampersad, M. V.; Jeffery, S. P.; Golden, M. L.; Lee, J.; Reibenspies, J. H.; Darensbourg, D. J.; Darensbourg, M. Y. *J. Am. Chem. Soc.* **2005**, *127*, 17323-17334.

30. Mills, D. K.; Hsiao, Y. M.; Farmer, P. J.; Atnip, E. V.; Reibenspies, J. H.; Darensbourg, M. Y. *J. Am. Chem. Soc.* **1991**, *113*, 1421-1423.

31. Tuntulani, T.; Reibenspies, J. H.; Farmer, P. J.; Darensbourg, M. Y. *Inorg. Chem.* **1992**, *31*, 3497-3499.

32. Musie, G.; Reibenspies, J. H.; Darensbourg, M. Y. *Inorg. Chem.* **1998**, *37*, 302-310.

33. Darnault, C.; Volbeda, A.; Kim, E. J.; Legrand, P.; Vernede, X.; Lindahl, P. A.; Fontecilla-Camps, J. C. *Nature Structural Biology* **2003**, *10*, 271.

34. Tolman, C. A. *Chem. Rev.* **1977**, *77*, 313-348.

35. Hess, J. L.; Conder, H. L.; Green, K. N.; Darensbourg, M. Y. *Inorg. Chem.* **2008**, *47*, 2056-2063.

36. Jeffrey, J. C.; Rauchfuss, T. B. *Inorg. Chem.* **1979**, *18*, 2658-2666.

37. Phelps, A. L.; Rampersad, M. V.; Fitch, S. B.; Darensbourg, M. Y.; Darensbourg, D. J. *Inorg. Chem.* **2005**, *45*, 119-126.

38. Jeffery, S. P.; Lee, J.; Darensbourg, M. Y. *Chem. Commun. (Cambridge, U. K.)* **2005**, *0*, 1122-1124.

39. Jeffery, S. P.; Green, K. N.; Rampersad, M. V.; Reibenspies, J. H.; Darensbourg, M. Y. *Dalton Trans.* **2006**, *0*, 4244-4252.

40. Golden, Melissa L.; Jeffery, Stephen P.; Miller, Matthew L.; Reibenspies, Joseph H.; Darensbourg, Marcetta Y. *Eur. J. Inorg. Chem.* **2004**, *2004*, 231-236.

41. Amoroso, A. J.; Chung, S. S. M.; Spencer, D. J. E.; Danks, J. P.; Glenny, M. W.; Blake, A. J.; Cooke, P. A.; Wilson, C.; Schroder, M. *Chem. Commun. (Cambridge, U. K.)* **2003**, *0*, 2020-2021.

42. Hatlevik, Ø.; Blanksma, M.; Mathrubootham, V.; Arif, A.; Hegg, E. *JBIC Journal of Biological Inorganic Chemistry* **2004**, *9*, 238-246.

43. Cotton, F. A. W., R. A. *Multiple Bonds Between Metal Atoms, 2nd ed*; Oxford University Press: Oxford, England, 1993.

44. Golden, M. L.; Rampersad, M. V.; Reibenspies, J. H.; Darensbourg, M. Y. *Chem. Commun. (Cambridge, U. K.)* **2003**, *0*, 1824-1825.

45. Golden, M. L.; Whaley, C. M.; Rampersad, M. V.; Reibenspies, J. H.; Hancock, R. D.; Darensbourg, M. Y. *Inorg. Chem.* **2005**, *44*, 875-883.

46. Hess, J. L.; Young, M. D.; Murillo, C. A.; Darensbourg, M. Y. *J. Mol. Struct.* **2008**, *890*, 70-74.

47. Krishnan, R.; Voo, J. K.; Riordan, C. G.; Zahkarov, L.; Rheingold, A. L. *J. Am. Chem. Soc.* **2003**, *125*, 4422-4423.

48. Bharadwaj, P. K.; John, E.; Xie, C. L.; Zhang, D.; Hendrickson, D. N.; Potenza, J. A.; Schugar, H. J. *Inorg. Chem.* **1986**, *25*, 4541-4546.

49. Rao, P. V.; Bhaduri, S.; Jiang, J.; Holm, R. H. *Inorg. Chem.* **2004**, *43*, 5833-5849.

50. Stibrany, R. T.; Fikar, R.; Brader, M.; Potenza, M. N.; Potenza, J. A.; Schugar, H. J. *Inorg. Chem.* **2002**, *41*, 5203-5215.

51. APEX2, version 7-0; Bruker AXS, Inc.: Madison, WI, 2009.

52. SAINTPLUS; 1034 version 6.63 ed.; Bruker AXS Inc: Madison, WI, 2007.

53. Sheldrick, G.; *SADABS Program for Absorption Correction Area Detector Frames;* Bruker AXS Inc: Madison, WI, 1999.

54. Sheldrick, G. *SHELXS-97, Program for Crytal Structure Soloution;* Institut fur Anorganische Chemie der Universitat Gottingen: Gottingen, Germany, 1997.

55. Sheldrick, G. S. *SHELXL-97, Program for Crytal Structure Refinement;* Institut fur Anorganische Chemie der Universitat Gottingen: Gottingen, Germany, 1997.

56. Volbeda, A. C., M.-H.; Piras, C.; Hatchilian, E. C.; Frey, M.; Fontecilla-Camps, J. C. *Nature* **1995**, *373*, 580-587.

57. Ito, M.; Kotera, M.; Matsumoto, T.; Tatsumi, K. *Proceedings of the National Academy of Sciences* **2009**, *106*, 11862-11866.

58. Ogo, S.; Kabe, R.; Uehara, K.; Kure, B.; Nishimura, T.; Menon, S. C.; Harada, R.; Fukuzumi, S.; Higuchi, Y.; Ohhara, T.; Tamada, T.; Kuroki, R. *Science* **2007**, *316*, 585-587.

59. Lai, C.-H.; Reibenspies, J. H.; Darensbourg, M. Y. *Angewandte Chemie International Edition in English* **1996**, *35*, 2390-2393.

60. Deák, A.; Megyes, T.; Tárkányi, G.; Király, P.; Biczók, L.; Pálinkás, G.; Stang, P. J. *J. Am. Chem. Soc.* **2006**, *128*, 12668-12670.

61. Ho, S. Y.; Cheng, E. C.-C.; Tiekink, E. R. T.; Yam, V. W.-W. *Inorg. Chem.* **2006**, *45*, 8165-8174.

62. Schmidbaur, H.; Schier, A. *Chem. Soc. Rev.* **2012**, *41*, 370-412.

63. Wang, S.; Fackler, J. P. *Inorg. Chem.* **1990**, *29*, 4404-4407.

64. Sutton, B. M.; McGusty, E.; Walz, D. T.; DiMartino, M. J. *J. Med. Chem.* **1972**, *15*, 1095-1098.

65. Taylor, P. C. *Curr. Opin. Pharmacol.* **2003**, *3*, 323-328.

66. Ott, I. *Coord. Chem. Rev.* **2009**, *253*, 1670-1681.

67. Watson, I. D. G.; Toste, F. D. *Chemical Science* **2012**, *3*, 2899-2919.

68. Tkatchouk, E.; Mankad, N. P.; Benitez, D.; Goddard, W. A.; Toste, F. D. *J. Am. Chem. Soc.* **2011**, *133*, 14293-14300.

69. Oliver-Meseguer, J.; Cabrero-Antonino, J. R.; Domínguez, I.; Leyva-Pérez, A.; Corma, A. *Science* **2012**, *338*, 1452-1455.

70. Taguchi, M.; Igashira-Kamiyama, A.; Kajiwara, T.; Konno, T. *Angewandte Chemie International Edition* **2007**, *46*, 2422-2425.

71. Konno, T.; Usami, M.; Toyota, A.; Hirotsu, M.; Kawamoto, T. *Chem. Lett.* **2005**, *34*, 1146-1147.

72. Lyon, E. J.; Musie, G.; Reibenspies, J. H.; Darensbourg, M. Y. *Inorg. Chem.* **1998**, *37*, 6942-6946.

73. Duff, S. E.; Barclay, J. E.; Davies, S. C.; Evans, D. J. *Inorg. Chem. Commun.* **2005**, *8*, 170-173.

74. Lever, A. B. P. *Inorganic Electronic Spectroscopy*; Elsevier: Amsterdam, 1968.

75. Musie, G.; Farmer, P. J.; Tuntulani, T.; Reibenspies, J. H.; Darensbourg, M. Y. *Inorg. Chem.* **1996**, *35*, 2176-2183.

76. Mohamed, A. A.; Bruce, A. E.; Bruce, M. R. M. *Metal-Based Drugs* **1999**, *6*, 233-238.

77. Zhu, W.; Marr, A. C.; Wang, Q.; Neese, F.; Spencer, D. J. E.; Blake, A. J.; Cooke, P. A.; Wilson, C.; Schröder, M. *Proc. Natl. Acad. Sci. U. S. A.* **2005**, *102*, 18280-18285.

78. Verhagen, Johanna A. W.; Lutz, M.; Spek, Anthony L.; Bouwman, E. *Eur. J. Inorg. Chem.* **2003**, *2003*, 3968-3974.

79. Liaw, W.-F.; Chiang, C.-Y.; Lee, G.-H.; Peng, S.-M.; Lai, C.-H.; Darensbourg, M. Y. *Inorg. Chem.* **2000**, *39*, 480-484.

80. Peters, J. W.; Lanzilotta, W. N.; Lemon, B. J.; Seefeldt, L. C. *Science* **1998**, *282*, 1853-1858.

81. Wang, Q.; Blake, A. J.; Davies, E. S.; McInnes, E. J. L.; Wilson, C.; Schroder, M. *Chem. Commun. (Cambridge, U. K.)* **2003**, 3012-3013.

82. Webster, C. E.; Darensbourg, M. Y.; Lindahl, P. A.; Hall, M. B. *J. Am. Chem. Soc.* **2004**, *126*, 3410-3411.

83. Amara, P.; Volbeda, A.; Fontecilla-Camps, J. C.; Field, M. J. *J. Am. Chem. Soc.* **2005**, *127*, 2776-2784.

84. Grapperhaus, C. A.; Darensbourg, M. Y. *Acc. Chem. Res.* **1998**, *31*, 451-459.

85. Osterloh, F.; Saak, W.; Haase, D.; Pohl, S. *Chem. Commun. (Cambridge, U. K.)* **1997**, *0*, 979-980.

86. Almaraz, E.; Foley, W. S.; Denny, J. A.; Reibenspies, J. H.; Golden, M. L.; Darensbourg, M. Y. *Inorg. Chem.* **2009**, *48*, 5288-5295.

87. Hsieh, C.-H.; Chupik, R. B.; Brothers, S. M.; Hall, M. B.; Darensbourg, M. Y. *Dalton Trans.* **2011**, *40*, 6047-6053.

88. Hansen, L.; Xu, X.; Lipowska, M.; Taylor, A.; Marzilli, L. G. *Inorg. Chem.* **1999**, *38*, 2890-2897.

89. Rao, T. N.; Adhikesavalu, D.; Camerman, A.; Fritzberg, A. R. *J. Am. Chem. Soc.* **1990**, *112*, 5798-5804.

90. Vanin, A. F. *Biochemistry (Moscow)* **1998**, *63*, 782-793.

91. Vanin, A. F.; Poltorakov, A. P.; Mikoyan, V. D.; Kubrina, L. N.; Burbaev, D. S. *Nitric Oxide* **2010**, *23*, 136-149.

92. Enemark, J. H.; Feltham, R. D. *Coord. Chem. Rev.* **1974**, *13*, 339-406.

93. Vanin, A. F. *Nitric Oxide* **2009**, *21*, 1-13.

94. Foster, M. W.; Cowan, J. A. *J. Am. Chem. Soc.* **1999**, *121*, 4093-4100.

95. Hess, J. L.; Hsieh, C.-H.; Reibenspies, J. H.; Darensbourg, M. Y. *Inorg. Chem.* **2011**, *50*, 8541-8552.

96. Tinberg, C. E.; Tonzetich, Z. J.; Wang, H.; Do, L. H.; Yoda, Y.; Cramer, S. P.; Lippard, S. J. *J. Am. Chem. Soc.* **2010**, *132*, 18168-18176.

97. Hung, M.-C.; Tsai, M.-C.; Lee, G.-H.; Liaw, W.-F. *Inorg. Chem.* **2006**, *45*, 6041-6047.

98. Tsai, M.-L.; Hsieh, C.-H.; Liaw, W.-F. *Inorg. Chem.* **2007**, *46*, 5110-5117.

99. Wang, J.-H.; Chen, C.-H. *Inorg. Chem.* **2010**, *49*, 7644-7646.

100. Hsieh, C.-H.; Darensbourg, M. Y. *J. Am. Chem. Soc.* **2010**, *132*, 14118-14125.

101. Anderson, J.; Anderson, W.; Hieber, J.; Mitarbeitern *Zeitschrift für anorganische Chemie (1892)* **1932**, *208*, 238-248.

102. Darensbourg, D. J.; Kump, R. L. *Inorg. Chem.* **1978**, *17*, 2680-2682.

103. Bryar, T. R.; Eaton, D. R. *Can. J. Chem.* **1992**, *70*, 1917-1926.

104. Arakawa, T.; Kawano, Y.; Kataoka, S.; Katayama, Y.; Kamiya, N.; Yohda, M.; Odaka, M. *J. Mol. Biol.* **2007**, *366*, 1497-1509.

105. Hashimoto, K.; Suzuki, H.; Taniguchi, K.; Noguchi, T.; Yohda, M.; Odaka, M. *J. Biol. Chem.* **2008**, *283*, 36617-36623.

106. Monga, V.; Thompson, K. H.; Yuen, V. G.; Sharma, V.; Patrick, B. O.; McNeill, J. H.; Orvig, C. *Inorg. Chem.* **2005**, *44*, 2678-2688.

APPENDIX

CRYSTALLOGRAPHIC DATA FOR STRUCTURES

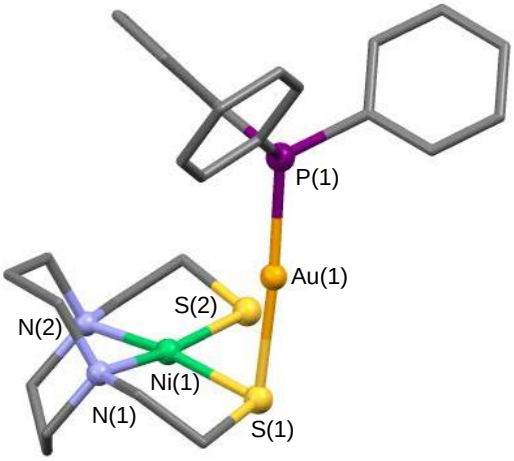

[{Ni(bme-daco)AuPPh$_3$}]$^+$(Cl$^-$)

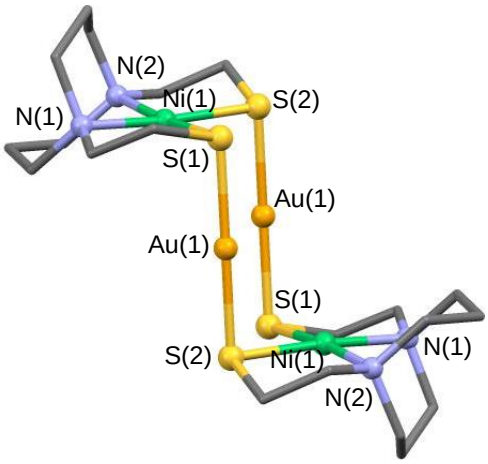

[Au$_2${Ni(bme-daco)}$_2$]$^{2+}$(Cl$^-$)$_2$

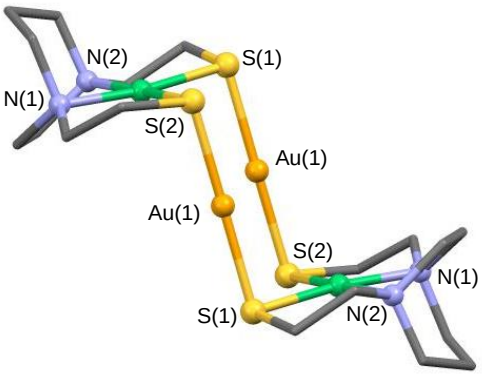

[Au$_2${Ni(bme-dach)}$_2$]$^{2+}$(Cl$^-$)$_2$

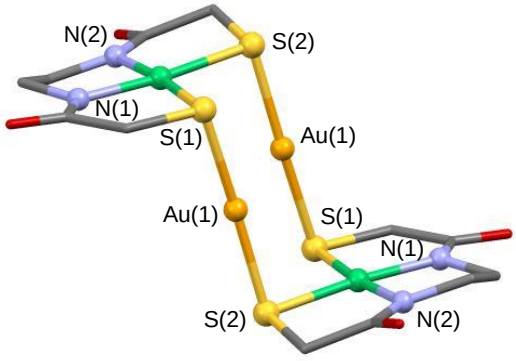

(Et$_4$N$^+$)$_2$ [Au$_2${Ni(ema)}$_2$]$^{2-}$

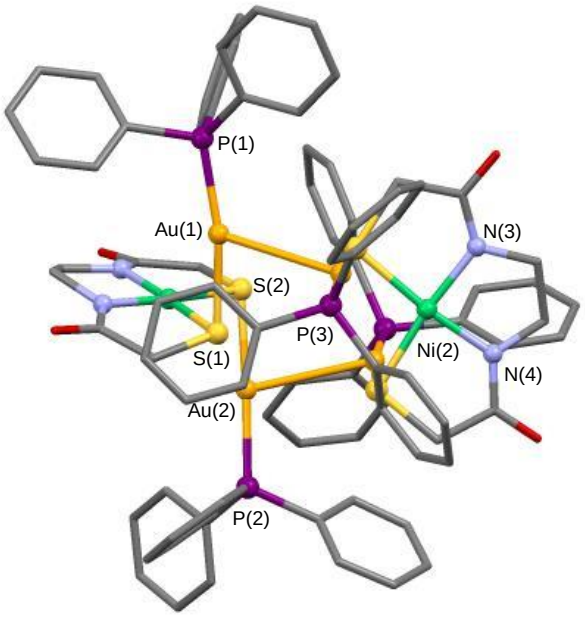

$[\{Ni(ema)\}_2Au_4(PPh_3)_4]$

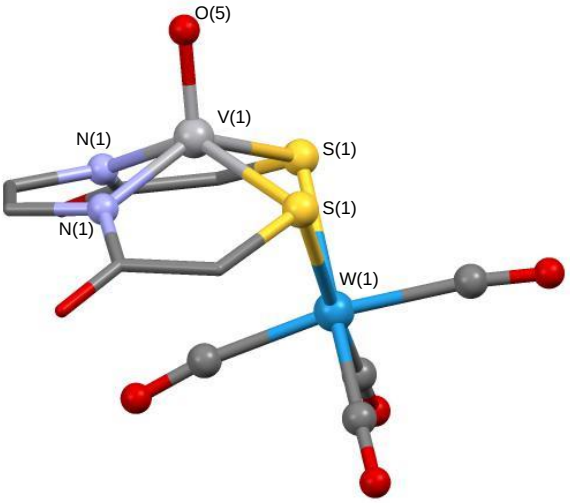

$[Et_4N^+]_2[V{\equiv}O(ema)W(CO)_4]^{2-}$

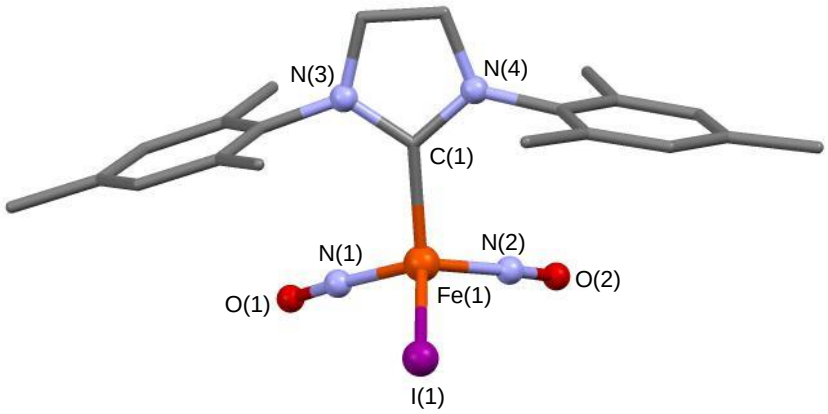

(IMes)Fe(NO)$_2$I

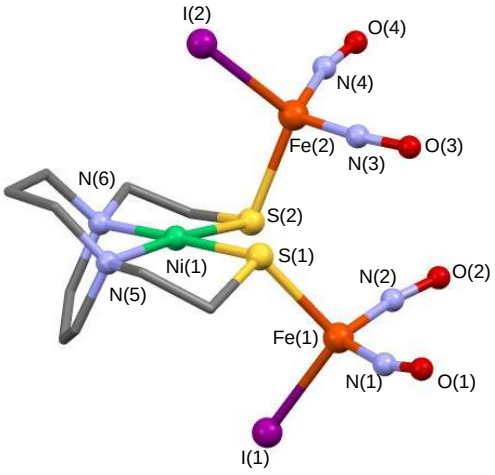

[Ni(bme-daco)•(Fe(NO)$_2$I)$_2$]

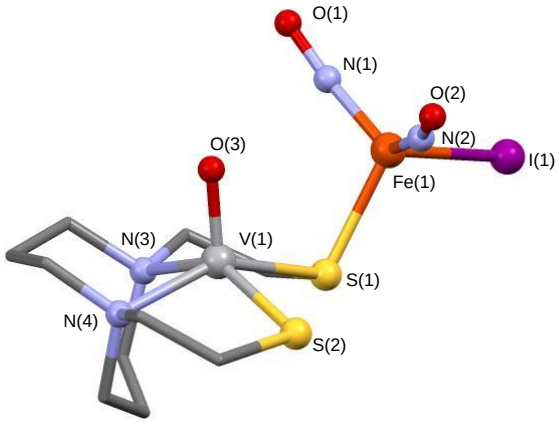

[V≡O(bme-daco)•Fe(NO)$_2$I]

Table A-1. Crystal data and structure refinement for [{Ni(bme-daco)}$AuPPh_3]^+$ Cl^-.

Identification code	datax	
Empirical formula	C28 H37 Au Cl N2 Ni O P S2	
Formula weight	803.81	
Temperature	110(2) K	
Wavelength	0.71073 Å	
Crystal system	Monoclinic	
Space group	P21/c	
Unit cell dimensions	a = 16.697(3) Å	α = 90°.
	b = 11.0833(19) Å	β = 102.978(2)°.
	c = 16.059(3) Å	γ = 90°.
Volume	2896.1(8) $Å^3$	
Z	4	
Density (calculated)	1.844 Mg/m^3	
Absorption coefficient	6.027 mm^{-1}	
F(000)	1592	
Crystal size	0.11 x 0.10 x 0.08 mm^3	
Theta range for data collection	2.22 to 28.33°.	
Index ranges	-22<=h<=22, -14<=k<=14, -21<=l<=21	
Reflections collected	33863	
Independent reflections	7153 [R(int) = 0.0370]	
Completeness to theta = 28.33°	99.0 %	
Absorption correction	Semi-empirical from equivalents	
Max. and min. transmission	0.6442 and 0.5569	
Refinement method	Full-matrix least-squares on F^2	
Data / restraints / parameters	7153 / 0 / 342	
Goodness-of-fit on F^2	1.075	
Final R indices [I>2sigma(I)]	R1 = 0.0214, wR2 = 0.0508	
R indices (all data)	R1 = 0.0244, wR2 = 0.0517	
Largest diff. peak and hole	0.813 and -1.292 e.$Å^{-3}$	

Table A-2. Bond lengths [Å] and angles [°] for [{Ni(bme-daco)}$AuPPh_3$]$^+$ Cl^- .

Au(1)-P(1)	2.2542(7)	C(6)-C(7)	1.508(4)
Au(1)-S(1)	2.3329(7)	C(6)-H(6A)	0.9900
Au(1)-Ni(1)	2.9533(6)	C(6)-H(6B)	0.9900
Ni(1)-N(2)	1.974(2)	C(7)-H(7A)	0.9900
Ni(1)-N(1)	1.980(2)	C(7)-H(7B)	0.9900
Ni(1)-S(2)	2.1706(8)	C(8)-C(9)	1.524(4)
Ni(1)-S(1)	2.1854(7)	C(8)-H(8A)	0.9900
S(1)-C(1)	1.829(3)	C(8)-H(8B)	0.9900
S(2)-C(3)	1.820(3)	C(9)-C(10)	1.523(4)
N(1)-C(5)	1.502(3)	C(9)-H(9A)	0.9900
N(1)-C(8)	1.503(3)	C(9)-H(9B)	0.9900
N(1)-C(2)	1.506(3)	C(10)-H(10A)	0.9900
N(2)-C(4)	1.506(3)	C(10)-H(10B)	0.9900
N(2)-C(7)	1.508(3)	C(11)-C(16)	1.394(3)
N(2)-C(10)	1.509(3)	C(11)-C(12)	1.399(3)
P(1)-C(11)	1.807(2)	C(12)-C(13)	1.389(4)
P(1)-C(23)	1.811(2)	C(12)-H(12)	0.9500
P(1)-C(17)	1.815(2)	C(13)-C(14)	1.383(4)
C(1)-C(2)	1.501(4)	C(13)-H(13)	0.9500
C(1)-H(1A)	0.9900	C(14)-C(15)	1.389(4)
C(1)-H(1B)	0.9900	C(14)-H(14)	0.9500
C(2)-H(2A)	0.9900	C(15)-C(16)	1.389(4)
C(2)-H(2B)	0.9900	C(15)-H(15)	0.9500
C(3)-C(4)	1.504(4)	C(16)-H(16)	0.9500
C(3)-H(3A)	0.9900	C(17)-C(22)	1.393(3)
C(3)-H(3B)	0.9900	C(17)-C(18)	1.397(3)
C(4)-H(4A)	0.9900	C(18)-C(19)	1.390(4)
C(4)-H(4B)	0.9900	C(18)-H(18)	0.9500
C(5)-C(6)	1.513(3)	C(19)-C(20)	1.385(4)
C(5)-H(5A)	0.9900	C(19)-H(19)	0.9500
C(5)-H(5B)	0.9900	C(20)-C(21)	1.387(4)

C(20)-H(20)	0.9500	C(3)-S(2)-Ni(1)	96.92(9)
C(21)-C(22)	1.383(4)	C(5)-N(1)-C(8)	111.53(19)
C(21)-H(21)	0.9500	C(5)-N(1)-C(2)	105.16(18)
C(22)-H(22)	0.9500	C(8)-N(1)-C(2)	109.14(19)
C(23)-C(28)	1.392(3)	C(5)-N(1)-Ni(1)	108.02(15)
C(23)-C(24)	1.397(3)	C(8)-N(1)-Ni(1)	110.74(15)
C(24)-C(25)	1.380(3)	C(2)-N(1)-Ni(1)	112.15(15)
C(24)-H(24)	0.9500	C(4)-N(2)-C(7)	109.2(2)
C(25)-C(26)	1.393(4)	C(4)-N(2)-C(10)	107.7(2)
C(25)-H(25)	0.9500	C(7)-N(2)-C(10)	109.6(2)
C(26)-C(27)	1.390(4)	C(4)-N(2)-Ni(1)	110.35(16)
C(26)-H(26)	0.9500	C(7)-N(2)-Ni(1)	108.47(15)
C(27)-C(28)	1.386(3)	C(10)-N(2)-Ni(1)	111.47(16)
C(27)-H(27)	0.9500	C(11)-P(1)-C(23)	105.64(11)
C(28)-H(28)	0.9500	C(11)-P(1)-C(17)	105.11(11)
O(1)-H(1)	0.79(5)	C(23)-P(1)-C(17)	105.00(11)
O(1)-H(2)	0.81(5)	C(11)-P(1)-Au(1)	114.19(8)
		C(23)-P(1)-Au(1)	110.46(8)
P(1)-Au(1)-S(1)	176.16(2)	C(17)-P(1)-Au(1)	115.56(8)
P(1)-Au(1)-Ni(1)	129.446(17)	C(2)-C(1)-S(1)	108.65(17)
S(1)-Au(1)-Ni(1)	47.052(17)	C(2)-C(1)-H(1A)	110.0
N(2)-Ni(1)-N(1)	90.69(9)	S(1)-C(1)-H(1A)	110.0
N(2)-Ni(1)-S(2)	91.18(7)	C(2)-C(1)-H(1B)	110.0
N(1)-Ni(1)-S(2)	170.72(6)	S(1)-C(1)-H(1B)	110.0
N(2)-Ni(1)-S(1)	171.05(6)	H(1A)-C(1)-H(1B)	108.3
N(1)-Ni(1)-S(1)	90.52(6)	C(1)-C(2)-N(1)	111.2(2)
S(2)-Ni(1)-S(1)	89.05(3)	C(1)-C(2)-H(2A)	109.4
N(2)-Ni(1)-Au(1)	137.36(6)	N(1)-C(2)-H(2A)	109.4
N(1)-Ni(1)-Au(1)	93.21(6)	C(1)-C(2)-H(2B)	109.4
S(2)-Ni(1)-Au(1)	79.30(2)	N(1)-C(2)-H(2B)	109.4
S(1)-Ni(1)-Au(1)	51.385(18)	H(2A)-C(2)-H(2B)	108.0
C(1)-S(1)-Ni(1)	97.53(9)	C(4)-C(3)-S(2)	106.78(19)
C(1)-S(1)-Au(1)	106.57(9)	C(4)-C(3)-H(3A)	110.4
Ni(1)-S(1)-Au(1)	81.56(2)	S(2)-C(3)-H(3A)	110.4

C(4)-C(3)-H(3B)	110.4	C(10)-C(9)-H(9A)	108.2
S(2)-C(3)-H(3B)	110.4	C(8)-C(9)-H(9A)	108.2
H(3A)-C(3)-H(3B)	108.6	C(10)-C(9)-H(9B)	108.2
C(3)-C(4)-N(2)	111.2(2)	C(8)-C(9)-H(9B)	108.2
C(3)-C(4)-H(4A)	109.4	H(9A)-C(9)-H(9B)	107.4
N(2)-C(4)-H(4A)	109.4	N(2)-C(10)-C(9)	113.0(2)
C(3)-C(4)-H(4B)	109.4	N(2)-C(10)-H(10A)	109.0
N(2)-C(4)-H(4B)	109.4	C(9)-C(10)-H(10A)	109.0
H(4A)-C(4)-H(4B)	108.0	N(2)-C(10)-H(10B)	109.0
N(1)-C(5)-C(6)	115.0(2)	C(9)-C(10)-H(10B)	109.0
N(1)-C(5)-H(5A)	108.5	H(10A)-C(10)-H(10B)	107.8
C(6)-C(5)-H(5A)	108.5	C(16)-C(11)-C(12)	119.7(2)
N(1)-C(5)-H(5B)	108.5	C(16)-C(11)-P(1)	121.29(18)
C(6)-C(5)-H(5B)	108.5	C(12)-C(11)-P(1)	118.96(18)
H(5A)-C(5)-H(5B)	107.5	C(13)-C(12)-C(11)	119.7(2)
C(7)-C(6)-C(5)	114.2(2)	C(13)-C(12)-H(12)	120.1
C(7)-C(6)-H(6A)	108.7	C(11)-C(12)-H(12)	120.1
C(5)-C(6)-H(6A)	108.7	C(14)-C(13)-C(12)	120.2(2)
C(7)-C(6)-H(6B)	108.7	C(14)-C(13)-H(13)	119.9
C(5)-C(6)-H(6B)	108.7	C(12)-C(13)-H(13)	119.9
H(6A)-C(6)-H(6B)	107.6	C(13)-C(14)-C(15)	120.4(2)
C(6)-C(7)-N(2)	113.3(2)	C(13)-C(14)-H(14)	119.8
C(6)-C(7)-H(7A)	108.9	C(15)-C(14)-H(14)	119.8
N(2)-C(7)-H(7A)	108.9	C(16)-C(15)-C(14)	119.8(2)
C(6)-C(7)-H(7B)	108.9	C(16)-C(15)-H(15)	120.1
N(2)-C(7)-H(7B)	108.9	C(14)-C(15)-H(15)	120.1
H(7A)-C(7)-H(7B)	107.7	C(15)-C(16)-C(11)	120.2(2)
N(1)-C(8)-C(9)	113.3(2)	C(15)-C(16)-H(16)	119.9
N(1)-C(8)-H(8A)	108.9	C(11)-C(16)-H(16)	119.9
C(9)-C(8)-H(8A)	108.9	C(22)-C(17)-C(18)	119.8(2)
N(1)-C(8)-H(8B)	108.9	C(22)-C(17)-P(1)	118.28(19)
C(9)-C(8)-H(8B)	108.9	C(18)-C(17)-P(1)	121.80(18)
H(8A)-C(8)-H(8B)	107.7	C(19)-C(18)-C(17)	119.8(2)
C(10)-C(9)-C(8)	116.3(2)	C(19)-C(18)-H(18)	120.1

C(17)-C(18)-H(18)	120.1	C(25)-C(24)-C(23)	120.2(2)
C(20)-C(19)-C(18)	120.0(3)	C(25)-C(24)-H(24)	119.9
C(20)-C(19)-H(19)	120.0	C(23)-C(24)-H(24)	119.9
C(18)-C(19)-H(19)	120.0	C(24)-C(25)-C(26)	119.8(2)
C(19)-C(20)-C(21)	120.3(2)	C(24)-C(25)-H(25)	120.1
C(19)-C(20)-H(20)	119.8	C(26)-C(25)-H(25)	120.1
C(21)-C(20)-H(20)	119.8	C(27)-C(26)-C(25)	120.1(2)
C(22)-C(21)-C(20)	120.1(3)	C(27)-C(26)-H(26)	119.9
C(22)-C(21)-H(21)	119.9	C(25)-C(26)-H(26)	119.9
C(20)-C(21)-H(21)	119.9	C(28)-C(27)-C(26)	120.1(3)
C(21)-C(22)-C(17)	120.0(2)	C(28)-C(27)-H(27)	119.9
C(21)-C(22)-H(22)	120.0	C(26)-C(27)-H(27)	119.9
C(17)-C(22)-H(22)	120.0	C(27)-C(28)-C(23)	119.8(2)
C(28)-C(23)-C(24)	119.8(2)	C(27)-C(28)-H(28)	120.1
C(28)-C(23)-P(1)	122.66(18)	C(23)-C(28)-H(28)	120.1
C(24)-C(23)-P(1)	117.49(18)	H(1)-O(1)-H(2)	109(4)

Symmetry transformations used to generate equivalent atoms:

Table A-3. Crystal data and structure refinement for $[Au_2\{Ni(bme\text{-}daco)\}_2]^{2+}(Cl^-)_2$.

Identification code	041213nibmedacoapph3inmeoh_0m-sr	
Empirical formula	C22 H48 Au2 Cl2 N4 Ni2 O2 S4	
Formula weight	1111.14	
Temperature	110(2) K	
Wavelength	0.71073 Å	
Crystal system	Monoclinic	
Space group	P21/c	
Unit cell dimensions	a = 8.661(2) Å	α = 90°.
	b = 15.988(4) Å	β = 100.346(3)°.
	c = 13.637(3) Å	γ = 90°.
Volume	1857.5(8) $Å^3$	
Z	2	
Density (calculated)	1.987 Mg/m^3	
Absorption coefficient	9.265 mm^{-1}	
F(000)	1072	
Crystal size	0.30 x 0.10 x 0.10 mm^3	
Theta range for data collection	1.98 to 28.28°.	
Index ranges	-11<=h<=11, 0<=k<=21, 0<=l<=18	
Reflections collected	4584	
Independent reflections	4584 [R(int) = 0.0000]	
Completeness to theta = 28.28°	99.4 %	
Absorption correction	Semi-empirical from equivalents	
Max. and min. transmission	0.4576 and 0.1676	
Refinement method	Full-matrix least-squares on F^2	
Data / restraints / parameters	4584 / 0 / 174	
Goodness-of-fit on F^2	1.049	
Final R indices [I>2sigma(I)]	R1 = 0.0198, wR2 = 0.0474	
R indices (all data)	R1 = 0.0234, wR2 = 0.0483	
Largest diff. peak and hole	1.041 and -1.301 $e.Å^{-3}$	

Table A-4. Bond lengths [Å] and angles [°] for $[Au_2\{Ni(bme\text{-}daco)\}_2]^{2+}(Cl^-)_2$.

Au(1)-S(2)#1	2.3000(8)	C(6)-H(6A)	0.9700
Au(1)-S(1)	2.3040(8)	C(6)-H(6B)	0.9700
Au(1)-Au(1)#1	3.1273(5)	C(7)-H(7A)	0.9700
Au(1)-Ni(1)	3.1782(6)	C(7)-H(7B)	0.9700
Ni(1)-N(2)	1.968(2)	C(8)-C(9)	1.507(4)
Ni(1)-N(1)	1.985(2)	C(8)-H(8A)	0.9700
Ni(1)-S(1)	2.1800(8)	C(8)-H(8B)	0.9700
Ni(1)-S(2)	2.1921(9)	C(9)-C(10)	1.510(4)
N(1)-C(8)	1.500(3)	C(9)-H(9A)	0.9700
N(1)-C(2)	1.504(3)	C(9)-H(9B)	0.9700
N(1)-C(7)	1.509(3)	C(10)-H(10A)	0.9700
N(2)-C(4)	1.498(3)	C(10)-H(10B)	0.9700
N(2)-C(10)	1.504(3)	C(11)-O(1)	1.413(3)
N(2)-C(5)	1.511(3)	C(11)-H(11A)	0.9600
S(1)-C(1)	1.829(3)	C(11)-H(11B)	0.9600
S(2)-C(3)	1.827(3)	C(11)-H(11C)	0.9600
S(2)-Au(1)#1	2.3000(8)	O(1)-H(1)	0.8200
C(1)-C(2)	1.505(4)		
C(1)-H(1A)	0.9700	S(2)#1-Au(1)-S(1)	177.98(2)
C(1)-H(1B)	0.9700	S(2)#1-Au(1)-Au(1)#1	87.601(19)
C(2)-H(2A)	0.9700	S(1)-Au(1)-Au(1)#1	90.47(2)
C(2)-H(2B)	0.9700	S(2)#1-Au(1)-Ni(1)	134.891(19)
C(3)-C(4)	1.501(4)	S(1)-Au(1)-Ni(1)	43.308(18)
C(3)-H(3A)	0.9700	Au(1)#1-Au(1)-Ni(1)	61.631(14)
C(3)-H(3B)	0.9700	N(2)-Ni(1)-N(1)	90.47(8)
C(4)-H(4A)	0.9700	N(2)-Ni(1)-S(1)	174.46(6)
C(4)-H(4B)	0.9700	N(1)-Ni(1)-S(1)	90.44(6)
C(5)-C(6)	1.523(3)	N(2)-Ni(1)-S(2)	90.17(6)
C(5)-H(5A)	0.9700	N(1)-Ni(1)-S(2)	175.23(7)
C(5)-H(5B)	0.9700	S(1)-Ni(1)-S(2)	88.47(3)
C(6)-C(7)	1.530(3)	N(2)-Ni(1)-Au(1)	138.87(6)

N(1)-Ni(1)-Au(1)	94.42(6)	C(4)-C(3)-H(3A)	110.1
S(1)-Ni(1)-Au(1)	46.46(2)	S(2)-C(3)-H(3A)	110.1
S(2)-Ni(1)-Au(1)	88.20(2)	C(4)-C(3)-H(3B)	110.1
C(8)-N(1)-C(2)	104.81(19)	S(2)-C(3)-H(3B)	110.1
C(8)-N(1)-C(7)	109.89(19)	H(3A)-C(3)-H(3B)	108.5
C(2)-N(1)-C(7)	110.0(2)	N(2)-C(4)-C(3)	111.8(2)
C(8)-N(1)-Ni(1)	113.50(16)	N(2)-C(4)-H(4A)	109.2
C(2)-N(1)-Ni(1)	111.96(15)	C(3)-C(4)-H(4A)	109.2
C(7)-N(1)-Ni(1)	106.71(15)	N(2)-C(4)-H(4B)	109.2
C(4)-N(2)-C(10)	104.50(19)	C(3)-C(4)-H(4B)	109.2
C(4)-N(2)-C(5)	109.87(18)	H(4A)-C(4)-H(4B)	107.9
C(10)-N(2)-C(5)	110.40(19)	N(2)-C(5)-C(6)	113.8(2)
C(4)-N(2)-Ni(1)	112.47(15)	N(2)-C(5)-H(5A)	108.8
C(10)-N(2)-Ni(1)	113.53(15)	C(6)-C(5)-H(5A)	108.8
C(5)-N(2)-Ni(1)	106.12(15)	N(2)-C(5)-H(5B)	108.8
C(1)-S(1)-Ni(1)	98.35(8)	C(6)-C(5)-H(5B)	108.8
C(1)-S(1)-Au(1)	106.11(10)	H(5A)-C(5)-H(5B)	107.7
Ni(1)-S(1)-Au(1)	90.23(3)	C(5)-C(6)-C(7)	118.6(2)
C(3)-S(2)-Ni(1)	97.82(9)	C(5)-C(6)-H(6A)	107.7
C(3)-S(2)-Au(1)#1	105.62(9)	C(7)-C(6)-H(6A)	107.7
Ni(1)-S(2)-Au(1)#1	91.93(3)	C(5)-C(6)-H(6B)	107.7
C(2)-C(1)-S(1)	108.48(18)	C(7)-C(6)-H(6B)	107.7
C(2)-C(1)-H(1A)	110.0	H(6A)-C(6)-H(6B)	107.1
S(1)-C(1)-H(1A)	110.0	N(1)-C(7)-C(6)	112.8(2)
C(2)-C(1)-H(1B)	110.0	N(1)-C(7)-H(7A)	109.0
S(1)-C(1)-H(1B)	110.0	C(6)-C(7)-H(7A)	109.0
H(1A)-C(1)-H(1B)	108.4	N(1)-C(7)-H(7B)	109.0
N(1)-C(2)-C(1)	111.8(2)	C(6)-C(7)-H(7B)	109.0
N(1)-C(2)-H(2A)	109.2	H(7A)-C(7)-H(7B)	107.8
C(1)-C(2)-H(2A)	109.2	N(1)-C(8)-C(9)	114.7(2)
N(1)-C(2)-H(2B)	109.2	N(1)-C(8)-H(8A)	108.6
C(1)-C(2)-H(2B)	109.2	C(9)-C(8)-H(8A)	108.6
H(2A)-C(2)-H(2B)	107.9	N(1)-C(8)-H(8B)	108.6
C(4)-C(3)-S(2)	107.84(17)	C(9)-C(8)-H(8B)	108.6

H(8A)-C(8)-H(8B)	107.6	N(2)-C(10)-H(10B)	108.7
C(8)-C(9)-C(10)	113.1(2)	C(9)-C(10)-H(10B)	108.7
C(8)-C(9)-H(9A)	109.0	H(10A)-C(10)-H(10B)	107.6
C(10)-C(9)-H(9A)	109.0	O(1)-C(11)-H(11A)	109.5
C(8)-C(9)-H(9B)	109.0	O(1)-C(11)-H(11B)	109.5
C(10)-C(9)-H(9B)	109.0	H(11A)-C(11)-H(11B)	109.5
H(9A)-C(9)-H(9B)	107.8	O(1)-C(11)-H(11C)	109.5
N(2)-C(10)-C(9)	114.3(2)	H(11A)-C(11)-H(11C)	109.5
N(2)-C(10)-H(10A)	108.7	H(11B)-C(11)-H(11C)	109.5
C(9)-C(10)-H(10A)	108.7	C(11)-O(1)-H(1)	109.5

Symmetry transformations used to generate equivalent atoms:
#1 -x+1,-y,-z+1

Table A-5. Crystal data and structure refinement for $[Au_2\{Ni(bme\text{-}dach)\}_2]^{2+}(Cl^-)_2$.

Identification code	mdau	
Empirical formula	C10 H22 Au Cl N2 Ni O S2	
Formula weight	541.54	
Temperature	110(2) K	
Wavelength	1.54178 Å	
Crystal system	Monoclinic	
Space group	P2(1)/n	
Unit cell dimensions	a = 8.3017(7) Å	α = 90°.
	b = 8.6040(8) Å	β = 95.316(5)°.
	c = 21.8658(17) Å	γ = 90°.
Volume	1555.1(2) $Å^3$	
Z	4	
Density (calculated)	2.313 Mg/m^3	
Absorption coefficient	22.996 mm^{-1}	
F(000)	1040	
Crystal size	0.20 x 0.20 x 0.10 mm^3	
Theta range for data collection	5.53 to 64.01°.	
Index ranges	-9<=h<=9, -9<=k<=9, -24<=l<=25	
Reflections collected	25177	
Independent reflections	2554 [R(int) = 0.0626]	
Completeness to theta = 64.01°	99.0 %	
Absorption correction	Semi-empirical from equivalents	
Max. and min. transmission	0.2331 and 0.0259	
Refinement method	Full-matrix least-squares on F^2	
Data / restraints / parameters	2554 / 0 / 164	
Goodness-of-fit on F^2	1.006	
Final R indices [I>2sigma(I)]	R1 = 0.0251, wR2 = 0.0607	
R indices (all data)	R1 = 0.0292, wR2 = 0.0617	
Largest diff. peak and hole	0.797 and -1.532 $e.Å^{-3}$	

Table A-6. Bond lengths [Å] and angles [°] for $[Au_2\{Ni(bme\text{-}dach)\}_2]^{2+}(Cl^-)_2$.

Au(1)-S(2)#1	2.2946(13)	C(6)-H(6B)	0.9900
Au(1)-S(1)	2.2995(12)	C(7)-C(8)	1.531(7)
Au(1)-Au(1)#1	3.1103(5)	C(7)-H(7A)	0.9900
Ni(1)-N(2)	1.922(4)	C(7)-H(7B)	0.9900
Ni(1)-N(1)	1.926(4)	C(8)-C(9)	1.534(7)
Ni(1)-S(2)	2.1802(14)	C(8)-H(8A)	0.9900
Ni(1)-S(1)	2.1845(15)	C(8)-H(8B)	0.9900
S(1)-C(1)	1.848(5)	C(9)-H(9A)	0.9900
S(2)-C(5)	1.829(5)	C(9)-H(9B)	0.9900
S(2)-Au(1)#1	2.2946(13)	C(1ME)-H(1MA)	0.9800
O(1ME)-C(1ME)	1.418(7)	C(1ME)-H(1MB)	0.9800
O(1ME)-H(1ME)	0.8653	C(1ME)-H(1MC)	0.9800
N(1)-C(7)	1.498(6)		
N(1)-C(6)	1.498(6)	S(2)#1-Au(1)-S(1)	177.35(4)
N(1)-C(4)	1.503(6)	S(2)#1-Au(1)-Au(1)#1	90.33(3)
N(2)-C(3)	1.494(6)	S(1)-Au(1)-Au(1)#1	92.28(3)
N(2)-C(9)	1.495(7)	N(2)-Ni(1)-N(1)	82.57(17)
N(2)-C(2)	1.515(6)	N(2)-Ni(1)-S(2)	173.42(13)
C(1)-C(2)	1.489(7)	N(1)-Ni(1)-S(2)	91.03(13)
C(1)-H(1A)	0.9900	N(2)-Ni(1)-S(1)	91.34(13)
C(1)-H(1B)	0.9900	N(1)-Ni(1)-S(1)	172.17(13)
C(2)-H(2A)	0.9900	S(2)-Ni(1)-S(1)	94.90(6)
C(2)-H(2B)	0.9900	C(1)-S(1)-Ni(1)	96.90(17)
C(3)-C(4)	1.544(7)	C(1)-S(1)-Au(1)	103.18(18)
C(3)-H(3A)	0.9900	Ni(1)-S(1)-Au(1)	93.13(5)
C(3)-H(3B)	0.9900	C(5)-S(2)-Ni(1)	97.57(17)
C(4)-H(4A)	0.9900	C(5)-S(2)-Au(1)#1	105.16(17)
C(4)-H(4B)	0.9900	Ni(1)-S(2)-Au(1)#1	94.40(5)
C(5)-C(6)	1.512(7)	C(1ME)-O(1ME)-H(1ME)	133.1
C(5)-H(5A)	0.9900	C(7)-N(1)-C(6)	110.8(4)
C(5)-H(5B)	0.9900	C(7)-N(1)-C(4)	110.1(4)
C(6)-H(6A)	0.9900	C(6)-N(1)-C(4)	110.2(4)

C(7)-N(1)-Ni(1)	104.0(3)	C(6)-C(5)-H(5A)	109.8
C(6)-N(1)-Ni(1)	112.8(3)	S(2)-C(5)-H(5A)	109.8
C(4)-N(1)-Ni(1)	108.7(3)	C(6)-C(5)-H(5B)	109.8
C(3)-N(2)-C(9)	111.1(4)	S(2)-C(5)-H(5B)	109.8
C(3)-N(2)-C(2)	110.6(4)	H(5A)-C(5)-H(5B)	108.3
C(9)-N(2)-C(2)	109.6(4)	N(1)-C(6)-C(5)	110.0(4)
C(3)-N(2)-Ni(1)	107.6(3)	N(1)-C(6)-H(6A)	109.7
C(9)-N(2)-Ni(1)	106.4(3)	C(5)-C(6)-H(6A)	109.7
C(2)-N(2)-Ni(1)	111.6(3)	N(1)-C(6)-H(6B)	109.7
C(2)-C(1)-S(1)	108.9(3)	C(5)-C(6)-H(6B)	109.7
C(2)-C(1)-H(1A)	109.9	H(6A)-C(6)-H(6B)	108.2
S(1)-C(1)-H(1A)	109.9	N(1)-C(7)-C(8)	112.2(4)
C(2)-C(1)-H(1B)	109.9	N(1)-C(7)-H(7A)	109.2
S(1)-C(1)-H(1B)	109.9	C(8)-C(7)-H(7A)	109.2
H(1A)-C(1)-H(1B)	108.3	N(1)-C(7)-H(7B)	109.2
C(1)-C(2)-N(2)	109.8(4)	C(8)-C(7)-H(7B)	109.2
C(1)-C(2)-H(2A)	109.7	H(7A)-C(7)-H(7B)	107.9
N(2)-C(2)-H(2A)	109.7	C(7)-C(8)-C(9)	114.5(4)
C(1)-C(2)-H(2B)	109.7	C(7)-C(8)-H(8A)	108.6
N(2)-C(2)-H(2B)	109.7	C(9)-C(8)-H(8A)	108.6
H(2A)-C(2)-H(2B)	108.2	C(7)-C(8)-H(8B)	108.6
N(2)-C(3)-C(4)	109.4(4)	C(9)-C(8)-H(8B)	108.6
N(2)-C(3)-H(3A)	109.8	H(8A)-C(8)-H(8B)	107.6
C(4)-C(3)-H(3A)	109.8	N(2)-C(9)-C(8)	112.5(4)
N(2)-C(3)-H(3B)	109.8	N(2)-C(9)-H(9A)	109.1
C(4)-C(3)-H(3B)	109.8	C(8)-C(9)-H(9A)	109.1
H(3A)-C(3)-H(3B)	108.3	N(2)-C(9)-H(9B)	109.1
N(1)-C(4)-C(3)	109.3(4)	C(8)-C(9)-H(9B)	109.1
N(1)-C(4)-H(4A)	109.8	H(9A)-C(9)-H(9B)	107.8
C(3)-C(4)-H(4A)	109.8	O(1ME)-C(1ME)-H(1MA)	109.5
N(1)-C(4)-H(4B)	109.8	O(1ME)-C(1ME)-H(1MB)	109.5
C(3)-C(4)-H(4B)	109.8	H(1MA)-C(1ME)-H(1MB)	109.5
H(4A)-C(4)-H(4B)	108.3	O(1ME)-C(1ME)-H(1MC)	109.5
C(6)-C(5)-S(2)	109.4(4)	H(1MA)-C(1ME)-H(1MC)	109.5

H(1MB)-C(1ME)-H(1MC)109.5

Symmetry transformations used to generate equivalent atoms:
#1 -x,-y,-z

Table A-7. Crystal data and structure refinement for $(Et_4N^+)_2[Au_2\{Ni(ema)\}_2]$.

Empirical formula	C28 H56 Au2 N6 Ni2 O4 S4	
Formula weight	1180.38	
Temperature	110(2) K	
Wavelength	0.71073 Å	
Crystal system	Monoclinic	
Space group	P21/c	
Unit cell dimensions	a = 8.308(2) Å	α = 90°.
	b = 24.096(6) Å	β = 110.431(3)°.
	c = 10.191(3) Å	γ = 90°.
Volume	1911.6(9) $Å^3$	
Z	2	
Density (calculated)	2.051 Mg/m^3	
Absorption coefficient	8.880 mm^{-1}	
F(000)	1152	
Crystal size	0.30 x 0.10 x 0.08 mm^3	
Theta range for data collection	2.29 to 28.64°.	
Index ranges	-11<=h<=11, -32<=k<=31, -13<=l<=13	
Reflections collected	22917	
Independent reflections	4844 [R(int) = 0.0487]	
Completeness to theta = 28.64°	98.4 %	
Absorption correction	Semi-empirical from equivalents	
Max. and min. transmission	0.5369 and 0.1759	
Refinement method	Full-matrix least-squares on F^2	
Data / restraints / parameters	4844 / 0 / 212	
Goodness-of-fit on F^2	1.014	
Final R indices [I>2sigma(I)]	R1 = 0.0269, wR2 = 0.0501	
R indices (all data)	R1 = 0.0418, wR2 = 0.0545	
Largest diff. peak and hole	0.814 and -0.970 e.$Å^{-3}$	

Table A-8. Bond lengths [Å] and angles [°] for $(Et_4N^+)_2[Au_2\{Ni(ema)\}_2]$.

Au(1)-S(2)#1	2.2914(11)	C(7)-C(8)	1.513(6)
Au(1)-S(1)	2.2952(11)	C(7)-H(7A)	0.9700
Au(1)-Au(1)#1	3.1169(7)	C(7)-H(7B)	0.9700
Ni(1)-N(1)	1.849(3)	C(8)-H(8A)	0.9600
Ni(1)-N(2)	1.854(3)	C(8)-H(8B)	0.9600
Ni(1)-S(1)	2.1854(11)	C(8)-H(8C)	0.9600
Ni(1)-S(2)	2.1991(11)	C(9)-C(10)	1.511(5)
S(1)-C(1)	1.831(4)	C(9)-H(9A)	0.9700
S(2)-C(3)	1.830(4)	C(9)-H(9B)	0.9700
S(2)-Au(1)#1	2.2914(11)	C(10)-H(10A)	0.9600
N(1)-C(2)	1.327(5)	C(10)-H(10B)	0.9600
N(1)-C(6)	1.461(5)	C(10)-H(10C)	0.9600
N(2)-C(4)	1.330(5)	C(11)-C(12)	1.514(5)
N(2)-C(5)	1.460(5)	C(11)-H(11A)	0.9700
N(3)-C(7)	1.510(5)	C(11)-H(11B)	0.9700
N(3)-C(9)	1.514(5)	C(12)-H(12A)	0.9600
N(3)-C(13)	1.515(5)	C(12)-H(12B)	0.9600
N(3)-C(11)	1.517(4)	C(12)-H(12C)	0.9600
O(1)-C(2)	1.245(4)	C(13)-C(14)	1.512(6)
O(2)-C(4)	1.239(5)	C(13)-H(13A)	0.9700
C(1)-C(2)	1.510(5)	C(13)-H(13B)	0.9700
C(1)-H(1A)	0.9700	C(14)-H(14A)	0.9600
C(1)-H(1B)	0.9700	C(14)-H(14B)	0.9600
C(3)-C(4)	1.518(6)	C(14)-H(14C)	0.9600
C(3)-H(3A)	0.9700		
C(3)-H(3B)	0.9700	S(2)#1-Au(1)-S(1)	175.35(3)
C(5)-C(6)	1.521(6)	S(2)#1-Au(1)-Au(1)#1	90.72(3)
C(5)-H(5A)	0.9700	S(1)-Au(1)-Au(1)#1	93.90(3)
C(5)-H(5B)	0.9700	N(1)-Ni(1)-N(2)	85.61(14)
C(6)-H(6A)	0.9700	N(1)-Ni(1)-S(1)	88.29(10)
C(6)-H(6B)	0.9700	N(2)-Ni(1)-S(1)	173.59(11)

N(1)-Ni(1)-S(2)	173.52(11)	S(2)-C(3)-H(3B)	109.2
N(2)-Ni(1)-S(2)	88.48(11)	H(3A)-C(3)-H(3B)	107.9
S(1)-Ni(1)-S(2)	97.70(4)	O(2)-C(4)-N(2)	126.5(4)
C(1)-S(1)-Ni(1)	98.15(13)	O(2)-C(4)-C(3)	120.4(4)
C(1)-S(1)-Au(1)	104.13(14)	N(2)-C(4)-C(3)	113.0(3)
Ni(1)-S(1)-Au(1)	92.44(4)	N(2)-C(5)-C(6)	107.1(3)
C(3)-S(2)-Ni(1)	96.61(14)	N(2)-C(5)-H(5A)	110.3
C(3)-S(2)-Au(1)#1	103.27(13)	C(6)-C(5)-H(5A)	110.3
Ni(1)-S(2)-Au(1)#1	95.12(4)	N(2)-C(5)-H(5B)	110.3
C(2)-N(1)-C(6)	118.2(3)	C(6)-C(5)-H(5B)	110.3
C(2)-N(1)-Ni(1)	125.4(3)	H(5A)-C(5)-H(5B)	108.6
C(6)-N(1)-Ni(1)	115.3(2)	N(1)-C(6)-C(5)	107.6(3)
C(4)-N(2)-C(5)	119.0(3)	N(1)-C(6)-H(6A)	110.2
C(4)-N(2)-Ni(1)	124.4(3)	C(5)-C(6)-H(6A)	110.2
C(5)-N(2)-Ni(1)	114.7(3)	N(1)-C(6)-H(6B)	110.2
C(7)-N(3)-C(9)	111.4(3)	C(5)-C(6)-H(6B)	110.2
C(7)-N(3)-C(13)	106.1(3)	H(6A)-C(6)-H(6B)	108.5
C(9)-N(3)-C(13)	110.9(3)	N(3)-C(7)-C(8)	115.0(3)
C(7)-N(3)-C(11)	110.9(3)	N(3)-C(7)-H(7A)	108.5
C(9)-N(3)-C(11)	106.6(3)	C(8)-C(7)-H(7A)	108.5
C(13)-N(3)-C(11)	111.1(3)	N(3)-C(7)-H(7B)	108.5
C(2)-C(1)-S(1)	112.8(3)	C(8)-C(7)-H(7B)	108.5
C(2)-C(1)-H(1A)	109.0	H(7A)-C(7)-H(7B)	107.5
S(1)-C(1)-H(1A)	109.0	C(7)-C(8)-H(8A)	109.5
C(2)-C(1)-H(1B)	109.0	C(7)-C(8)-H(8B)	109.5
S(1)-C(1)-H(1B)	109.0	H(8A)-C(8)-H(8B)	109.5
H(1A)-C(1)-H(1B)	107.8	C(7)-C(8)-H(8C)	109.5
O(1)-C(2)-N(1)	126.0(4)	H(8A)-C(8)-H(8C)	109.5
O(1)-C(2)-C(1)	119.1(3)	H(8B)-C(8)-H(8C)	109.5
N(1)-C(2)-C(1)	114.9(3)	C(10)-C(9)-N(3)	116.0(3)
C(4)-C(3)-S(2)	111.9(3)	C(10)-C(9)-H(9A)	108.3
C(4)-C(3)-H(3A)	109.2	N(3)-C(9)-H(9A)	108.3
S(2)-C(3)-H(3A)	109.2	C(10)-C(9)-H(9B)	108.3
C(4)-C(3)-H(3B)	109.2	N(3)-C(9)-H(9B)	108.3

H(9A)-C(9)-H(9B)	107.4	C(11)-C(12)-H(12C)	109.5
C(9)-C(10)-H(10A)	109.5	H(12A)-C(12)-H(12C)	109.5
C(9)-C(10)-H(10B)	109.5	H(12B)-C(12)-H(12C)	109.5
H(10A)-C(10)-H(10B)	109.5	C(14)-C(13)-N(3)	115.3(3)
C(9)-C(10)-H(10C)	109.5	C(14)-C(13)-H(13A)	108.4
H(10A)-C(10)-H(10C)	109.5	N(3)-C(13)-H(13A)	108.4
H(10B)-C(10)-H(10C)	109.5	C(14)-C(13)-H(13B)	108.4
C(12)-C(11)-N(3)	114.5(3)	N(3)-C(13)-H(13B)	108.4
C(12)-C(11)-H(11A)	108.6	H(13A)-C(13)-H(13B)	107.5
N(3)-C(11)-H(11A)	108.6	C(13)-C(14)-H(14A)	109.5
C(12)-C(11)-H(11B)	108.6	C(13)-C(14)-H(14B)	109.5
N(3)-C(11)-H(11B)	108.6	H(14A)-C(14)-H(14B)	109.5
H(11A)-C(11)-H(11B)	107.6	C(13)-C(14)-H(14C)	109.5
C(11)-C(12)-H(12A)	109.5	H(14A)-C(14)-H(14C)	109.5
C(11)-C(12)-H(12B)	109.5	H(14B)-C(14)-H(14C)	109.5
H(12A)-C(12)-H(12B)	109.5		

Symmetry transformations used to generate equivalent atoms:

#1 -x+1,-y+2,-z+1

Table A-9. Crystal data and structure refinement for $[\{Ni(ema)\}_2Au_4(PPh_3)_4]$.

Identification code	niau	
Empirical formula	C96 H100 Au4 N10 Ni2 O7 P4 S4	
Formula weight	2663.26	
Temperature	110(2) K	
Wavelength	0.71073 Å	
Crystal system	Triclinic	
Space group	P-1	
Unit cell dimensions	a = 13.465(2) Å	α = 75.987(2)°.
	b = 16.178(2) Å	β = 78.277(2)°.
	c = 25.137(4) Å	γ = 71.395(2)°.
Volume	4987.9(13) $Å^3$	
Z	2	
Density (calculated)	1.773 Mg/m^3	
Absorption coefficient	6.436 mm^{-1}	
F(000)	2596	
Crystal size	0.100 x 0.100 x 0.050 mm^3	
Theta range for data collection	2.101 to 28.382°.	
Index ranges	-17<=h<=18, -21<=k<=21, -33<=l<=33	
Reflections collected	59144	
Independent reflections	24138 [R(int) = 0.0455]	
Completeness to theta = 25.242°	99.5 %	
Absorption correction	Semi-empirical from equivalents	
Max. and min. transmission	0.7457 and 0.3136	
Refinement method	Full-matrix least-squares on F^2	
Data / restraints / parameters	24138 / 171 / 1159	
Goodness-of-fit on F^2	1.125	
Final R indices [I>2sigma(I)]	R1 = 0.0430, wR2 = 0.0993	
R indices (all data)	R1 = 0.0567, wR2 = 0.1039	
Extinction coefficient	0	
Largest diff. peak and hole	3.615 and -1.925 $e.Å^{-3}$	

Table A-10. Bond lengths [Å] and angles [°] for [{Ni(ema)}$_2$Au$_4$(PPh$_3$)$_4$].

Au(1)-Au(3)	3.0544(6)	C(25)-C(26)	1.39(1)
Au(2)-Au(4)	3.1268(5)	C(26)-C(27)	1.40(1)
C(9)-C(10)	1.52(1)	C(27)-C(28)	1.38(1)
S(4)-C(10)	1.835(8)	C(28)-C(29)	1.38(1)
N(4)-C(11)	1.458(9)	C(1A)-C(2A)	1.22(2)
C(11)-C(12)	1.527(9)	C(1B)-C(2B)	1.34(2)
N(3)-C(12)	1.45(1)	C(1C)-C(2C)	1.35(2)
P(1)-C(13)	1.812(7)	C(1D)-C(2D)	1.20(1)
C(13)-C(14)	1.385(9)	C(1E)-C(2E)	1.34(1)
C(14)-C(15)	1.38(1)	C(1F)-C(2F)	1.24(2)
C(15)-C(16)	1.36(1)	N(2)-C(3)	1.469(8)
C(16)-C(17)	1.39(1)	C(25)-C(30)	1.41(1)
C(17)-C(18)	1.38(1)	C(29)-C(30)	1.38(1)
C(13)-C(18)	1.38(1)	P(2)-C(31)	1.807(7)
N(1A)-C(1A)	1.34(2)	C(31)-C(32)	1.40(1)
N(1B)-C(1B)	1.20(2)	C(32)-C(33)	1.38(1)
N(1C)-C(1C)	1.21(2)	C(33)-C(34)	1.39(1)
N(1D)-C(1D)	1.35(2)	C(34)-C(35)	1.38(2)
N(1E)-C(1E)	1.23(1)	C(31)-C(36)	1.384(9)
N(1F)-C(1F)	1.34(2)	C(35)-C(36)	1.40(1)
S(2)-C(1I)	1.828(8)	P(2)-C(37)	1.826(7)
N(2)-C(1J)	1.313(8)	C(37)-C(38)	1.39(1)
C(1I)-C(1J)	1.510(9)	C(38)-C(39)	1.38(1)
O(2)-C(1J)	1.270(9)	N(9)-C(4)	1.46(1)
C(19)-C(20)	1.37(1)	C(3)-C(4)	1.506(9)
C(20)-C(21)	1.37(1)	C(39)-C(40)	1.38(1)
C(21)-C(22)	1.37(1)	C(40)-C(41)	1.37(2)
C(22)-C(23)	1.40(1)	C(41)-C(42)	1.39(1)
C(19)-C(24)	1.41(1)	C(37)-C(42)	1.394(9)
C(23)-C(24)	1.38(1)	P(2)-C(43)	1.815(7)
P(1)-C(24)	1.807(7)	C(43)-C(44)	1.39(1)
P(1)-C(25)	1.808(7)	C(44)-C(45)	1.38(1)

C(45)-C(46)	1.39(1)	C(70)-C(71)	1.38(1)
C(46)-C(47)	1.37(1)	C(67)-C(72)	1.386(9)
C(47)-C(48)	1.40(1)	C(71)-C(72)	1.41(1)
C(43)-C(48)	1.40(1)	P(4)-C(73)	1.813(7)
P(3)-C(49)	1.808(6)	C(73)-C(74)	1.38(1)
N(9)-C(5)	1.306(8)	C(74)-C(75)	1.40(1)
O(1)-C(5)	1.259(8)	C(75)-C(76)	1.39(2)
C(49)-C(50)	1.399(8)	C(76)-C(77)	1.38(1)
C(50)-C(51)	1.382(9)	C(73)-C(78)	1.39(1)
C(51)-C(52)	1.38(1)	C(77)-C(78)	1.39(1)
C(52)-C(53)	1.39(1)	P(4)-C(79)	1.808(8)
C(49)-C(54)	1.38(1)	C(7)-C(8)	1.52(1)
C(53)-C(54)	1.37(1)	O(3)-C(8)	1.235(8)
P(3)-C(55)	1.797(7)	N(3)-C(8)	1.311(8)
C(55)-C(56)	1.41(1)	C(79)-C(80)	1.39(1)
C(56)-C(57)	1.38(1)	C(80)-C(81)	1.40(1)
C(57)-C(58)	1.39(1)	C(81)-C(82)	1.37(1)
C(58)-C(59)	1.38(1)	C(82)-C(83)	1.37(1)
C(5)-C(6)	1.51(1)	C(83)-C(84)	1.39(1)
S(1)-C(6)	1.817(7)	C(79)-C(84)	1.40(1)
C(55)-C(60)	1.393(8)	N(4)-C(9)	1.316(7)
C(59)-C(60)	1.39(1)	O(4)-C(9)	1.24(1)
P(3)-C(61)	1.830(8)	C(10)-H(10A)	0.990(7)
C(61)-C(62)	1.388(9)	C(10)-H(10B)	0.989(5)
C(62)-C(63)	1.39(1)	C(11)-H(11A)	0.990(6)
C(63)-C(64)	1.38(1)	C(11)-H(11B)	0.989(8)
C(64)-C(65)	1.37(1)	C(12)-H(12A)	0.991(6)
C(65)-C(66)	1.39(1)	C(12)-H(12B)	0.989(7)
C(61)-C(66)	1.39(1)	C(14)-H(14)	0.949(6)
P(4)-C(67)	1.808(6)	C(15)-H(15)	0.950(7)
C(67)-C(68)	1.40(1)	C(16)-H(16)	0.951(8)
C(68)-C(69)	1.37(1)	C(17)-H(17)	0.950(7)
S(3)-C(7)	1.836(6)	C(18)-H(18)	0.950(7)
C(69)-C(70)	1.37(1)	C(19)-H(19)	0.950(7)

C(1I)-H(1IA)	0.990(7)	C(33)-H(33)	0.95(1)
C(1I)-H(1IB)	0.990(6)	C(34)-H(34)	0.95(1)
O(1W)-H(1WA)	0.870(6)	C(35)-H(35)	0.950(7)
O(1W)-H(1WB)	0.871(8)	C(36)-H(36)	0.950(8)
C(20)-H(20)	0.95(1)	C(38)-H(38)	0.949(6)
C(21)-H(21)	0.949(8)	C(39)-H(39)	0.95(1)
C(22)-H(22)	0.948(9)	C(3)-H(3A)	0.991(7)
C(23)-H(23)	0.950(8)	C(3)-H(3B)	0.990(9)
C(26)-H(26)	0.949(8)	O(3W)-H(3WA)	0.870(7)
C(27)-H(27)	0.95(1)	O(3W)-H(3WB)	0.870(6)
C(28)-H(28)	0.949(8)	C(40)-H(40)	0.950(9)
C(29)-H(29))	0.950(8)	C(41)-H(41)	0.951(8)
C(2A)-H(2AA)	0.98(1)	C(42)-H(42)	0.949(9)
C(2A)-H(2AB)	0.98(1)	C(44)-H(44)	0.950(7)
C(2A)-H(2AC)	0.98(1)	C(45)-H(45)	0.949(9)
C(2B)-H(2BA)	0.98(1)	C(46)-H(46)	0.949(9)
C(2B)-H(2BB)	0.98(1)	C(47)-H(47)	0.950(7)
C(2B)-H(2BC)	0.98(1)	C(48)-H(48)	0.951(8)
C(2C)-H(2CA)	0.98(1)	C(4)-H(4A)	0.988(7)
C(2C)-H(2CB)	0.98(1)	C(4)-H(4B)	0.991(6)
C(2C)-H(2CC)	0.98(1)	C(50)-H(50)	0.950(6)
C(2D)-H(2DA)	0.98(1)	C(51)-H(51)	0.951(7)
C(2D)-H(2DB)	0.98(1)	C(52)-H(52)	0.951(7)
C(2D)-H(2DC)	0.98(1)	C(53)-H(53)	0.950(8)
C(2E)-H(2EA)	0.98(1)	C(54)-H(54)	0.950(7)
C(2E)-H(2EB)	0.98(1)	C(56)-H(56)	0.950(6)
C(2E)-H(2EC)	0.98(1)	C(57)-H(57)	0.95(1)
C(2F)-H(2FA)	0.98(1)	C(58)-H(58)	0.949(8)
C(2F)-H(2FB)	0.98(1)	C(59)-H(59)	0.950(7)
C(2F)-H(2FC)	0.98(2)	C(60)-H(60)	0.949(8)
O(2W)-H(2WA)	0.870(8)	C(62)-H(62)	0.950(7)
O(2W)-H(2WB)	0.870(5)	C(63)-H(63)	0.951(8)
C(30)-H(30)	0.95(1)	C(64)-H(64)	0.950(9)
C(32)-H(32)	0.950(6)	C(65)-H(65)	0.951(8)

C(66)-H(66)	0.950(8)	Ni(1)-S(2)	2.207(2)
C(68)-H(68)	0.950(7)	Au(2)-S(2)	2.350(2)
C(69)-H(69)	0.950(9)	Ni(2)-S(3)	2.204(2)
C(6)-H(6A)	0.990(8)	Au(3)-S(3)	2.352(2)
C(6)-H(6B)	0.990(6)	Au(4)-S(4)	2.324(2)
C(70)-H(70)	0.950(7)	Ni(2)-S(4)	2.198(2)
C(71)-H(71)	0.949(8)		
C(72)-H(72)	0.949(8)	N(1A)-C(1A)-C(2A)	178(1)
C(74)-H(74)	0.950(9)	C(1A)-C(2A)-H(2AA)	110(1)
C(75)-H(75)	0.950(9)	C(1A)-C(2A)- H(2AB)	109(1)
C(76)-H(76)	0.950(8)	C(1A)-C(2A)-H(2AC)	109(1)
C(77)-H(77)	0.95(1)	H(2AA)-C(2A)-H(2AB)	109(1)
C(78)-H(78)	0.948(8)	H(2AA)-C(2A)-H(2AC)	109(1)
C(7)-H(7A)	0.989(7)	H(2AB)-C(2A)-H(2AC)	109(1)
C(7)-H(7B)	0.990(6)	N(1B)-C(1B)-C(2B)	177(1)
C(80)-H(80)	0.949(7)	C(1B)-C(2B)-H(2BA)	110(1)
C(81)-H(81)	0.95(1)	C(1B)-C(2B)-H(2BB)	109(1)
C(82)-H(82)	0.95(1)	C(1B)-C(2B)-H(2BC)	110(1)
C(83)-H(83)	0.950(8)	H(2BA)-C(2B)-H(2BB)	110(1)
C(84)-H(84)	0.95(1)	H(2BA)-C(2B)-H(2BC)	109(1)
Ni(1)-N(2)	1.848(5)	H(2BB)-C(2B)-H(2BC)	109(1)
Ni(2)-N(3)	1.861(5)	N(1C)-C(1C)-C(2C)	174(1)
Ni(2)-N(4)	1.852(6)	C(1C)-C(2C)-H(2CA)	109(1)
Ni(1)-N(9)	1.861(5)	C(1C)-C(2C)-H(2CB)	109(1)
Au(2)-Ni(1)	2.9227(9)	C(1C)-C(2C)-H(2CC)	109(1)
Au(1)-Ni(1)	3.1411(8)	H(2CA)-C(2C)-H(2CB)	110(1)
Au(4)-Ni(2)	3.3127(9)	H(2CA)-C(2C)-H(2CC)	110(1)
Au(3)-Ni(2)	2.9040(9)	H(2CB)-C(2C)-H(2CC)	109(1)
Au(1)-P(1)	2.269(2)	N(1D)-C(1D)-C(2D)	173(1)
Au(2)-P(2)	2.266(2)	C(1D)-C(2D)-H(2DA)	109(1)
Au(3)-P(3)	2.259(2)	C(1D)-C(2D)-H(2DB)	110(1)
Au(4)-P(4)	2.268(2)	C(1D)-C(2D)-H(2DC)	109(1)
Au(1)-S(1)	2.330(2)	H(2DA)-C(2D)-H(2DB)	110(1)
Ni(1)-S(1)	2.186(2)	H(2DA)-C(2D)-H(2DC)	109(1)

H(2DB)-C(2D)-H(2DC)	110(1)	Ni(2)-Au(3)-P(3)	125.69(5)
N(1E)-C(1E)-C(2E)	176(1)	S(3)-Au(3)-P(3)	172.22(6)
C(1E)-C(2E)-H(2EA)	109(1)	Au(2)-Au(4)-Ni(2)	112.77(2)
C(1E)-C(2E)-H(2EB)	110(1)	Au(2)-Au(4)-S(4)	76.45(4)
C(1E)-C(2E)-H(2EC)	109(1)	Au(2)-Au(4)-P(4)	106.91(5)
H(2EA)-C(2E)-H(2EB)	109(1)	Ni(2)-Au(4)-S(4)	41.43(4)
H(2EA)-C(2E)-H(2EC)	109(1)	Ni(2)-Au(4)-P(4)	133.64(5)
H(2EB)-C(2E)-H(2EC)	110(1)	S(4)-Au(4)-P(4)	174.76(6)
N(1F)-C(1F)-C(2F)	172(2)	Au(1)-Ni(1)-Au(2)	118.52(3)
C(1F)-C(2F)-H(2FA)	109(1)	Au(1)-Ni(1)-S(1)	47.86(5)
C(1F)-C(2F)-H(2FB)	109(1)	Au(1)-Ni(1)-S(2)	80.89(5)
C(1F)-C(2F)-H(2FC)	110(1)	Au(1)-Ni(1)-N(9)	104.5(2)
H(2FA)-C(2F)-H(2FB)	109(1)	Au(1)-Ni(1)-N(2)	134.1(2)
H(2FA)-C(2F)-H(2FC)	110(1)	Au(2)-Ni(1)-S(1)	97.37(5)
H(2FB)-C(2F)-H(2FC)	110(1)	Au(2)-Ni(1)-S(2)	52.29(5)
H(1WA)-O(1W)-H(1WB)	109.4(7)	Au(2)-Ni(1)-N(9)	126.0(2)
H(2WA)-O(2W)-H(2WB)	109.5(7)	Au(2)-Ni(1)-N(2)	86.6(2)
H(3WA)-O(3W)-H(3WB)	109.5(8)	S(1)-Ni(1)-S(2)	98.61(7)
Au(3)-Au(1)-Ni(1)	116.09(2)	S(1)-Ni(1)-N(9)	87.9(2)
Au(3)-Au(1)-S(1)	80.67(4)	S(1)-Ni(1)-N(2)	173.5(2)
Au(3)-Au(1)-P(1)	101.95(5)	S(2)-Ni(1)-N(9)	173.4(2)
Ni(1)-Au(1)-S(1)	44.07(4)	S(2)-Ni(1)-N(2)	87.9(2)
Ni(1)-Au(1)-P(1)	131.23(5)	N(9)-Ni(1)-N(2)	85.6(2)
S(1)-Au(1)-P(1)	174.95(6)	Au(3)-Ni(2)-Au(4)	117.61(3)
Au(4)-Au(2)-Ni(1)	116.32(2)	Au(3)-Ni(2)-S(3)	52.68(5)
Au(4)-Au(2)-S(2)	78.18(4)	Au(3)-Ni(2)-S(4)	92.92(5)
Au(4)-Au(2)-P(2)	114.40(4)	Au(3)-Ni(2)-N(3)	90.3(2)
Ni(1)-Au(2)-S(2)	47.99(4)	Au(3)-Ni(2)-N(4)	127.6(2)
Ni(1)-Au(2)-P(2)	120.19(5)	Au(4)-Ni(2)-S(3)	85.95(5)
S(2)-Au(2)-P(2)	167.14(6)	Au(4)-Ni(2)-S(4)	44.40(5)
Au(1)-Au(3)-Ni(2)	116.66(2)	Au(4)-Ni(2)-N(3)	137.9(2)
Au(1)-Au(3)-S(3)	84.17(4)	Au(4)-Ni(2)-N(4)	98.6(2)
Au(1)-Au(3)-P(3)	103.57(4)	S(3)-Ni(2)-S(4)	98.72(7)
Ni(2)-Au(3)-S(3)	48.19(4)	S(3)-Ni(2)-N(3)	87.9(2)

S(3)-Ni(2)-N(4)	173.6(2)	Au(4)-P(4)-C(67)	108.8(2)
S(4)-Ni(2)-N(3)	173.4(2)	Au(4)-P(4)-C(73)	115.7(2)
S(4)-Ni(2)-N(4)	87.7(2)	Au(4)-P(4)-C(79)	113.8(2)
N(3)-Ni(2)-N(4)	85.7(2)	C(67)-P(4)-C(73)	105.4(3)
Au(1)-S(1)-Ni(1)	88.07(6)	C(67)-P(4)-C(79)	106.7(3)
Au(1)-S(1)-C(6)	106.5(2)	C(73)-P(4)-C(79)	105.8(3)
Ni(1)-S(1)-C(6)	98.3(2)	Ni(1)-N(9)-C(4)	114.8(4)
Au(2)-S(2)-Ni(1)	79.71(6)	Ni(1)-N(9)-C(5)	124.4(5)
Au(2)-S(2)-C(1I)	102.5(2)	C(4)-N(9)-C(5)	118.7(5)
Ni(1)-S(2)-C(1I)	96.1(2)	Ni(1)-N(2)-C(1J)	125.0(5)
Au(3)-S(3)-Ni(2)	79.13(6)	Ni(1)-N(2)-C(3)	114.8(4)
Au(3)-S(3)-C(7)	100.9(2)	C(1J)-N(2)-C(3)	119.8(6)
Ni(2)-S(3)-C(7)	97.6(2)	Ni(2)-N(3)-C(8)	125.8(5)
Au(4)-S(4)-Ni(2)	94.17(7)	Ni(2)-N(3)-C(12)	114.7(4)
Au(4)-S(4)-C(10)	104.8(2)	C(8)-N(3)-C(12)	118.7(5)
Ni(2)-S(4)-C(10)	98.3(2)	Ni(2)-N(4)-C(9)	125.6(5)
Au(1)-P(1)-C(13)	114.5(2)	Ni(2)-N(4)-C(11)	115.1(4)
Au(1)-P(1)-C(24)	114.9(2)	C(9)-N(4)-C(11)	117.2(5)
Au(1)-P(1)-C(25)	109.0(2)	S(2)-C(1I)-H(1IA)	109.3(5)
C(13)-P(1)-C(24)	104.0(3)	S(2)-C(1I)-H(1IB)	109.2(5)
C(13)-P(1)-C(25)	106.9(3)	S(2)-C(1I)-C(1J)	111.9(5)
C(24)-P(1)-C(25)	106.9(3)	H(1IA)-C(1I)-H(1IB)	108.0(6)
Au(2)-P(2)-C(31)	119.6(2)	H(1IA)-C(1I)-C(1J)	109.2(6)
Au(2)-P(2)-C(37)	109.2(2)	H(1IB)-C(1I)-C(1J)	109.2(6)
Au(2)-P(2)-C(43)	111.3(2)	O(2)-C(1J)-N(2)	125.8(6)
C(31)-P(2)-C(37)	107.3(3)	O(2)-C(1J)-C(1I)	119.4(6)
C(31)-P(2)-C(43)	104.3(3)	N(2)-C(1J)-C(1I)	114.8(6)
C(37)-P(2)-C(43)	104.1(3)	N(2)-C(3)-H(3A)	110.3(6)
Au(3)-P(3)-C(49)	112.4(2)	N(2)-C(3)-H(3B)	110.3(6)
Au(3)-P(3)-C(55)	115.6(2)	N(2)-C(3)-C(4)	107.0(6)
Au(3)-P(3)-C(61)	112.3(2)	H(3A)-C(3)-H(3B)	108.5(7)
C(49)-P(3)-C(55)	105.2(3)	H(3A)-C(3)-C(4)	110.4(6)
C(49)-P(3)-C(61)	104.9(3)	H(3B)-C(3)-C(4)	110.3(6)
C(55)-P(3)-C(61)	105.6(3)	N(9)-C(4)-C(3)	108.8(6)

N(9)-C(4)-H(4A)	110.0(6)	N(4)-C(11)-C(12)	107.7(5)
N(9)-C(4)-H(4B)	109.7(6)	H(11A)-C(11)-H(11B)	108.5(6)
C(3)-C(4)-H(4A)	110.0(6)	H(11A)-C(11)-C(12)	110.1(6)
C(3)-C(4)-H(4B)	109.9(6)	H(11B)-C(11)-C(12)	110.2(6)
H(4A)-C(4)-H(4B)	108.3(6)	N(3)-C(12)-C(11)	107.4(5)
O(1)-C(5)-N(9)	125.0(6)	N(3)-C(12)-H(12A)	110.3(6)
O(1)-C(5)-C(6)	119.3(6)	N(3)-C(12)-H(12B)	110.2(6)
N(9)-C(5)-C(6)	115.7(6)	C(11)-C(12)-H(12A)	110.1(6)
S(1)-C(6)-C(5)	112.4(5)	C(11)-C(12)-H(12B)	110.2(6)
S(1)-C(6)-H(6A)	109.1(5)	H(12A)-C(12)-H(12B)	108.5(6)
S(1)-C(6)-H(6B)	109.1(5)	P(1)-C(13)-C(14)	120.1(5)
C(5)-C(6)-H(6A)	109.2(6)	P(1)-C(13)-C(18)	120.5(6)
C(5)-C(6)-H(6B)	109.1(6)	C(14)-C(13)-C(18)	119.3(7)
H(6A)-C(6)-H(6B)	107.9(6)	C(13)-C(14)-H(14)	119.9(7)
S(3)-C(7)-H(7A)	109.3(5)	C(13)-C(14)-C(15)	120.3(7)
S(3)-C(7)-H(7B)	109.2(5)	H(14)-C(14)-C(15)	119.8(7)
S(3)-C(7)-C(8)	111.9(5)	C(14)-C(15)-H(15)	120.1(8)
H(7A)-C(7)-H(7B)	107.9(6)	C(14)-C(15)-C(16)	119.9(7)
H(7A)-C(7)-C(8)	109.2(6)	H(15)-C(15)-C(16)	120.0(8)
H(7B)-C(7)-C(8)	109.2(6)	C(15)-C(16)-H(16)	119.4(8)
O(3)-C(8)-N(3)	125.5(6)	C(15)-C(16)-C(17)	121.1(8)
O(3)-C(8)-C(7)	119.6(6)	H(16)-C(16)-C(17)	119.5(8)
N(3)-C(8)-C(7)	114.9(6)	C(16)-C(17)-H(17)	120.5(8)
O(4)-C(9)-N(4)	126.1(6)	C(16)-C(17)-C(18)	119.0(7)
O(4)-C(9)-C(10)	119.4(6)	H(17)-C(17)-C(18)	120.5(8)
N(4)-C(9)-C(10)	114.5(6)	C(13)-C(18)-C(17)	120.3(7)
S(4)-C(10)-C(9)	111.6(5)	C(13)-C(18)-H(18)	119.9(8)
S(4)-C(10)-H(10A)	109.3(5)	C(17)-C(18)-H(18)	119.8(8)
S(4)-C(10)-H(10B)	109.3(5)	H(19)-C(19)-C(20)	120.4(7)
C(9)-C(10)-H(10A)	109.3(6)	H(19)-C(19)-C(24)	120.5(7)
C(9)-C(10)-H(10B)	109.3(6)	C(20)-C(19)-C(24)	119.1(7)
H(10A)-C(10)-H(10B)	108.0(6)	C(19)-C(20)-H(20)	119.2(9)
N(4)-C(11)-H(11A)	110.2(6)	C(19)-C(20)-C(21)	121.6(8)
N(4)-C(11)-H(11B)	110.2(6)	H(20)-C(20)-C(21)	119.2(9)

C(20)-C(21)-H(21)	120.1(9)	C(31)-C(32)-C(33)	120.5(7)
C(20)-C(21)-C(22)	120.0(9)	H(32)-C(32)-C(33)	119.8(8)
H(21)-C(21)-C(22)	119.9(9)	C(32)-C(33)-H(33)	120.5(9)
C(21)-C(22)-H(22)	120.2(9)	C(32)-C(33)-C(34)	119.2(8)
C(21)-C(22)-C(23)	119.7(9)	H(33)-C(33)-C(34)	120.3(9)
H(22)-C(22)-C(23)	120.2(9)	C(33)-C(34)-H(34)	119.6(9)
C(22)-C(23)-H(23)	119.9(8)	C(33)-C(34)-C(35)	121.1(9)
C(22)-C(23)-C(24)	120.2(7)	H(34)-C(34)-C(35)	119.4(9)
H(23)-C(23)-C(24)	119.9(8)	C(34)-C(35)-H(35)	120.3(9)
P(1)-C(24)-C(19)	117.1(5)	C(34)-C(35)-C(36)	119.4(8)
P(1)-C(24)-C(23)	123.7(6)	H(35)-C(35)-C(36)	120.3(8)
C(19)-C(24)-C(23)	119.3(7)	C(31)-C(36)-C(35)	119.9(7)
P(1)-C(25)-C(26)	122.6(6)	C(31)-C(36)-H(36)	120.1(7)
P(1)-C(25)-C(30)	118.5(5)	C(35)-C(36)-H(36)	120.0(7)
C(26)-C(25)-C(30)	118.7(7)	P(2)-C(37)-C(38)	118.8(5)
C(25)-C(26)-H(26)	119.8(8)	P(2)-C(37)-C(42)	121.3(5)
C(25)-C(26)-C(27)	120.0(7)	C(38)-C(37)-C(42)	119.9(7)
H(26)-C(26)-C(27)	120.2(8)	C(37)-C(38)-H(38)	120.4(7)
C(26)-C(27)-H(27)	119.8(8)	C(37)-C(38)-C(39)	118.9(7)
C(26)-C(27)-C(28)	120.3(8)	H(38)-C(38)-C(39)	120.7(7)
H(27)-C(27)-C(28)	119.9(9)	C(38)-C(39)-H(39)	119.2(8)
C(27)-C(28)-H(28)	120.2(8)	C(38)-C(39)-C(40)	121.4(8)
C(27)-C(28)-C(29)	119.7(8)	H(39)-C(39)-C(40)	119.4(9)
H(28)-C(28)-C(29)	120.0(8)	C(39)-C(40)-H(40)	120.2(9)
C(28)-C(29)-H(29)	119.7(8)	C(39)-C(40)-C(41)	119.7(8)
C(28)-C(29)-C(30)	120.6(7)	H(40)-C(40)-C(41)	120.1(9)
H(29)-C(29)-C(30)	119.7(8)	C(40)-C(41)-H(41)	120.1(9)
C(25)-C(30)-C(29)	120.6(7)	C(40)-C(41)-C(42)	120.2(8)
C(25)-C(30)-H(30)	119.7(8)	H(41)-C(41)-C(42)	119.8(8)
C(29)-C(30)-H(30)	119.7(8)	C(37)-C(42)-C(41)	119.9(7)
P(2)-C(31)-C(32)	117.7(5)	C(37)-C(42)-H(42)	120.0(8)
P(2)-C(31)-C(36)	122.0(5)	C(41)-C(42)-H(42)	120.1(8)
C(32)-C(31)-C(36)	119.8(7)	P(2)-C(43)-C(44)	123.0(6)
C(31)-C(32)-H(32)	119.8(7)	P(2)-C(43)-C(48)	117.6(5)

C(44)-C(43)-C(48)	119.3(7)	P(3)-C(55)-C(56)	118.1(5)
C(43)-C(44)-H(44)	119.6(8)	P(3)-C(55)-C(60)	123.4(5)
C(43)-C(44)-C(45)	120.8(7)	C(56)-C(55)-C(60)	118.5(6)
H(44)-C(44)-C(45)	119.6(8)	C(55)-C(56)-H(56)	119.6(7)
C(44)-C(45)-H(45)	119.9(9)	C(55)-C(56)-C(57)	120.8(7)
C(44)-C(45)-C(46)	120.3(8)	H(56)-C(56)-C(57)	119.6(7)
H(45)-C(45)-C(46)	119.8(9)	C(56)-C(57)-H(57)	120.1(8)
C(45)-C(46)-H(46)	120.3(9)	C(56)-C(57)-C(58)	119.8(8)
C(45)-C(46)-C(47)	119.3(8)	H(57)-C(57)-C(58)	120.1(9)
H(46)-C(46)-C(47)	120.4(9)	C(57)-C(58)-H(58)	120.1(9)
C(46)-C(47)-H(47)	119.2(8)	C(57)-C(58)-C(59)	120.0(8)
C(46)-C(47)-C(48)	121.7(8)	H(58)-C(58)-C(59)	119.9(9)
H(47)-C(47)-C(48)	119.1(8)	C(58)-C(59)-H(59)	119.7(9)
C(43)-C(48)-C(47)	118.6(7)	C(58)-C(59)-C(60)	120.6(8)
C(43)-C(48)-H(48)	120.6(8)	H(59)-C(59)-C(60)	119.7(8)
C(47)-C(48)-H(48)	120.7(8)	C(55)-C(60)-C(59)	120.4(7)
P(3)-C(49)-C(50)	118.6(5)	C(55)-C(60)-H(60)	119.8(7)
P(3)-C(49)-C(54)	122.6(6)	C(59)-C(60)-H(60)	119.8(7)
C(50)-C(49)-C(54)	118.8(7)	P(3)-C(61)-C(62)	119.3(5)
C(49)-C(50)-H(50)	120.0(7)	P(3)-C(61)-C(66)	120.6(5)
C(49)-C(50)-C(51)	120.1(7)	C(62)-C(61)-C(66)	120.1(7)
H(50)-C(50)-C(51)	120.0(7)	C(61)-C(62)-H(62)	120.4(7)
C(50)-C(51)-H(51)	119.8(8)	C(61)-C(62)-C(63)	119.2(7)
C(50)-C(51)-C(52)	120.6(7)	H(62)-C(62)-C(63)	120.5(7)
H(51)-C(51)-C(52)	119.6(8)	C(62)-C(63)-H(63)	119.9(8)
C(51)-C(52)-H(52)	120.4(8)	C(62)-C(63)-C(64)	120.3(7)
C(51)-C(52)-C(53)	119.3(8)	H(63)-C(63)-C(64)	119.8(8)
H(52)-C(52)-C(53)	120.3(8)	C(63)-C(64)-H(64)	119.6(8)
C(52)-C(53)-H(53)	119.9(9)	C(63)-C(64)-C(65)	120.9(7)
C(52)-C(53)-C(54)	120.2(8)	H(64)-C(64)-C(65)	119.5(8)
H(53)-C(53)-C(54)	119.9(9)	C(64)-C(65)-H(65)	120.3(8)
C(49)-C(54)-C(53)	121.0(7)	C(64)-C(65)-C(66)	119.5(7)
C(49)-C(54)-H(54)	119.5(8)	H(65)-C(65)-C(66)	120.2(8)
C(53)-C(54)-H(54)	119.5(8)	C(61)-C(66)-C(65)	120.0(7)

C(61)-C(66)-H(66)	120.1(8)	C(75)-C(76)-H(76)	119.1(9)
C(65)-C(66)-H(66)	119.9(8)	C(75)-C(76)-C(77)	121.8(9)
P(4)-C(67)-C(68)	121.6(5)	H(76)-C(76)-C(77)	119.1(9)
P(4)-C(67)-C(72)	118.9(5)	C(76)-C(77)-H(77)	120.2(9)
C(68)-C(67)-C(72)	119.5(7)	C(76)-C(77)-C(78)	119.5(8)
C(67)-C(68)-H(68)	120.0(8)	H(77)-C(77)-C(78)	120.2(9)
C(67)-C(68)-C(69)	119.9(7)	C(73)-C(78)-C(77)	120.0(8)
H(68)-C(68)-C(69)	120.1(8)	C(73)-C(78)-H(78)	119.9(8)
C(68)-C(69)-H(69)	119.1(8)	C(77)-C(78)-H(78)	120.1(9)
C(68)-C(69)-C(70)	121.5(8)	P(4)-C(79)-C(80)	123.1(6)
H(69)-C(69)-C(70)	119.4(8)	P(4)-C(79)-C(84)	119.4(6)
C(69)-C(70)-H(70)	120.2(9)	C(80)-C(79)-C(84)	117.5(7)
C(69)-C(70)-C(71)	119.5(8)	C(79)-C(80)-H(80)	119.5(8)
H(70)-C(70)-C(71)	120.3(9)	C(79)-C(80)-C(81)	121.1(7)
C(70)-C(71)-H(71)	119.8(8)	H(80)-C(80)-C(81)	119.5(8)
C(70)-C(71)-C(72)	120.5(8)	C(80)-C(81)-H(81)	120.2(9)
H(71)-C(71)-C(72)	119.7(8)	C(80)-C(81)-C(82)	119.7(8)
C(67)-C(72)-C(71)	119.1(7)	H(81)-C(81)-C(82)	120.1(9)
C(67)-C(72)-H(72)	120.5(8)	C(81)-C(82)-H(82)	119.7(9)
C(71)-C(72)-H(72)	120.4(8)	C(81)-C(82)-C(83)	120.7(9)
P(4)-C(73)-C(74)	120.8(6)	H(82)-C(82)-C(83)	119.5(9)
P(4)-C(73)-C(78)	118.6(6)	C(82)-C(83)-H(83)	120.0(9)
C(74)-C(73)-C(78)	119.6(7)	C(82)-C(83)-C(84)	119.8(8)
C(73)-C(74)-H(74)	119.4(8)	H(83)-C(83)-C(84)	120.2(8)
C(73)-C(74)-C(75)	121.4(7)	C(79)-C(84)-C(83)	121.2(8)
H(74)-C(74)-C(75)	119.2(8)	C(79)-C(84)-H(84)	119.4(8)
C(74)-C(75)-H(75)	121.2(9)	C(83)-C(84)-H(84)	119.4(8)
C(74)-C(75)-C(76)	117.6(8)		
H(75)-C(75)-C(76)	121.2(9)		

Symmetry transformations used to generate equivalent atoms:

Table A-11. Crystal data and structure refinement for $[Et_4N^+]_2[V{\equiv}O(ema)W(CO)_4]^{2-}$.

Identification code	vow	
Empirical formula	C26 H48 N4 O7 S2 V W	
Formula weight	827.60	
Temperature	110(2) K	
Wavelength	0.71073 ≈	
Crystal system	Orthorhombic	
Space group	Pnma	
Unit cell dimensions	a = 22.1643(16) Å	α= 90°
	b = 15.6695(12) Å	β= 90°
	c = 10.7813(8) Å	γ = 90°
Volume	3744.4(5) Å^3	
Z	4	
Density (calculated)	1.468 Mg/m^3	
Absorption coefficient	3.478 mm^{-1}	
F(000)	1792	
Crystal size	0.30 x 0.10 x 0.10 mm^3	
Theta range for data collection	1.84 to 25.00°	
Index ranges	-26<=h<=26, -18<=k<=18, -12<=l<=12	
Reflections collected	34263	
Independent reflections	3386 [R(int) = 0.0768]	
Completeness to theta = 25.00°	98.5 %	
Absorption correction	Semi-empirical from equivalents	
Max. and min. transmission	0.7224 and 0.4218	
Refinement method	Full-matrix least-squares on F^2	
Data / restraints / parameters	3386 / 167 / 279	
Goodness-of-fit on F^2	1.012	
Final R indices [I>2sigma(I)]	R1 = 0.0319, wR2 = 0.0694	
R indices (all data)	R1 = 0.0459, wR2 = 0.0723	
Largest diff. peak and hole	0.768 and -1.013 e.Å^{-3}	

Table A-12. Bond lengths [Å] and angles [°] for $[Et_4N^+]_2[V{\equiv}O(ema)W(CO)_4]^{2-}$.

W(1)-C(1)	1.934(6)	C21-H2B1	0.9800
W(1)-C(1)#1	1.934(6)	C21-H2C1	0.9800
W(1)-C(3)	2.027(8)	C31-C41	1.490(9)
W(1)-C(2)	2.039(8)	C31-H3A1	0.9900
W(1)-S(1)	2.5857(13)	C31-H3B1	0.9900
W(1)-S(1)#1	2.5857(13)	C41-H4C1	0.9800
V(1)-O(5)	1.612(5)	C41-H4D1	0.9800
V(1)-N(1)#1	1.992(4)	C41-H4E1	0.9800
V(1)-N(1)	1.992(4)	C51-C61	1.490(9)
V(1)-S(1)	2.3834(15)	C51-H5A1	0.9900
V(1)-S(1)#1	2.3834(15)	C51-H5B1	0.9900
S(1)-C(6)	1.823(5)	C61-H6C1	0.9800
O(1)-C(1)	1.184(6)	C61-H6D1	0.9800
O(2)-C(2)	1.145(8)	C61-H6E1	0.9800
O(3)-C(3)	1.141(8)	C71-C81	1.497(9)
O(4)-C(5)	1.247(6)	C71-H7A1	0.9900
N(1)-C(5)	1.325(7)	C71-H7B1	0.9900
N(1)-C(4)	1.464(6)	C81-H8A1	0.9800
C(4)-C(4)#1	1.451(11)	C81-H8B1	0.9800
C(4)-H(4A)	0.9701	C81-H8C1	0.9800
C(4)-H(4B)	0.9698	N12-C72	1.506(8)
C(6)-C(5)	1.516(7)	N12-C12	1.509(8)
C(6)-H(6A)	0.9900	N12-C52	1.515(8)
C(6)-H(6B)	0.9900	N12-C32	1.519(8)
N11-C11	1.503(8)	C12-C22	1.478(9)
N11-C51	1.509(8)	C12-H1C2	0.9900
N11-C71	1.516(8)	C12-H1D2	0.9900
N11-C31	1.525(8)	C22-H2D2	0.9800
C11-C21	1.471(9)	C22-H2E2	0.9800
C11-H1A1	0.9900	C22-H2F2	0.9800
C11-H1B1	0.9900	C32-C42	1.527(9)
C21-H2A1	0.9800	C32-H3C2	0.9900

C32-H3D2	0.9900	N(1)#1-V(1)-N(1)	79.4(3)
C42-H4F2	0.9800	O(5)-V(1)-S(1)	110.01(13)
C42-H4G2	0.9800	N(1)#1-V(1)-S(1)	140.49(14)
C42-H4H2	0.9800	N(1)-V(1)-S(1)	82.74(12)
C52-C62	1.495(8)	O(5)-V(1)-S(1)#1	110.01(13)
C52-H5C2	0.9900	N(1)#1-V(1)-S(1)#1	82.74(12)
C52-H5D2	0.9900	N(1)-V(1)-S(1)#1	140.49(14)
C62-H6F2	0.9800	S(1)-V(1)-S(1)#1	89.36(7)
C62-H6G2	0.9800	C(6)-S(1)-V(1)	98.37(17)
C62-H6H2	0.9800	C(6)-S(1)-W(1)	108.71(18)
C72-C82	1.502(9)	V(1)-S(1)-W(1)	83.06(5)
C72-H7C2	0.9900	C(5)-N(1)-C(4)	117.4(5)
C72-H7D2	0.9900	C(5)-N(1)-V(1)	127.5(3)
C82-H8D2	0.9800	C(4)-N(1)-V(1)	114.3(4)
C82-H8E2	0.9800	O(1)-C(1)-W(1)	178.2(5)
C82-H8F2	0.9800	O(2)-C(2)-W(1)	173.4(7)
		O(3)-C(3)-W(1)	171.9(7)
C(1)-W(1)-C(1)#1	93.5(3)	C(4)#1-C(4)-N(1)	111.9(3)
C(1)-W(1)-C(3)	86.4(2)	C(4)#1-C(4)-H(4A)	109.2
C(1)#1-W(1)-C(3)	86.4(2)	N(1)-C(4)-H(4A)	110.4
C(1)-W(1)-C(2)	87.6(2)	C(4)#1-C(4)-H(4B)	109.2
C(1)#1-W(1)-C(2)	87.6(2)	N(1)-C(4)-H(4B)	108.2
C(3)-W(1)-C(2)	171.3(3)	H(4A)-C(4)-H(4B)	107.9
C(1)-W(1)-S(1)	173.51(16)	C(5)-C(6)-S(1)	115.1(4)
C(1)#1-W(1)-S(1)	92.82(17)	C(5)-C(6)-H(6A)	108.5
C(3)-W(1)-S(1)	95.27(16)	S(1)-C(6)-H(6A)	108.5
C(2)-W(1)-S(1)	91.33(16)	C(5)-C(6)-H(6B)	108.5
C(1)-W(1)-S(1)#1	92.82(17)	S(1)-C(6)-H(6B)	108.5
C(1)#1-W(1)-S(1)#1	173.51(16)	H(6A)-C(6)-H(6B)	107.5
C(3)-W(1)-S(1)#1	95.27(16)	O(4)-C(5)-N(1)	126.9(5)
C(2)-W(1)-S(1)#1	91.33(16)	O(4)-C(5)-C(6)	117.4(5)
S(1)-W(1)-S(1)#1	80.80(6)	N(1)-C(5)-C(6)	115.6(5)
O(5)-V(1)-N(1)#1	109.06(19)	C11-N11-C51	110.7(6)
O(5)-V(1)-N(1)	109.06(19)	C11-N11-C71	109.2(6)

C51-N11-C71	110.6(6)	C51-C61-H6C1	109.5
C11-N11-C31	110.4(6)	C51-C61-H6D1	109.5
C51-N11-C31	108.4(6)	H6C1-C61-H6D1	109.5
C71-N11-C31	107.6(6)	C51-C61-H6E1	109.5
C21-C11-N11	115.4(8)	H6C1-C61-H6E1	109.5
C21-C11-H1A1	108.4	H6D1-C61-H6E1	109.5
N11-C11-H1A1	108.4	C81-C71-N11	113.5(7)
C21-C11-H1B1	108.4	C81-C71-H7A1	108.9
N11-C11-H1B1	108.4	N11-C71-H7A1	108.9
H1A1-C11-H1B1	107.5	C81-C71-H7B1	108.9
C11-C21-H2A1	109.5	N11-C71-H7B1	108.9
C11-C21-H2B1	109.5	H7A1-C71-H7B1	107.7
H2A1-C21-H2B1	109.5	C71-C81-H8A1	109.5
C11-C21-H2C1	109.5	C71-C81-H8B1	109.5
H2A1-C21-H2C1	109.5	H8A1-C81-H8B1	109.5
H2B1-C21-H2C1	109.5	C71-C81-H8C1	109.5
C41-C31-N11	113.7(8)	H8A1-C81-H8C1	109.5
C41-C31-H3A1	108.8	H8B1-C81-H8C1	109.5
N11-C31-H3A1	108.8	C72-N12-C12	109.7(6)
C41-C31-H3B1	108.8	C72-N12-C52	110.4(6)
N11-C31-H3B1	108.8	C12-N12-C52	111.9(8)
H3A1-C31-H3B1	107.7	C72-N12-C32	109.5(6)
C31-C41-H4C1	109.5	C12-N12-C32	107.2(6)
C31-C41-H4D1	109.5	C52-N12-C32	108.1(6)
H4C1-C41-H4D1	109.5	C22-C12-N12	114.4(8)
C31-C41-H4E1	109.5	C22-C12-H1C2	108.7
H4C1-C41-H4E1	109.5	N12-C12-H1C2	108.7
H4D1-C41-H4E1	109.5	C22-C12-H1D2	108.7
C61-C51-N11	114.5(7)	N12-C12-H1D2	108.7
C61-C51-H5A1	108.6	H1C2-C12-H1D2	107.6
N11-C51-H5A1	108.6	C12-C22-H2D2	109.5
C61-C51-H5B1	108.6	C12-C22-H2E2	109.5
N11-C51-H5B1	108.6	H2D2-C22-H2E2	109.5
H5A1-C51-H5B1	107.6	C12-C22-H2F2	109.5

H2D2-C22-H2F2	109.5	H5C2-C52-H5D2	107.7
H2E2-C22-H2F2	109.5	C52-C62-H6F2	109.5
N12-C32-C42	111.0(7)	C52-C62-H6G2	109.5
N12-C32-H3C2	109.4	H6F2-C62-H6G2	109.5
C42-C32-H3C2	109.4	C52-C62-H6H2	109.5
N12-C32-H3D2	109.4	H6F2-C62-H6H2	109.5
C42-C32-H3D2	109.4	H6G2-C62-H6H2	109.5
H3C2-C32-H3D2	108.0	C82-C72-N12	112.4(7)
C32-C42-H4F2	109.5	C82-C72-H7C2	109.1
C32-C42-H4G2	109.5	N12-C72-H7C2	109.1
H4F2-C42-H4G2	109.5	C82-C72-H7D2	109.1
C32-C42-H4H2	109.5	N12-C72-H7D2	109.1
H4F2-C42-H4H2	109.5	H7C2-C72-H7D2	107.9
H4G2-C42-H4H2	109.5	C72-C82-H8D2	109.5
C62-C52-N12	113.7(7)	C72-C82-H8E2	109.5
C62-C52-H5C2	108.8	H8D2-C82-H8E2	109.5
N12-C52-H5C2	108.8	C72-C82-H8F2	109.5
C62-C52-H5D2	108.8	H8D2-C82-H8F2	109.5
N12-C52-H5D2	108.8	H8E2-C82-H8F2	109.5

Symmetry transformations used to generate equivalent atoms:

#1 x,-y+1/2,z

Table A-13. Crystal data and structure refinement for (IMes)Fe$(NO)_2$I.

Identification code	IMesI	
Empirical formula	C21 H24 Fe I N4 O2	
Formula weight	547.19	
Temperature	110(2) K	
Wavelength	0.71073 Å	
Crystal system	Orthorhombic	
Space group	Pbca	
Unit cell dimensions	a = 14.303(5) Å	α= 90°.
	b = 16.389(6) Å	β= 90°.
	c = 19.923(7) Å	γ = 90°.
Volume	4670(3) $Å^3$	
Z	8	
Density (calculated)	1.556 Mg/m^3	
Absorption coefficient	1.990 mm^{-1}	
F(000)	2184	
Crystal size	0.08 x 0.05 x 0.02 mm^3	
Theta range for data collection	2.04 to 28.31°.	
Index ranges	-18<=h<=19, -21<=k<=21, -26<=l<=26	
Reflections collected	53589	
Independent reflections	5787 [R(int) = 0.0788]	
Completeness to theta = 28.31°	99.6 %	
Absorption correction	Semi-empirical from equivalents	
Max. and min. transmission	0.9613 and 0.8570	
Refinement method	Full-matrix least-squares on F^2	
Data / restraints / parameters	5787 / 0 / 268	
Goodness-of-fit on F^2	1.025	
Final R indices [I>2sigma(I)]	R1 = 0.0334, wR2 = 0.0703	
R indices (all data)	R1 = 0.0561, wR2 = 0.0793	
Largest diff. peak and hole	0.646 and -0.458 $e.Å^{-3}$	

Table A-14. Bond lengths [Å] and angles [°] for (IMes)Fe$(NO)_2$I.

Fe(1)-N(2)	1.689(3)		
Fe(1)-N(1)	1.688(3)	N(2)-Fe(1)-N(1)	111.95(13)
Fe(1)-C(1)	2.041(3)	N(2)-Fe(1)-C(1)	106.09(12)
Fe(1)-I(1)	2.5727(8)	N(1)-Fe(1)-C(1)	107.20(12)
N(1)-O(1)	1.169(3)	N(2)-Fe(1)-I(1)	113.06(9)
N(2)-O(2)	1.172(3)	N(1)-Fe(1)-I(1)	108.98(9)
C(1)-N(4)	1.355(3)	C(1)-Fe(1)-I(1)	109.34(8)
C(1)-N(3)	1.360(3)	O(1)-N(1)-Fe(1)	167.3(2)
C(2)-C(3)	1.340(4)	O(2)-N(2)-Fe(1)	162.6(3)
C(2)-N(3)	1.392(4)	N(4)-C(1)-N(3)	103.8(2)
C(3)-N(4)	1.383(4)	N(4)-C(1)-Fe(1)	129.0(2)
C(4)-C(5)	1.384(4)	N(3)-C(1)-Fe(1)	127.10(19)
C(4)-C(9)	1.394(4)	C(3)-C(2)-N(3)	106.5(3)
C(4)-N(3)	1.451(3)	C(2)-C(3)-N(4)	106.9(3)
C(5)-C(6)	1.397(4)	C(5)-C(4)-C(9)	123.4(3)
C(5)-C(11)	1.506(4)	C(5)-C(4)-N(3)	118.7(2)
C(6)-C(7)	1.396(4)	C(9)-C(4)-N(3)	117.8(2)
C(7)-C(8)	1.385(4)	C(4)-C(5)-C(6)	117.2(3)
C(7)-C(12)	1.509(4)	C(4)-C(5)-C(11)	122.2(3)
C(8)-C(9)	1.393(4)	C(6)-C(5)-C(11)	120.6(3)
C(9)-C(10)	1.507(4)	C(7)-C(6)-C(5)	121.7(3)
C(13)-C(14)	1.392(4)	C(8)-C(7)-C(6)	118.7(3)
C(13)-C(18)	1.395(4)	C(8)-C(7)-C(12)	120.7(3)
C(13)-N(4)	1.455(3)	C(6)-C(7)-C(12)	120.6(3)
C(14)-C(15)	1.393(4)	C(7)-C(8)-C(9)	121.8(3)
C(14)-C(19)	1.512(4)	C(8)-C(9)-C(4)	117.3(3)
C(15)-C(16)	1.391(4)	C(8)-C(9)-C(10)	121.1(3)
C(16)-C(17)	1.392(4)	C(4)-C(9)-C(10)	121.6(3)
C(16)-C(20)	1.507(4)	C(14)-C(13)-C(18)	122.7(3)
C(17)-C(18)	1.394(4)	C(14)-C(13)-N(4)	117.7(2)
C(18)-C(21)	1.503(4)	C(18)-C(13)-N(4)	119.5(2)

C(13)-C(14)-C(15)	117.8(3)	C(17)-C(18)-C(21)	120.8(3)
C(13)-C(14)-C(19)	122.0(3)	C(13)-C(18)-C(21)	121.9(3)
C(15)-C(14)-C(19)	120.2(3)	C(1)-N(3)-C(2)	111.3(2)
C(16)-C(15)-C(14)	121.7(3)	C(1)-N(3)-C(4)	125.6(2)
C(15)-C(16)-C(17)	118.5(3)	C(2)-N(3)-C(4)	123.1(2)
C(15)-C(16)-C(20)	120.5(3)	C(1)-N(4)-C(3)	111.6(2)
C(17)-C(16)-C(20)	121.0(3)	C(1)-N(4)-C(13)	126.3(2)
C(16)-C(17)-C(18)	122.0(3)	C(3)-N(4)-C(13)	121.5(2)
C(17)-C(18)-C(13)	117.3(3)		

Symmetry transformations used to generate equivalent atoms:

Table A-15. Crystal data and structure refinement for [Ni(bme-daco)•$(Fe(NO)_2I)_2$].

Identification code	NidacoFeNO2	
Empirical formula	C10 H20 Fe2 I2 N6 Ni O4 S2	
Formula weight	776.65	
Temperature	110(2) K	
Wavelength	0.71073 Å	
Crystal system	Monoclinic	
Space group	P21/n	
Unit cell dimensions	a = 10.274(3) Å	α= 90°.
	b = 15.992(5) Å	β= 91.237(3)°.
	c = 13.674(4) Å	γ = 90°.
Volume	2246.2(11) $Å^3$	
Z	4	
Density (calculated)	2.297 Mg/m^3	
Absorption coefficient	5.066 mm^{-1}	
F(000)	1488	
Crystal size	0.10 x 0.09 x 0.05 mm^3	
Theta range for data collection	2.36 to 28.35°.	
Index ranges	-13<=h<=13, -21<=k<=20, -18<=l<=18	
Reflections collected	26134	
Independent reflections	5561 [R(int) = 0.0410]	
Completeness to theta = 28.35°	99.0 %	
Absorption correction	Semi-empirical from equivalents	
Max. and min. transmission	0.7858 and 0.6313	
Refinement method	Full-matrix least-squares on F^2	
Data / restraints / parameters	5561 / 12 / 244	
Goodness-of-fit on F^2	1.040	
Final R indices [I>2sigma(I)]	R1 = 0.0371, wR2 = 0.0861	
R indices (all data)	R1 = 0.0427, wR2 = 0.0890	
Largest diff. peak and hole	2.046 and -1.944 $e.Å^{-3}$	

Table A-16. Bond lengths [Å] and angles [°] for [Ni(bme-daco)•$(Fe(NO)_2I)_2$].

I(1)-Fe(1)	2.5775(9)	C(6)-C(7)	1.479(8)
I(2)-Fe(2)	2.5704(9)	C(6)-C(5)	1.510(7)
Ni(1)-N(5)	1.970(4)	C(6)-H(6A)	0.9900
Ni(1)-N(6)	1.976(3)	C(6)-H(6B)	0.9900
Ni(1)-S(1)	2.1765(12)	C(5)-H(5A)	0.9900
Ni(1)-S(2)	2.1884(11)	C(5)-H(5B)	0.9900
Fe(2)-N(3)	1.688(4)	C(2)-C(1)	1.401(9)
Fe(2)-N(4)	1.785(5)	C(2)-H(2A)	0.9900
Fe(2)-S(2)	2.3381(12)	C(2)-H(2B)	0.9900
Fe(1)-N(2)	1.680(4)	C(1)-H(1B)	0.9900
Fe(1)-N(1)	1.765(5)	C(1)-H(1C)	0.9900
Fe(1)-S(1)	2.3213(13)	C(7)-H(7A)	0.9900
S(1)-C(1)	1.803(5)	C(7)-H(7B)	0.9900
S(2)-C(3)	1.824(4)	C(10)-C(9)	1.442(9)
N(3)-O(3)	1.154(5)	C(10)-H(10A)	0.9900
N(2)-O(2)	1.169(5)	C(10)-H(10B)	0.9900
N(1)-O(1)	0.993(5)	C(9)-H(9A)	0.9900
O(4)-N(4)	0.984(6)	C(9)-H(9B)	0.9900
N(6)-C(5)	1.501(6)		
N(6)-C(8)	1.503(6)	N(5)-Ni(1)-N(6)	89.62(16)
N(6)-C(4)	1.505(5)	N(5)-Ni(1)-S(1)	90.17(12)
C(3)-C(4)	1.505(6)	N(6)-Ni(1)-S(1)	174.28(11)
C(3)-H(3A)	0.9900	N(5)-Ni(1)-S(2)	178.97(15)
C(3)-H(3B)	0.9900	N(6)-Ni(1)-S(2)	89.89(10)
C(4)-H(4A)	0.9900	S(1)-Ni(1)-S(2)	90.23(4)
C(4)-H(4B)	0.9900	N(3)-Fe(2)-N(4)	110.57(18)
N(5)-C(7)	1.483(7)	N(3)-Fe(2)-S(2)	109.86(12)
N(5)-C(10)	1.484(8)	N(4)-Fe(2)-S(2)	103.42(13)
N(5)-C(2)	1.537(7)	N(3)-Fe(2)-I(2)	110.34(13)
C(8)-C(9)	1.450(8)	N(4)-Fe(2)-I(2)	115.34(12)
C(8)-H(8A)	0.9900	S(2)-Fe(2)-I(2)	106.95(3)
C(8)-H(8B)	0.9900	N(2)-Fe(1)-N(1)	111.58(17)

N(2)-Fe(1)-S(1)	103.00(13)	C(7)-N(5)-C(2)	101.1(4)
N(1)-Fe(1)-S(1)	111.25(13)	C(10)-N(5)-C(2)	112.8(5)
N(2)-Fe(1)-I(1)	109.35(13)	C(7)-N(5)-Ni(1)	115.2(3)
N(1)-Fe(1)-I(1)	109.51(13)	C(10)-N(5)-Ni(1)	106.4(4)
S(1)-Fe(1)-I(1)	112.01(4)	C(2)-N(5)-Ni(1)	110.0(3)
C(1)-S(1)-Ni(1)	98.04(19)	C(9)-C(8)-N(6)	116.8(5)
C(1)-S(1)-Fe(1)	111.5(3)	C(9)-C(8)-H(8A)	108.1
Ni(1)-S(1)-Fe(1)	99.02(4)	N(6)-C(8)-H(8A)	108.1
C(3)-S(2)-Ni(1)	96.95(14)	C(9)-C(8)-H(8B)	108.1
C(3)-S(2)-Fe(2)	101.32(15)	N(6)-C(8)-H(8B)	108.1
Ni(1)-S(2)-Fe(2)	111.37(4)	H(8A)-C(8)-H(8B)	107.3
O(3)-N(3)-Fe(2)	166.6(4)	C(7)-C(6)-C(5)	114.8(4)
O(2)-N(2)-Fe(1)	168.5(3)	C(7)-C(6)-H(6A)	108.6
O(1)-N(1)-Fe(1)	161.6(4)	C(5)-C(6)-H(6A)	108.6
C(5)-N(6)-C(8)	112.3(4)	C(7)-C(6)-H(6B)	108.6
C(5)-N(6)-C(4)	105.6(3)	C(5)-C(6)-H(6B)	108.6
C(8)-N(6)-C(4)	108.8(4)	H(6A)-C(6)-H(6B)	107.5
C(5)-N(6)-Ni(1)	112.0(3)	N(6)-C(5)-C(6)	115.9(4)
C(8)-N(6)-Ni(1)	106.7(3)	N(6)-C(5)-H(5A)	108.3
C(4)-N(6)-Ni(1)	111.4(2)	C(6)-C(5)-H(5A)	108.3
O(4)-N(4)-Fe(2)	160.9(5)	N(6)-C(5)-H(5B)	108.3
C(4)-C(3)-S(2)	105.1(3)	C(6)-C(5)-H(5B)	108.3
C(4)-C(3)-H(3A)	110.7	H(5A)-C(5)-H(5B)	107.4
S(2)-C(3)-H(3A)	110.7	C(1)-C(2)-N(5)	112.6(5)
C(4)-C(3)-H(3B)	110.7	C(1)-C(2)-H(2A)	109.1
S(2)-C(3)-H(3B)	110.7	N(5)-C(2)-H(2A)	109.1
H(3A)-C(3)-H(3B)	108.8	C(1)-C(2)-H(2B)	109.1
N(6)-C(4)-C(3)	111.6(3)	N(5)-C(2)-H(2B)	109.1
N(6)-C(4)-H(4A)	109.3	H(2A)-C(2)-H(2B)	107.8
C(3)-C(4)-H(4A)	109.3	C(2)-C(1)-S(1)	111.7(4)
N(6)-C(4)-H(4B)	109.3	C(2)-C(1)-H(1B)	109.3
C(3)-C(4)-H(4B)	109.3	S(1)-C(1)-H(1B)	109.3
H(4A)-C(4)-H(4B)	108.0	C(2)-C(1)-H(1C)	109.3
C(7)-N(5)-C(10)	111.4(5)	S(1)-C(1)-H(1C)	109.3

H(1B)-C(1)-H(1C)	107.9	C(9)-C(10)-H(10B)	108.0
C(6)-C(7)-N(5)	116.2(4)	N(5)-C(10)-H(10B)	108.0
C(6)-C(7)-H(7A)	108.2	H(10A)-C(10)-H(10B)	107.2
N(5)-C(7)-H(7A)	108.2	C(10)-C(9)-C(8)	131.1(6)
C(6)-C(7)-H(7B)	108.2	C(10)-C(9)-H(9A)	104.5
N(5)-C(7)-H(7B)	108.2	C(8)-C(9)-H(9A)	104.5
H(7A)-C(7)-H(7B)	107.4	C(10)-C(9)-H(9B)	104.5
C(9)-C(10)-N(5)	117.4(5)	C(8)-C(9)-H(9B)	104.5
C(9)-C(10)-H(10A)	108.0	H(9A)-C(9)-H(9B)	105.6
N(5)-C(10)-H(10A)	108.0		

Symmetry transformations used to generate equivalent atoms:

Table A-17. Crystal data and structure refinement for [V≡O(bme-daco)•$Fe(NO)_2I$].

Identification code	VOdacoI	
Empirical formula	C14 H28 Fe I N4 O4 S2 V	
Formula weight	614.21	
Temperature	110(2) K	
Wavelength	0.71073 Å	
Crystal system	Triclinic	
Space group	P-1	
Unit cell dimensions	a = 8.764(7) Å	α= 102.983(9)°.
	b = 10.583(8) Å	β= 99.382(9)°.
	c = 13.888(11) Å	γ = 113.174(9)°.
Volume	1107.5(15) $Å^3$	
Z	2	
Density (calculated)	1.842 Mg/m^3	
Absorption coefficient	2.685 mm^{-1}	
F(000)	612	
Crystal size	0.25 x 0.10 x 0.10 mm^3	
Theta range for data collection	2.21 to 25.99°.	
Index ranges	-10<=h<=10, -13<=k<=13, -17<=l<=17	
Reflections collected	11303	
Independent reflections	4321 [R(int) = 0.0354]	
Completeness to theta = 25.99°	99.4 %	
Absorption correction	Semi-empirical from equivalents	
Max. and min. transmission	0.7750 and 0.5533	
Refinement method	Full-matrix least-squares on F^2	
Data / restraints / parameters	4321 / 0 / 244	
Goodness-of-fit on F^2	1.079	
Final R indices [I>2sigma(I)]	R1 = 0.0275, wR2 = 0.0611	
R indices (all data)	R1 = 0.0355, wR2 = 0.0642	
Largest diff. peak and hole	0.715 and -0.702 e.$Å^{-3}$	

Table A-18. Bond lengths [Å] and angles [°] for [V≡O(bme-daco)•Fe(NO)$_2$I].

Fe(1)-N(1)	1.682(3)	C(6)-C(7)	1.521(5)
Fe(1)-N(2)	1.694(3)	C(6)-H(6A)	0.9900
Fe(1)-S(1)	2.3234(19)	C(6)-H(6B)	0.9900
Fe(1)-I(1)	2.5987(16)	C(7)-H(7A)	0.9900
N(1)-O(1)	1.172(4)	C(7)-H(7B)	0.9900
N(2)-O(2)	1.160(4)	C(8)-C(9)	1.516(4)
S(1)-C(3)	1.834(4)	C(8)-H(8A)	0.9900
S(1)-V(1)	2.4206(17)	C(8)-H(8B)	0.9900
S(2)-C(1)	1.830(4)	C(9)-C(10)	1.521(5)
S(2)-V(1)	2.322(2)	C(9)-H(9A)	0.9900
V(1)-O(3)	1.594(2)	C(9)-H(9B)	0.9900
V(1)-N(4)	2.127(3)	C(10)-H(10A)	0.9900
V(1)-N(3)	2.149(3)	C(10)-H(10B)	0.9900
N(3)-C(4)	1.496(4)	O(4)-C(14)	1.424(4)
N(3)-C(10)	1.506(4)	O(4)-C(11)	1.427(4)
N(3)-C(5)	1.511(4)	C(14)-C(13)	1.511(5)
N(4)-C(8)	1.492(4)	C(14)-H(14A)	0.9900
N(4)-C(7)	1.507(4)	C(14)-H(14B)	0.9900
N(4)-C(2)	1.509(4)	C(12)-C(11)	1.511(5)
C(1)-C(2)	1.512(5)	C(12)-C(13)	1.519(5)
C(1)-H(1A)	0.9900	C(12)-H(12A)	0.9900
C(1)-H(1B)	0.9900	C(12)-H(12B)	0.9900
C(2)-H(2A)	0.9900	C(11)-H(11A)	0.9900
C(2)-H(2B)	0.9900	C(11)-H(11B)	0.9900
C(3)-C(4)	1.508(5)	C(13)-H(13A)	0.9900
C(3)-H(3A)	0.9900	C(13)-H(13B)	0.9900
C(3)-H(3B)	0.9900		
C(4)-H(4A)	0.9900	N(1)-Fe(1)-N(2)	117.07(16)
C(4)-H(4B)	0.9900	N(1)-Fe(1)-S(1)	110.53(11)
C(5)-C(6)	1.530(4)	N(2)-Fe(1)-S(1)	105.72(10)
C(5)-H(5A)	0.9900	N(1)-Fe(1)-I(1)	104.73(10)
C(5)-H(5B)	0.9900	N(2)-Fe(1)-I(1)	111.46(11)

S(1)-Fe(1)-I(1)	107.01(6)	H(1A)-C(1)-H(1B)	107.9
O(1)-N(1)-Fe(1)	170.2(3)	N(4)-C(2)-C(1)	112.7(3)
O(2)-N(2)-Fe(1)	166.2(3)	N(4)-C(2)-H(2A)	109.0
C(3)-S(1)-Fe(1)	103.26(12)	C(1)-C(2)-H(2A)	109.0
C(3)-S(1)-V(1)	99.34(11)	N(4)-C(2)-H(2B)	109.0
Fe(1)-S(1)-V(1)	103.71(7)	C(1)-C(2)-H(2B)	109.0
C(1)-S(2)-V(1)	99.84(11)	H(2A)-C(2)-H(2B)	107.8
O(3)-V(1)-N(4)	102.32(12)	C(4)-C(3)-S(1)	110.5(2)
O(3)-V(1)-N(3)	104.22(11)	C(4)-C(3)-H(3A)	109.5
N(4)-V(1)-N(3)	84.38(10)	S(1)-C(3)-H(3A)	109.5
O(3)-V(1)-S(2)	111.50(9)	C(4)-C(3)-H(3B)	109.5
N(4)-V(1)-S(2)	84.82(8)	S(1)-C(3)-H(3B)	109.5
N(3)-V(1)-S(2)	144.11(8)	H(3A)-C(3)-H(3B)	108.1
O(3)-V(1)-S(1)	108.69(11)	N(3)-C(4)-C(3)	113.0(3)
N(4)-V(1)-S(1)	148.61(7)	N(3)-C(4)-H(4A)	109.0
N(3)-V(1)-S(1)	83.46(8)	C(3)-C(4)-H(4A)	109.0
S(2)-V(1)-S(1)	88.30(4)	N(3)-C(4)-H(4B)	109.0
C(4)-N(3)-C(10)	106.2(2)	C(3)-C(4)-H(4B)	109.0
C(4)-N(3)-C(5)	110.5(2)	H(4A)-C(4)-H(4B)	107.8
C(10)-N(3)-C(5)	110.0(2)	N(3)-C(5)-C(6)	111.9(2)
C(4)-N(3)-V(1)	108.87(19)	N(3)-C(5)-H(5A)	109.2
C(10)-N(3)-V(1)	109.99(19)	C(6)-C(5)-H(5A)	109.2
C(5)-N(3)-V(1)	111.12(18)	N(3)-C(5)-H(5B)	109.2
C(8)-N(4)-C(7)	111.0(2)	C(6)-C(5)-H(5B)	109.2
C(8)-N(4)-C(2)	106.4(2)	H(5A)-C(5)-H(5B)	107.9
C(7)-N(4)-C(2)	110.9(2)	C(7)-C(6)-C(5)	117.9(3)
C(8)-N(4)-V(1)	111.54(19)	C(7)-C(6)-H(6A)	107.8
C(7)-N(4)-V(1)	110.20(19)	C(5)-C(6)-H(6A)	107.8
C(2)-N(4)-V(1)	106.71(18)	C(7)-C(6)-H(6B)	107.8
C(2)-C(1)-S(2)	111.9(2)	C(5)-C(6)-H(6B)	107.8
C(2)-C(1)-H(1A)	109.2	H(6A)-C(6)-H(6B)	107.2
S(2)-C(1)-H(1A)	109.2	N(4)-C(7)-C(6)	113.0(3)
C(2)-C(1)-H(1B)	109.2	N(4)-C(7)-H(7A)	109.0
S(2)-C(1)-H(1B)	109.2	C(6)-C(7)-H(7A)	109.0

N(4)-C(7)-H(7B)	109.0	O(4)-C(14)-H(14A)	110.5
C(6)-C(7)-H(7B)	109.0	C(13)-C(14)-H(14A)	110.5
H(7A)-C(7)-H(7B)	107.8	O(4)-C(14)-H(14B)	110.5
N(4)-C(8)-C(9)	115.2(3)	C(13)-C(14)-H(14B)	110.5
N(4)-C(8)-H(8A)	108.5	H(14A)-C(14)-H(14B)	108.7
C(9)-C(8)-H(8A)	108.5	C(11)-C(12)-C(13)	102.2(3)
N(4)-C(8)-H(8B)	108.5	C(11)-C(12)-H(12A)	111.3
C(9)-C(8)-H(8B)	108.5	C(13)-C(12)-H(12A)	111.3
H(8A)-C(8)-H(8B)	107.5	C(11)-C(12)-H(12B)	111.3
C(8)-C(9)-C(10)	115.5(3)	C(13)-C(12)-H(12B)	111.3
C(8)-C(9)-H(9A)	108.4	H(12A)-C(12)-H(12B)	109.2
C(10)-C(9)-H(9A)	108.4	O(4)-C(11)-C(12)	107.0(3)
C(8)-C(9)-H(9B)	108.4	O(4)-C(11)-H(11A)	110.3
C(10)-C(9)-H(9B)	108.4	C(12)-C(11)-H(11A)	110.3
H(9A)-C(9)-H(9B)	107.5	O(4)-C(11)-H(11B)	110.3
N(3)-C(10)-C(9)	114.6(3)	C(12)-C(11)-H(11B)	110.3
N(3)-C(10)-H(10A)	108.6	H(11A)-C(11)-H(11B)	108.6
C(9)-C(10)-H(10A)	108.6	C(14)-C(13)-C(12)	102.5(3)
N(3)-C(10)-H(10B)	108.6	C(14)-C(13)-H(13A)	111.3
C(9)-C(10)-H(10B)	108.6	C(12)-C(13)-H(13A)	111.3
H(10A)-C(10)-H(10B)	107.6	C(14)-C(13)-H(13B)	111.3
C(14)-O(4)-C(11)	109.9(3)	C(12)-C(13)-H(13B)	111.3
O(4)-C(14)-C(13)	106.2(3)	H(13A)-C(13)-H(13B)	109.2

Symmetry transformations used to generate equivalent atoms: